PEOPLE'S DEMOCRATIC REPUBLIC OF ALGERIA

Ministry of Higher Education And Scientific Research

KASDY MERBAH UNIVERSITY OF OUARGLA

FACULTY OF MATHEMATICS AND MATERIAL SCIENCES

DEPARTMENT OF MATHEMATICS

Doctorate In Mathematics

Order No:

Serial No:

Specialization

Analysis

Theme

The homotopy method for nonlinear problems

Presented by

Mouaad BOUAKKAZ

Defended on 03 May 2026 befor the jury:

Djamel Ahmed CHACHA	Professor	Kasdi Merbah University-Ouargla	Chairman
Mabrouk MEFLAH	Professor	Kasdi Merbah University-Ouargla	Supervisor
Nouria ARAR	Professor	University Constantine 1, Brothers Mentouri	Co-supervisor
Ibrahim Talleb	Professor	Kasdi Merbah University-Ouargla	Examiner
Abdelkader AMARA	Professor	Kasdi Merbah University-Ouargla	Examiner
Ammar YOUKANA	Professor	University of Batna 2	Examiner
Chahrazade MATMAT	MCA	University Constantine 1, Brothers Mentouri	Examiner

Academic year: 2025/2026

DEDICATION

I dedicate this work to:

My late mother, may Allah have mercy on her.

My father, for his sacrifices, guidance, and unwavering support.

My wife, for her continuous support, patience, and encouragement.

My daughter, who is a constant source of inspiration, hope, and strength.

My siblings, for their support and the strong bond that unites us.

ACKNOWLEDGEMENTS

First and foremost, I would like to thank Allah for granting me the strength, patience, and determination to complete this work.

With deep gratitude, I would like to express my sincere appreciation to my supervisor, Professor Mabrouk MEFLAH, for his continuous guidance, valuable support, and constant encouragement throughout my doctoral studies.

I would especially like to express my deepest gratitude to my co-supervisor, Professor Nouria ARAR, for her exceptional support, continuous encouragement, and invaluable guidance throughout this work. I am profoundly grateful for the considerable time and effort he devoted to reviewing my research, discussing my ideas, and providing insightful remarks and constructive suggestions.

I am honored to express my sincere gratitude to the members of the examination committee: Prof. Djamel Ahmed CHACHA, as Chair, and Prof. Ibrahim TALLAB, Prof. Abdelkader AMARA, Dr. Chahrazade MATMAT, and Prof. Ammar YOUKANA as Examiners, for the honor they have given me by evaluating this thesis.

I would also like to thank the members of the Laboratory of Applied Mathematics (LMA) for their support and encouragement.

Finally, my deepest gratitude goes to my family and friends for their patience, unconditional support, and unwavering belief in me. Their encouragement has been a constant source of strength and motivation throughout this journey.

TABLE OF CONTENTS

LIST OF FIGURES

LIST OF TABLES

ABSTRACT

In this work, we present a comprehensive study of the homotopy method and its numerical extensions for solving both classical and fractional nonlinear differential equations. After establishing the theoretical foundations of the Homotopy Analysis Method (HAM), we applied it to various nonlinear problems, including the Burgers equation and another nonlinear model, to illustrate its accuracy and robustness. Subsequently, we developed the Spectral Homotopy Analysis Method (SHAM), which combines the analytical power of HAM with the numerical precision of spectral techniques. The SHAM was first implemented using Chebyshev polynomials to solve the Duffing and Van der Pol equations. Then, an improved version employing Chelyshkov polynomials was proposed and successfully applied to the Lane–Emden equation, marking the first use of these polynomials within this framework. Finally, the method was extended to the fractional case and tested on the fractional Duffing equation, demonstrating SHAM's ability to effectively handle fractional-order derivatives and strong nonlinearities simultaneously. The obtained numerical results show excellent agreement with analytical solutions, fast convergence, and high numerical stability. These findings confirm the efficiency, flexibility, and accuracy of the HAM and SHAM approaches in addressing a wide range of nonlinear differential problems.

Keywords: Nonlinear equations; Homotopy analysis method; Spectral homotopy analysis method; Chebyshev polynomials; Chelyshkov polynomials.

RÉSUMÉ

Dans ce travail, nous présentons une étude complète de la méthode d'homotopie et de ses extensions numériques pour la résolution des équations différentielles non linéaires classiques et fractionnaires. Après avoir établi les fondements théoriques de la Méthode d'Analyse par Homotopie (HAM), celle-ci a été appliquée à divers problèmes non linéaires, notamment à l'équation de Burgers et à un autre modèle non linéaire, afin d'illustrer sa précision et sa robustesse. Par la suite, nous avons développé la Méthode Spectrale d'Analyse par Homotopie (SHAM), qui combine la puissance analytique de la HAM avec la précision numérique des techniques spectrales. La SHAM a d'abord été mise en œuvre à laide des polynômes de Chebyshev pour résoudre les équations de Duffing et de Van der Pol. Ensuite, une version améliorée utilisant les polynômes de Chelyshkov a été proposée et appliquée avec succès à l'équation de Lane–Emden, marquant la première utilisation de ces polynômes dans ce cadre. Enfin, la méthode a été étendue au cas fractionnaire et testée sur l'équation de Duffing fractionnaire, démontrant la capacité de la SHAM à traiter simultanément les dérivées d'ordre fractionnaire et les non-linéarités fortes. Les résultats numériques obtenus montrent un excellent accord avec les solutions analytiques, une convergence rapide et une grande stabilité numérique. Ces résultats confirment l'efficacité, la flexibilité et la précision des approches HAM et SHAM dans le traitement d'une grande variété de problèmes différentiels non linéaires.

Mots-clés : Équations non linéaires ; Méthode d'analyse homotopique ; Méthode d'analyse homotopique spectrale ; Polynômes de Chebyshev ; Polynômes de Chelyshkov.

ملخص

في هذا العمل، نقدم دراسة شاملة لطريقة **الهوموتوبي** وامتداداتها العددية لحل المعادلات التفاضلية غير الخطية الكلاسيكية والكسرية.
بعد عرض الأسس النظرية **لطريقة التحليل بالهوموتوبي**، قمنا بتطبيقها على عدد من المسائل غير الخطية، بما في ذلك معادلة **بيرغرز** ومعادلة غير خطية أخرى، لإبراز دقتها وفعاليتها.

بعد ذلك، طورنا **طريقة التحليل الطيفي بالهوموتوبي**، التي تجمع بين القوة التحليلية **لطريقة التحليل بالهوموتوبي** والدقة العددية للطرق الطيفية. وقد تم تطبيق هذه الطريقة أولا باستخدام كثيرات حدود **تشيبيشيف** لحل معادلات **دافينغ** و**فان دير بول** .ثم تم اقتراح نسخة محسّنة تعتمد على كثيرات حدود **تشيليشكوف** وتطبيقها بنجاح على معادلة **لين–إمدن**، لتكون هذه أول مرة تستخدم فيها هذه كثيرات الحدود ضمن هذا الإطار.

وأخيرا، تم تعميم الطريقة إلى الحالة الكسرية وتطبيقها على معادلة **دافينغ** الكسرية، مما أظهر قدرة **طريقة التحليل الطيفي بالهوموتوبي** على التعامل بفعالية مع المشتقات ذات الرتبة الكسرية واللاخطيات القوية في الوقت نفسه.

النتائج العددية المتحصّل عليها أظهرت توافقا ممتازا مع الحلول التحليلية، وسرعة في التقارب، واستقرارا عدديا عاليا.
وتؤكد هذه النتائج كفاءة ومرونة ودقة طريقتي **التحليل بالهوموتوبي** و **التحليل الطيفي بالهوموتوبي** في معالجة طيف واسع من المعادلات التفاضلية غير الخطية.

الكلمات المفتاحية: المعادلات غير الخطية؛ طريقة التحليل بالهوموتوبي؛ طريقة التحليل الطيفي بالهوموتوبي ؛ متعددات حدود تشيبيشيف؛ متعددات حدود تشيليشكوف.

FOUNDATIONAL INTRODUCTION

Nonlinear differential equations play a fundamental role in modeling a wide range of complex physical, biological, and engineering phenomena, including oscillatory systems, fluid dynamics, astrophysical models, and chemical processes. However, the inherent nonlinearity of these equations often makes obtaining exact analytical solutions nearly impossible, motivating the development of numerous numerical and semi-analytical techniques to achieve high-accuracy approximations. Among these approaches, methods such as the Adomian Decomposition Method (ADM) [12], the Variational Iteration Method (VIM) [51], Runge-Kutta method [10], the Homotopy Perturbation Method (HPM) [16, 48], and particularly the Homotopy Analysis Method (HAM) [25] have proven to be remarkably effective in tackling nonlinear problems. The *Homotopy Analysis Method* (HAM), introduced by Liao [28, 32], is a powerful semi-analytical technique inspired by the *homotopy concept in topology* [17, 45], which constructs a continuous deformation between a simple solvable problem and the original nonlinear one using an embedding parameter $p \in [0, 1]$. Unlike traditional perturbation methods that rely on small parameters, HAM provides a flexible framework capable of handling strongly nonlinear systems without such restrictions. One of its most notable features is the convergence-control parameter ς, which allows direct regulation of convergence speed and stability of the series solution.

In the theoretical part of this work, we present a comprehensive and detailed exposition of the HAM, including its mathematical formulation, deformation equations, convergence analysis, and error estimation. This theoretical foundation not only clarifies the analytical power of the method but also establishes a solid basis for its extension toward spectral-based frame-

works that significantly enhance computational efficiency and numerical accuracy.

Spectral methods are known for their *exponential convergence* and exceptional precision when applied to smooth problems [4, 5, 18, 23, 24, 35]. They approximate the unknown function as a truncated series of orthogonal polynomials such as Chebyshev[9], Legendre, or Chelyshkov [11, 14] polynomials. Through their matrix formulation, differential operators can be represented as derivative matrices, simplifying computation, preserving stability, and allowing highly accurate enforcement of boundary conditions. Due to their superior accuracy and efficiency, spectral methods have become indispensable tools in modern numerical analysis [4, 5, 18, 24]. Building upon this theoretical foundation, we first applied the HAM to two classical nonlinear differential equations, namely the *Burgers equation* and another nonlinear model, to verify its flexibility and robustness in treating a variety of nonlinearities. Subsequently, the study extends toward the *Spectral Homotopy Analysis Method (SHAM)* proposed by Motsa et al. [38], which combines the analytical versatility of HAM [13, 28, 32, 39] with the numerical precision of spectral techniques. In this work, SHAM was initially applied using *Chebyshev polynomials* to solve the *Duffing* and *Van der Pol* equations. The obtained results demonstrated excellent agreement with analytical solutions and rapid convergence behavior. To further extend the approach, we employed *Chelyshkov polynomials* as spectral basis functions within the SHAM framework representing the first application of SHAM using these polynomials and applied it to the *Lane-Emden equation*, a fundamental model in astrophysics. This adaptation highlighted the method's flexibility and its ability to handle different spectral bases while maintaining high accuracy and stability.

Finally, the SHAM was generalized to fractional systems and successfully applied to the *fractional Duffing equation* as an illustrative example. This generalization demonstrated the method's capability to handle both fractional derivatives and strong nonlinearities simultaneously, confirming its effectiveness as a unified framework for solving a wide class of nonlinear problems. Overall, the numerical results confirm that both HAM and SHAM exhibit *high precision, strong convergence behavior, and excellent computational efficiency*. The combination of the homotopy deformation concept with spectral representations provides a powerful and reliable framework for solving nonlinear both classical and fractional differential equations with superior accuracy and stability.

The remainder of this dissertation is organized as follows: Chapter 1 provides a set of essential mathematical preliminaries, including the definitions and properties of fractional deriva-

tives and integrals, along with an overview of Chebyshev and Chelyshkov polynomials and their corresponding matrix formulations. Chapter 2 is devoted to the theoretical study of the *Homotopy Analysis Method* (HAM), presenting its mathematical foundations, construction of deformation equations, convergence-control mechanisms, and practical implementation strategies. Chapter 3 introduces the *Spectral Homotopy Analysis Method* (SHAM) based on Chebyshev polynomials and illustrates its application to nonlinear equations such as the Duffing and Van der Pol models. The results presented in this chapter are in fact the subject of an article [6] published in a renowned international scientific journal. Chapter 4 extends the SHAM formulation by employing Chelyshkov polynomials as spectral basis functions and applies it to the Lane-Emden equation, marking the first integration of these polynomials into the SHAM framework. The results presented in this chapter are in fact the subject of an article [7] published in a renowned international scientific journal. Finally, Chapter 5 generalizes the SHAM approach to fractional-order systems, with the fractional Duffing equation serving as a representative example, demonstrating the method's robustness and adaptability in handling fractional nonlinear dynamics. A general conclusion summarizes the key findings and highlights potential directions for future research.

Chapter 1

Preliminaries

CHAPTER 1

PRELIMINARIES

1.1 Some elements of functional analysis

Definition 1.1. *[22] Let Ω be a finite or infinite interval of the real axis $\mathbb{R}$. We denote by $L^p(\Omega)$, for $1 \leq p \leq \infty$, the set of all Lebesgue measurable complex-valued functions f defined on Ω such that $\|f\|_p < \infty$, where*

$$\|f\|_p = \left(\int_\Omega |f(t)|^p \, dt \right)^{1/p}, \qquad 1 \leq p < \infty,$$

and

$$\|f\|_\infty = \operatorname*{ess\,sup}_{x \in \Omega} |f(x)|.$$

Here, $\operatorname{ess\,sup}$ *denotes the essential supremum of $|f(x)|$.*

Definition 1.2. *[22] Let Ω be a finite or infinite interval of the real axis $\mathbb{R}$, and let $n \in \mathbb{N}$. We denote by $C^n(\Omega)$ the space of all functions f that are n times continuously differentiable on Ω, endowed with the norm*

$$\|f\|_{C^n} = \sum_{k=0}^{n} \|f^{(k)}\|_C = \sum_{k=0}^{n} \sup_{x \in \Omega} |f^{(k)}(x)|.$$

In particular, for $n = 0$, we have $C^0(\Omega) \equiv C(\Omega)$, the space of continuous functions on Ω,

with the norm

$$\|f\|_C = \sup_{x\in\Omega} |f(x)|.$$

1.2 Fractional calculus

We begin this section by introducing fundamental definitions related to fractional integration and differentiation, which form the core of fractional calculus, as detailed in [22, 41, 44].

1.2.1 The Gamma function

The Euler Gamma function is a fundamental function in fractional calculus. It generalizes the factorial $n!$ and allows n to take real or even complex values.

Definition 1.3. *[22] The Gamma function is defined by the integral:*

$$\Gamma(z) = \int_0^\infty t^{z-1}e^{-t}\,dt, \quad \textit{for } \Re(z) > 0. \tag{1.1}$$

By integration by parts, we obtain the recurrence relation:

$$\Gamma(z+1) = z\Gamma(z), \quad \Re(z) > 0. \tag{1.2}$$

In particular, for all $n \in \mathbb{N}$:

$$\Gamma(n+1) = n!. \tag{1.3}$$

1.2.2 The Beta function

The Beta function is another essential function in fractional calculus. It plays an important role, particularly in combination with the Gamma function.

Definition 1.4. *[22] The Beta function is defined by:*

$$B(z,w) = \int_0^1 t^{z-1}(1-t)^{w-1}\,dt, \quad \Re(z) > 0,\ \Re(w) > 0. \tag{1.4}$$

Relation between Beta and Gamma functions

The Beta and Gamma functions are related by the identity:

$$B(z,w) = \frac{\Gamma(z)\Gamma(w)}{\Gamma(z+w)}. \tag{1.5}$$

This implies the symmetry property:

$$B(z,w) = B(w,z).$$

Definition 1.5. *[22] [Riemann-Liouville fractional integral] Let $f \in L^1[a,b]$ and let $\alpha > 0$. The Riemann–Liouville fractional integral of order α is defined as:*

$$J_a^\alpha f(x) = \frac{1}{\Gamma(\alpha)} \int_a^x (x-t)^{\alpha-1} f(t)\, dt, \tag{1.6}$$

where $\Gamma(\cdot)$ denotes the Gamma function. When α tends to 0, this operator becomes the identity: $\lim_{\alpha\to 0} J_a^\alpha f(x) = f(x)$.

Definition 1.6. *[22] [Caputo fractional derivative] The Caputo derivative of order α, where $n = \lceil \alpha \rceil$, is given by:*

$$D^\alpha f(x) = \frac{1}{\Gamma(n-\alpha)} \int_0^x (x-t)^{n-\alpha-1} f^{(n)}(t)\, dt, \tag{1.7}$$

where $f^{(n)}$ denotes the n-th order derivative of f, and $\lceil \alpha \rceil$ denotes the smallest integer greater than or equal to α.

This form of the fractional derivative satisfies the following identity for monomials x^k, with $k \in \mathbb{N}_0$:

$$D^\alpha x^k = \begin{cases} 0, & \text{if } k < \lceil \alpha \rceil, \\ \frac{\Gamma(k+1)}{\Gamma(k-\alpha+1)} x^{k-\alpha}, & \text{if } k \geq \lceil \alpha \rceil. \end{cases} \tag{1.8}$$

1.3 Chebyshev polynomials

Chebyshev polynomials of the first kind are defined over the interval $[-1,1]$ by the expression:

$$\mathcal{T}_m(\eta) = \cos\left(m \cos^{-1}(\eta)\right). \tag{1.9}$$

They can also be generated recursively using the following relations:

$$\mathcal{T}_0(\eta) = 1, \quad \mathcal{T}_1(\eta) = \eta, \quad \mathcal{T}_{m+1}(\eta) = 2\eta\mathcal{T}_m(\eta) - \mathcal{T}_{m-1}(\eta), \quad m = 1, 2, \ldots \tag{1.10}$$

An explicit representation of $T_p(\eta)$ as a polynomial in η is given by:

$$\mathcal{T}_m(\eta) = \sum_{i=0}^{\lfloor m/2 \rfloor} \left[(-1)^i \sum_{r=i}^{\lfloor m/2 \rfloor} \binom{m}{2r} \binom{r}{i} \right] \eta^{m-2i}, \tag{1.11}$$

where $\lfloor m/2 \rfloor$ denotes the greatest integer less than or equal to $m/2$. Alternatively, the Chebyshev polynomial can be expressed in the form:

$$\mathcal{T}_m(\eta) = \sum_{i=0}^{\lfloor m/2 \rfloor} c_i^{(m)} \eta^{m-2i}, \tag{1.12}$$

with the coefficients defined as:

$$c_i^{(m)} = (-1)^i 2^{m-2i-1} \cdot \frac{m}{m-i} \binom{m-i}{i}. \tag{1.13}$$

The inverse relation of Equation (1.11) is given by:

$$\eta^m = 2^{1-m} \sum_{i=0}^{\lfloor m/2 \rfloor}{}' \binom{m}{i} \mathcal{T}_{m-2i}(\eta), \tag{1.14}$$

where the prime on the summation indicates that the final term should be halved when m is even and $i = m/2$. The first derivative of the Chebyshev polynomial $\mathcal{T}_m(\eta)$ can be written as:

$$\frac{d}{d\eta}\mathcal{T}_m(\eta) = 2m \sum_{\substack{i=0 \\ m-i \text{ even}}}^{m-1}{}' \mathcal{T}_i(\eta), \tag{1.15}$$

and the second derivative is given by:

$$\frac{d^2}{d\eta^2}\mathcal{T}_m(\eta) = \sum_{\substack{i=0 \\ m-i \text{ even}}}^{m-2} m(m-i)(m+i)\mathcal{T}_i(\eta). \tag{1.16}$$

For detailed derivations and properties, refer to [34, 42].

In our numerical method, we discretize the interval $[-1, 1]$ using $(N + 1)$ Gauss-Lobatto

collocation points defined as:

$$\eta_m = \cos\left(\frac{m\pi}{N}\right), \quad m = 0, 1, \ldots, N. \tag{1.17}$$

If the function $\mathcal{Y}$ belongs to $\mathbb{L}^2[-1, 1]$, its truncated Chebyshev series expansion at the collocation points is given by:

$$\mathcal{Y}(\eta_m) = \sum_{i=0}^{N} a_i \mathcal{T}_i(\eta_m), \quad m = 0, 1, \ldots, N, \tag{1.18}$$

where the Chebyshev coefficients a_i are computed as:

$$a_i = \frac{2}{\pi\gamma_i} \int_{-1}^{1} \frac{\mathcal{Y}(\eta)\mathcal{T}_i(\eta)}{\sqrt{1-\eta^2}} d\eta, \quad \gamma_i = \begin{cases} 2, & i = 0, \\ 1, & i \geq 1. \end{cases} \tag{1.19}$$

To apply the spectral method on a general interval $[a, b]$, we transform the variable η using the linear mapping:

$$t = \frac{(b-a)\eta}{2} + \frac{(b+a)}{2}, \quad t \in [a, b]. \tag{1.20}$$

The derivative of $\mathcal{Y}$ at the collocation points is then approximated by:

$$\frac{d\mathcal{Y}}{d\eta} = \sum_{i=0}^{N} \mathbf{D}_{im} \mathcal{Y}(\eta_m) = \mathbf{DY}, \quad \mathbf{D} = \frac{2}{b-a} D, \tag{1.21}$$

where $D = (D_{im})$ is the Chebyshev differentiation matrix, defined as follows:

$$D_{im} = \begin{cases} \frac{\chi_m}{\chi_i} \cdot \frac{(-1)^{m+i}}{\eta_m - \eta_i}, & i \neq m, \\ -\frac{\eta_i}{2(1-\eta_i^2)}, & 1 \leq i = m \leq N-1, \\ \frac{2N^2+1}{6}, & i = m = 0, \\ -\frac{2N^2+1}{6}, & i = m = N. \end{cases} \tag{1.22}$$

Here, the weights χ_i are defined by:

$$\chi_i = \begin{cases} 2, & i = 0, N, \\ 1, & 1 \leq i \leq N-1. \end{cases} \tag{1.23}$$

The vector $\mathbf{Y}$ holds the values of the function $\mathcal{Y}$ evaluated at the collocation nodes:

$$\mathbf{Y} = (\mathcal{Y}(\eta_0), \mathcal{Y}(\eta_1), \ldots, \mathcal{Y}(\eta_N))^T. \tag{1.24}$$

Higher-order derivatives are obtained by raising the matrix $\mathbf{D}$ to the corresponding power:

$$\frac{d^k \mathcal{Y}}{d\eta^k} = \mathbf{D}^k \mathbf{Y}, \quad k \geq 1. \tag{1.25}$$

1.4 Chelyshkov polynomials

To lay the groundwork for this study, we first revisit essential definitions and foundational principles related to the Chelyshkov function, highlighting several results that play a crucial role in our analysis. The Chelyshkov polynomials, recently developed by Chelyshkov, form an orthogonal set over the interval $[0, 1]$ and are given explicitly by

$$C_{N,i}(t) = \sum_{s=0}^{N-i} (-1)^s \binom{N-i}{s} \binom{N+i+s+1}{N-i} t^{i+s}, \quad i = 0, 1, \cdots, N. \tag{1.26}$$

This yields the Rodrigues' type representation,

$$C_{N,i}(t) = \frac{1}{(N-i)! t^{i+1}} \frac{\mathrm{d}^{N-i}}{t\, \mathrm{d}^{N-i}} \left(t^{N+i+1} (1-t)^{N-i} \right), \quad i = 0, 1, \cdots, N$$

The Chelyshkov polynomials meets the following orthogonality condition

$$\int_0^1 C_{N,r}(t) C_{N,s}(t) \mathrm{dt} = \begin{cases} \frac{1}{r+s+1}, & \text{for } r = s, \\ 0, & \text{for } r \neq s \end{cases} \qquad r, s = 0, 1, \cdots, N. \tag{1.27}$$

Chelyshkov polynomials $C_{Ni}(t)$ offer a natural approach for solving, expanding, and interpreting solutions. Actually, these polynomials can be expressed in terms of the Jacobi polynomials $P_k^{(\alpha,\beta)}$ by the following relation

$$C_{N,i}(t) = t^i P_{N-i}^{2i,1}(1-2t), \quad i = 0, 1 \cdots, N.$$

Consider a function $y(t)$, square-integrable over the interval $[0, 1]$, which can be represented using Chelyshkov polynomials as

$$y(t)|_{t_j} \approx y_N(t_j) = \sum_{i=0}^{N} e_i C_{N,i}(t_j) \quad j = 0, 1, \ldots, N. \tag{1.28}$$

Also,

$$\begin{aligned} y'_N(t_j) &= \sum_{i=0}^{N} e_i C'_{N,i}(t_j) \\ y''_N(t_j) &= \sum_{i=0}^{N} e_i C''_{N,i}(t_j), \\ &\vdots \\ y_N^{(m)}(t_j) &= \sum_{i=0}^{N} e_i C_{N,i}^{(m)}(t_j), \quad j = 0, 1, \ldots, N, m = 3, 4, ... \end{aligned} \tag{1.29}$$

where e_i are the unknown coefficients, $C_{N,i}, \quad i = 0, 1, \cdots, N$ represent the Chelyshkov orthogonal polynomials of degree N (with N=2,3,...), and $t_0, t_1, \ldots, t_N$ are the Gauss-Lobatto collocation points, expressed as

$$t_j = \frac{1 + \cos\left(\frac{\pi j}{N}\right)}{2}, \quad j = 0, 1, \ldots, N. \tag{1.30}$$

1.4.1 Operational matrix for the fractional derivative

The derivative of the Chelyshkov polynomial vector $C(x)$ can be represented using an operational matrix as follows:

$$\frac{dC(x)}{dx} = D^{(1)} C(x) = \mathbf{C} D^{(1)} \mathbf{X}, \tag{1.31}$$

where

$$D^{(1)} = \begin{pmatrix} 0 & 1 & 0 & \cdots & 0 \\ 0 & 0 & 2 & \cdots & 0 \\ 0 & 0 & 0 & \ddots & \vdots \\ \vdots & \vdots & \vdots & \ddots & N \\ 0 & 0 & 0 & \cdots & 0 \end{pmatrix}_{(N+1)\times(N+1)}, \quad \mathbf{X} = \begin{bmatrix} 1 \\ x \\ x^2 \\ \vdots \\ x^N \end{bmatrix},$$

If N is odd, from (1.26) and (1.27), we have

$$\mathbf{C} = \begin{pmatrix} \binom{N}{0}\binom{N+1}{N} & 0 & \cdots & 0 & 0 \\ -\binom{N}{1}\binom{N+2}{N} & \binom{N-1}{0}\binom{N+2}{N-1} & \cdots & 0 & 0 \\ \vdots & \vdots & \ddots & \vdots & \vdots \\ \binom{N}{N-1}\binom{2N}{N} & -\binom{N-1}{N-2}\binom{2N}{N-1} & \cdots & \binom{1}{0}\binom{2}{N} & 0 \\ -\binom{N}{N}\binom{2N+1}{N} & \binom{N-1}{N-1}\binom{2N+1}{N-1} & \cdots & -\binom{1}{1}\binom{2N+1}{1} & 1 \end{pmatrix}_{(N+1)\times(N+1)}.$$

If N is even, then

$$\mathbf{C} = \begin{pmatrix} \binom{N}{0}\binom{N+1}{N} & 0 & \cdots & 0 & 0 \\ -\binom{N}{1}\binom{N+2}{N} & \binom{N-1}{0}\binom{N+2}{N-1} & \cdots & 0 & 0 \\ \vdots & \vdots & \ddots & \vdots & \vdots \\ -\binom{N}{N-1}\binom{2N}{N} & \binom{N-1}{N-2}\binom{2N}{N-1} & \cdots & \binom{1}{0}\binom{2}{N} & 0 \\ \binom{N}{N}\binom{2N+1}{N} & -\binom{N-1}{N-1}\binom{2N+1}{N-1} & \cdots & -\binom{1}{1}\binom{2N+1}{1} & 1 \end{pmatrix}_{(N+1)\times(N+1)}.$$

The higher-order derivatives are computed using powers of $D^{(1)}$:

$$\frac{d^m C(x)}{dx^m} = \left(D^{(1)}\right)^m C(x), \quad m \in \mathbb{N}_0, \tag{1.32}$$

which implies:

$$D^{(m)} = \left(D^{(1)}\right)^m, \quad m = 1, 2, \ldots \tag{1.33}$$

Theorem 1.1. *[47] Let $C(x)$ denote the Chelyshkov polynomial vector, and let $\alpha \in \mathbb{R}^+$. Then, the Caputo fractional derivative of $C(x)$ can be approximated as:*

$$D^\alpha C(x) \approx D^{(\alpha)} C(x), \tag{1.34}$$

where $D^{(\alpha)}$ is the $(N+1)\times(N+1)$ matrix defined by:

$$D^{(\alpha)} = \begin{pmatrix} \lambda_{0,0}^{\alpha} & \lambda_{0,1}^{\alpha} & \cdots & \lambda_{0,N}^{\alpha} \\ \lambda_{1,0}^{\alpha} & \lambda_{1,1}^{\alpha} & \cdots & \lambda_{1,N}^{\alpha} \\ \vdots & \vdots & \ddots & \vdots \\ \lambda_{N,0}^{\alpha} & \lambda_{N,1}^{\alpha} & \cdots & \lambda_{N,N}^{\alpha} \end{pmatrix}, \tag{1.35}$$

with each element given by:

$$\lambda_{n,l}^{\alpha} = \sum_{j=\lceil\alpha\rceil}^{N} (-1)^{j-n} \binom{N-n}{j-n} \binom{N+j+1}{N-n} \frac{\Gamma(j+1)}{\Gamma(j+1-\alpha)} d_{l,j}, \quad n,l = 0,1,\ldots,N. \tag{1.36}$$

with the coefficients $d_{l,j}$ obtained as:

$$d_{l,j} = (2l+1)\int_0^1 x^{j-\alpha} C_{N,l}(x)\,dx. \tag{1.37}$$

Proof. Starting from the definition of Chelyshkov polynomials, we express the Caputo fractional derivative of $C_{N,n}(x)$ as:

$$D^{\alpha} C_{N,n}(x) = \sum_{j=n}^{N} (-1)^{j-n} \binom{N-n}{j-n} \binom{N+n+j+1}{N-n} \frac{\Gamma(j+1)}{\Gamma(j+1-\alpha)} x^{j-\alpha}. \tag{1.38}$$

To approximate $x^{j-\alpha}$ in the Chelyshkov polynomial basis, we write:

$$x^{j-\alpha} \approx \sum_{l=0}^{N} d_{l,j} C_{N,l}(x), \tag{1.39}$$

where

$$\begin{aligned} d_{l,j} &= (2l+1)\int_0^1 x^{j-\alpha} C_{N,l}(x)\,dx \\ &= \sum_{s=0}^{N-l} (-1)^s \binom{N-l}{s} \binom{N+l+s+1}{N-l} \frac{2l+1}{j-\alpha+l+s+1}. \end{aligned} \tag{1.40}$$

Substituting this expansion into the fractional derivative expression yields:

$$D^{\alpha} C_{N,n}(x) \approx \sum_{j=\lceil\alpha\rceil}^{N} \sum_{l=0}^{N} (-1)^{j-n} \binom{N-n}{j-n} \binom{N+j+1}{N-n} \frac{\Gamma(j+1)}{\Gamma(j+1-\alpha)} d_{l,j} C_{N,l}(x). \tag{1.41}$$

This leads to the approximation:

$$D^{\alpha} C_{N,n}(x) \approx \sum_{l=0}^{N} \lambda_{n,l}^{\alpha} C_{N,l}(x), \tag{1.42}$$

and in vector notation, this can be compactly expressed as:

$$D^{\alpha} C_{N,n}(x) \approx \left[\lambda_{n,0}^{\alpha}, \lambda_{n,1}^{\alpha}, \ldots, \lambda_{n,N}^{\alpha}\right] C(x), \quad n = 0, \ldots, N. \tag{1.43}$$

□

Remark . *When $\alpha = m \in \mathbb{N}$, the above formulation reduces to the classical derivative case as shown in* (1.32).

Chapter 2

Homotopy analysis method

CHAPTER 2

HOMOTOPY ANALYSIS METHOD

The **homotopy analysis method (HAM)**, initially developed by Liao in 1992 [31], is based on the application of homotopy [17], a key concept from topology [45], to construct analytic approximations for nonlinear differential equations. To solve a general nonlinear differential equation of the form

$$\mathcal{M}[u(x,t)] = 0, \quad x \in \Omega \times \mathbb{R}^+, \tag{2.1}$$

where $\mathcal{M}$ is a nonlinear operator, x denotes an independent variable within the domain Ω, t denotes the temporal independent variable and $u(x,t)$ is the unknown function, respectivelly, Liao constructed a one-parameter family of equations parameterized by an embedding parameter $p \in [0,1]$. This formulation, known as the *zeroth-order deformation equation*, is given by

$$(1-p)\mathscr{A}[\phi(x,t;p) - u_0(x,t)] + p\mathcal{M}[\phi(x,t;p)] = 0, \quad (x,t) \in \Omega \times \mathbb{R}^+, \quad p \in [0,1], \tag{2.2}$$

where $\mathscr{A}$ is an auxiliary linear operator and $u_0(x,t)$ is an initial guess for the solution $u(x,t)$, and $\phi(x,t;p)$ is an unknown function. The homotopy-based approach offers freedom to choose both the auxiliary linear operator $\mathscr{A}$ and the initial guess $u_0(x,t)$. At the endpoints of the embedding parameter, the solution satisfies $\phi(x,t;0) = u_0(x,t)$ and $\phi(x,t;1) = u(x,t)$.

Assuming $\phi(x,t;p)$ is analytic in p, it can be expanded as

$$\phi(x,t;p) = u_0(x,t) + \sum_{s=1}^{\infty} u_s(x,t)p^s. \tag{2.3}$$

where

$$u_s = \frac{1}{s!}\frac{\partial^s \phi(x,t;p)}{\partial p^s}|_{p=0}. \tag{2.4}$$

If this series converges at $p = 1$, the resulting *homotopy-series solution*

$$u(x,t) = u_0(x,t) + \sum_{s=1}^{\infty} u_s(x,t) \tag{2.5}$$

satisfies the original nonlinear equation $\mathcal{M}[u(x,t)] = 0$, as rigorously proved by Liao [27, 28]. Each term $u_s(x,t)$ is obtained from a linear differential equation related to the auxiliary operator $\mathscr{A}$, which is generally easier to solve than the original nonlinear problem, provided appropriate choices of $\mathscr{A}$ and $u_0(x,t)$. Nevertheless, the original homotopy-analysis method did not always guarantee convergence of the series solution. To overcome this, Liao [26] introduced an auxiliary convergence-control parameter ς, thereby generalizing the zeroth-order deformation equation to

$$(1-p)\mathscr{A}[\phi(x,t;p) - u_0(x,t)] = \varsigma p \mathcal{M}[\phi(x,t;p)], \quad x \in \Omega \times \mathbb{R}^+, \quad p \in [0,1]. \tag{2.6}$$

This additional parameter ς allows adjustment and control of the convergence region and rate of the homotopy-series solution. Although ς has no physical meaning, it provides an extra degree of freedom that significantly improves the methods convergence properties. As a result, ς is now commonly referred to as the *convergence-control parameter*. Assuming that $\mathscr{A}$, $u_0(t)$, and ς are appropriately chosen to ensure the series (2.5) converges, which satisfies the original equation (2.1). For more details, see [28].

By differentiating (2.6) s times with respect to p, then dividing by $s!$ and setting $p = 0$, we derive the high-order deformation equation

$$\mathscr{A}(u_s(x,t) - \chi_s u_{s-1}(x,t)) = \varsigma \mathscr{R}_s(u_0, u_1, \ldots, u_{s-1}), \tag{2.7}$$

where

$$\mathscr{R}_s(u_0, u_1, \ldots, u_{s-1}) = \frac{1}{(s-1)!}\frac{\partial^{s-1}\mathcal{M}(\phi(x,t;p))}{\partial p^{s-1}}|_{p=0} \tag{2.8}$$

and

$$\chi_s = \begin{cases} 0 \quad , & s \leq 1, \\ 1 \quad , & s > 1. \end{cases} \tag{2.9}$$

An M^{th}-order approximate analytic solution of practical interest is given by truncating the homotopy series (2.5):

$$u_M(x,t) = u_0(x,t) + \sum_{k=1}^{M} u_k(x,t), \tag{2.10}$$

and the exact solution is given by the limit:

$$u(x,t) = \lim_{M \to \infty} u_M(x,t). \tag{2.11}$$

It should be reminded that the homotopy terms $u_1(x,t), u_2(x,t), \ldots, u_k(x,t)$ strongly depend on both the physical variable (x,t) and the convergence control parameter ς.

Definition 2.1. *[32] Let ϕ be a function of the homotopy-parameter p, then*

$$\mathfrak{D}_s(\phi) = \frac{1}{s!} \frac{d^s \phi}{dp^s}\bigg|_{p=0}$$

is called the m^{th}-order homotopy-derivative of ϕ, where $s \geq 0$ is an integer, and $\mathfrak{D}_s$ is called the operator of the m^{th}-order homotopy-derivative.

Theorem 2.1. *[32, 36] For two arbitrary homotopy-Maclaurin series*

$$\phi = \sum_{k=0}^{+\infty} u_k p^k, \quad \psi = \sum_{k=0}^{+\infty} w_k p^k$$

where ϕ and ψ are analytic in $p \in [0, a)$, it holds

$$\begin{aligned} &(a)\mathfrak{D}_s(\phi) = u_s, \\ &(b)\mathfrak{D}_s\left(p^k \phi\right) = \mathfrak{D}_{s-k}(\phi) = \begin{cases} u_{s-k}, & \text{when } 0 \leq k \leq s, \\ 0, & \text{otherwise}, \end{cases} \\ &(c)\mathfrak{D}_s(\phi\psi) = \textstyle\sum_{k=0}^{s} u_k w_{s-k} = \sum_{k=0}^{s} u_{s-k} w_k. \end{aligned}$$

Theorem 2.2. *[32, 36] For an arbitrary homotopy-Maclaurin series*

$$\phi = \sum_{k=0}^{+\infty} u_k p^k,$$

it holds,

$$\mathfrak{D}_s\left(\phi^{\sigma}\right)=\sum_{k_1=0}^{s}u_{s-k_1}\sum_{k_2=0}^{k_1}u_{k_1-k_2}\sum_{k_3=0}^{k_2}u_{k_2-k_3}\cdots\sum_{k_{\sigma-1}=0}^{k_{\sigma-2}}u_{k_{\sigma-2}-k_{\sigma-1}}u_{k_{\sigma-1}},$$

where $s\geq 0$ and $\sigma\geq 2$ are positive integer.

Theorem 2.3. *[32] If $\phi=\sum_{k=0}^{+\infty}u_kp^k$ and $\psi=\sum_{k=0}^{+\infty}w_kp^k$ are two homotopy-Maclaurin series, where ϕ and ψ are analytic in $p\in[0,a)$. f and g are independent of the homotopy-parameter $p\in[0,1]$, then it holds*

$$\mathfrak{D}_s(f\phi+g\psi)=f\mathfrak{D}_s(\phi)+g\mathfrak{D}_s(\psi)=fu_s+gw_s$$

Theorem 2.4. *[32] Let $\mathscr{A}$ denote a linear operator independent of the homotopy-parameter $p\in[0,1]$. For two homotopy-Maclawin series*

$$\phi=\sum_{k=0}^{+\infty}u_kp^k,\quad \psi=\sum_{k=0}^{+\infty}w_kp^k,$$

where ϕ and ψ are analytic in $p\in[0,a)$, it holds

$$\mathfrak{D}_s(\mathscr{A}\phi)=\mathscr{A}\left[\mathfrak{D}_s(\phi)\right]=\mathscr{A}u_s$$

and

$$\mathfrak{D}_s(\psi\mathscr{A}\phi)=\sum_{k=0}^{s}\mathfrak{D}_{s-k}(\psi)\mathscr{A}\left[\mathfrak{D}_k(\phi)\right]=\sum_{k=0}^{s}w_{s-k}\mathscr{A}u_k.$$

where $s\geq 0$ is an integer.

Theorem 2.5. *[32] For two homotopy-Macianin series*

$$\phi=\sum_{i=0}^{+\infty}u_ip^i,\quad \psi=\sum_{j=0}^{+\infty}w_jp^j,$$

where ϕ and ψ are analytic in $p\in[0,a)$, if $\phi=\psi$ in $p\in[0,a)$, then $u_s=w_s$ and $\mathfrak{D}_s(\phi)=\mathfrak{D}_s(\psi)$ for any integer $s\geq 0$ and a real number $a>0$.

Theorem 2.6. *[32] Let $f(\phi),g(\psi)$ denote no smooth functions. For two homotopy-Maclaurin*

series

$$\phi = \sum_{i=0}^{+\infty} u_i p^i, \quad \psi = \sum_{j=0}^{+\infty} w_j p^j,$$

if $f(\phi) = g(\psi)$ *in a domain* $p \in [0, a)$*, then*

$$\mathfrak{D}_s[f(\phi)] = \mathfrak{D}_s[g(\psi)]$$

for any integer $s \geq 0$ *and* a *real number* $a > 0$*.*

Theorem 2.7. *[32] For a homotopy-Maclaurin series*

$$\phi = \sum_{k=0}^{+\infty} u_k p^k,$$

it holds the recursion formulas

$$\begin{aligned}
\mathfrak{D}_0\left(e^{\alpha\phi}\right) &= e^{\alpha u_0}, \\
\mathfrak{D}_s\left(e^{\alpha\phi}\right) &= \alpha \sum_{k=0}^{s-1} \left(1 - \frac{k}{s}\right) \mathfrak{D}_{s-k}(\phi) \mathfrak{D}_k\left(e^{\alpha\phi}\right) \\
&= \alpha \sum_{k=0}^{s-1} \left(1 - \frac{k}{s}\right) u_{s-k} \mathfrak{D}_k\left(e^{\alpha\phi}\right),
\end{aligned}$$

where $s \geq 1$ *is an integer, and* $\alpha \neq 0$ *is independent of the homotopy-paramerer* p*.*

Theorem 2.8. *[32] For a homotopy-Maclaurin series*

$$\phi = \sum_{i=0}^{+\infty} u_k p^k,$$

it holds the recurrion formulas

$$\begin{aligned}
\mathfrak{D}_0(\sin\phi) &= \sin(u_0), \quad \mathfrak{D}_0(\cos\phi) = \cos(u_0) \\
\mathfrak{D}_s(\sin\phi) &= \sum_{s=0}^{s-1}\left(1-\frac{k}{s}\right)\mathfrak{D}_{s-k}(\phi)\mathfrak{D}_k(\cos\phi) \\
&= \sum_{k=0}^{s-1}\left(1-\frac{k}{s}\right)u_{s-k}\mathfrak{D}_k(\cos\phi) \\
\mathfrak{D}_s(\cos\phi) &= -\sum_{k=0}^{s-1}\left(1-\frac{k}{s}\right)\mathfrak{D}_{s-k}(\phi)\mathfrak{D}_k(\sin\phi) \\
&= -\sum_{k=0}^{s-1}\left(1-\frac{k}{s}\right)u_{s-k}\mathfrak{D}_k(\sin\phi)
\end{aligned}$$

where $s \geq 1$ is an integer.

Theorem 2.9. *[32] Define an operator*

$$\mathfrak{D}_s\phi = \frac{1}{s!}\frac{\partial^s\phi}{\partial p^s}.$$

For a smooth function $f \in C^\infty(a,b)$ and a homotopy-Maclaurin series

$$\phi = \sum_{k=0}^{+\infty} u_k p^k,$$

it holds

$$\mathfrak{D}_0[f(\phi)] = f(\phi), \tag{2.12}$$

$$\mathfrak{D}_s[f(\phi)] = \sum_{k=0}^{s-1}\left(1-\frac{k}{s}\right)\mathfrak{D}_{s-k}(\phi)\frac{\partial}{\partial\phi}\left\{\mathfrak{D}_k[f(\phi)]\right\}, \tag{2.13}$$

and

$$\mathfrak{D}_s[f(\phi)] = \left\{\mathfrak{D}_s[f(\phi)]\right\}\Big|_{p=0}. \tag{2.14}$$

Theorem 2.10. *[32] For a smooth function $f(u)$ and a homotopy-Maclaurin serie*

$$\phi = \sum_{k=0}^{+\infty} u_k p^k,$$

it holds

$$\mathfrak{D}_0[f(\phi)] = f(u_0), \tag{2.15}$$

$$\mathfrak{D}_s[f(\phi)] = \sum_{k=0}^{s-1} \left(1 - \frac{k}{s}\right) u_{s-k} \frac{\partial}{\partial u_0} \left\{\mathfrak{D}_k[f(\phi)]\right\}, \tag{2.16}$$

and

$$\mathfrak{D}_s[f(\phi)] = \sum_{k=0}^{s-1} \left(1 - \frac{k}{s}\right) u_{s-k} \mathfrak{D}_k\left[f'(\phi)\right], \tag{2.17}$$

for $s \geq 1$.

2.1 Convergence

Theorem 2.11. *[29] As long as the series*

$$u_0(x,t) + \sum_{s=1}^{+\infty} u_s(x,t)$$

is convergent, where $u_s(x,t)$ *is governed by the high-order deformation equation* (2.7) *under the definitions* (2.8) *and* (2.9)*, it must be a solution of quation* (2.1)*.*

Proof. [29] Let

$$S(x,t) = u_0(x,t) + \sum_{s=1}^{+\infty} u_s(x,t)$$

denote the convergent series. Using (2.7) and (2.9), we have

$$\begin{aligned}
&\varsigma \sum_{s=1}^{+\infty} \mathscr{R}_s\left(u_{s-1}, x, t\right) \\
=&\sum_{s=1}^{+\infty} \mathscr{A}\left[u_s(x,t) - \chi_s u_{s-1}(x,t)\right] \\
=&\mathscr{A}\left[\sum_{s=1}^{+\infty} u_s(x,t) - \sum_{s=1}^{+\infty} \chi_s u_{s-1}(x,t)\right] \\
=&\mathscr{A}[0] \\
=&0.
\end{aligned}$$

which gives, since $\varsigma \neq 0$,

$$\sum_{s-1}^{+\infty} \mathscr{R}_s\left(u_{s-1}, x, t\right) = 0$$

it holds

$$\sum_{s=0}^{+\infty} \frac{1}{s!} \frac{\partial^s \mathcal{M}[\phi(x,t;p)]}{\partial p^s}\bigg|_{p=0} = 0$$

In general, $\phi(x,t;p)$ does not satisfy the original nonlinear equation (2.1). Let

$$\mathcal{E}(x,t;p) = \mathcal{M}[\phi(x,t;p)]$$

denote the residual error of (2.1). Clearly,

$$\mathcal{E}(x,t;p) = 0$$

corresponds to the exact solution of the original equation (2.1). According to the above definition, the Maclaurin series of the residual error $\mathcal{E}(x,t;p)$ about the embedding parameter p is

$$\sum_{s=0}^{+\infty} \frac{p^s}{s!} \frac{\partial^s \mathcal{E}(x,t;p)}{\partial p^s}\bigg|_{p=0} = \sum_{s=0}^{+\infty} \frac{p^s}{s!} \frac{\partial^s \mathcal{M}[\phi(x,t;p)]}{\partial p^s}\bigg|_{p=0}.$$

When $p = 1$, the above expression gives,

$$\mathcal{E}(x,t;1) = \sum_{s=0}^{+\infty} \frac{1}{s!} \frac{\partial^s \mathcal{E}(x,t;p)}{\partial p^s}\bigg|_{p=0} = 0$$

This means, according to the definition of $\mathcal{E}(x,t;p)$, that we gain the exact solution of the original equation (2.1) when $p = 1$. Thus, as long as the series

$$u_0(x,t) + \sum_{s=1}^{+\infty} u_s(x,t)$$

is convergent, it must be one solution of the original equation (2.1). □

In the two theorems that follow, the function θ depends only on x.

Theorem 2.12. *[30] Suppose that Ω be a Banach space endowed with a suitable norm $\|.\|_\Omega$ (depending on the physical problem under consideration), over which the functional sequence $u_k(x)$ of (2.3) is defined for a prescribed value of ς. Assume also that the initial approximation $u_0(x)$ remains inside the ball of the solution $u(x)$ of (2.1). Taking $r \in \mathbb{R}^+$ be a constant, the following statements hold true:*

(i) For a prescribed convergence control parameter ς, if $\|u_{k+1}(x)\| \leq r \|u_k(x)\|$ for all k, provided that $0 < r < 1$, then the series solution $\phi(x,p)$ defined in (2.3) converges absolutely at $p = 1$ to $u(x)$ given by (2.5) over the domain Ω.

(ii) For a prescribed convergence control parameter ς, if $\|u_{k+1}(x)\| \geq r \|u_k(x)\|$ for all k, given some $r > 1$, then the series solution $\phi(x,p)$ defined in (2.3) diverges at $p = 1$ over the domain Ω.

Proof. [30]

(i) If $S_n(x)$ denote the sequence of partial sum of the series (2.5), it is demanded that $S_n(x)$ be a Cauchy sequence in Ω. For this purpose, the subsequent inequalities are constructed

$$\begin{aligned} \|S_{n+1}(x) - S_n(x)\| = \|u_{n+1}(x)\| &\leq r \|u_n(x)\| \\ &\leq r^2 \|u_{n-1}(x)\| \leq \cdots \leq r^{n+1} \|u_0(x)\| \end{aligned} \tag{2.18}$$

For every $m, n \in \mathbb{N}$, such that $n \geq m$, the following results in making use of (2.18) and the triangle inequality successively,

$$\begin{aligned} \|S_n(x) - S_m(x)\| &= \|(S_n(x) - S_{n-1}(x)) + \cdots + (S_{m+1}(x) - S_m(x))\| \\ &\leq \left(\frac{1 - r^{n-m}}{1 - r}\right) r^{m+1} \|u_0(x)\| \end{aligned} \tag{2.19}$$

Since by the hypothesis $0 < r < 1$, we get from (2.19)

$$\lim_{n,m \to \infty} \|S_n(x) - S_m(x)\| = 0 \tag{2.20}$$

Therefore, $S_n(x)$ is a Cauchy sequence in the Banach space Ω, which implies that the series solution (2.5) is indeed convergent. This completes the proof (i). The proof of (ii) follows from the fact that under the hypothesis supplied in (ii), there exist a number $l, l > r > 1$, so that the interval of convergence of the power series (2.3) is $|p| < \frac{1}{l} < 1$, which obviously excludes the case of $p = 1$. □

Theorem 2.13. *[30] Assume that the series solution defined in (2.5) is convergent to the solution $u(x)$ for a prescribed value of ς. If the truncated series $u_M(x)$ expressed in equation (2.10) is used as an approximation to the solution $u(x)$ of problem (2.1), then an upper bound for the error, that is, $E_M(x)$, is estimated as*

$$E_M(x) \leq \frac{r^{M+1}}{1 - r} \|u_0(x)\| \tag{2.21}$$

Proof. [30] Making use of the inequality (2.18) , we immediately obtain

$$\|u(x) - u_M(x)\| \leq \left(\frac{1 - r^{n-M}}{1 - r}\right) r^{M+1} \|u_0(x)\| \tag{2.22}$$

and taking into account the constraint $\left(1 - r^{n-M}\right) < 1$, (2.22) leads to the desired formula (2.21). This completes the proof. □

2.2 Choice of initial guess, auxiliary linear operator, convergence control parameter and auxiliary function

2.2.1 Initial guess

The process of selecting an initial guess plays a pivotal yet often overlooked role in the implementation of the Homotopy Analysis Method (HAM). While the task itself may appear straightforward, the implications of this choice are significant. An effective initial approximation should inherently satisfy the initial or boundary conditions defined by the nonlinear problem, which helps simplify the integral operations required to solve the m^{th}-order deformation equations used to construct the series terms $u_m(x)$. Although this requirement constrains the choice to some extent, practitioners still retain considerable flexibility in defining the form of the initial guess. Alongside the choice of the auxiliary linear operator, the selected initial approximation influences the overall structure and convergence behavior of the solution series. Because the HAM framework involves successive integration of inhomogeneous terms and manipulation of the operator's inverse, the mathematical form of the initial guess can significantly affect computational complexity. For instance, using polynomials will typically yield series terms composed of polynomial expressions and their integrals, often combined with the homogeneous solutions of the linear operator. In contrast, selecting exponential decay functions as the initial guess generally results in solutions formed from combinations of exponential terms and their derivatives or integrals. Furthermore, when the original nonlinear operator explicitly depends on specific functions of the independent variable x, these components are expected to appear in the series as well. To keep the solution expression compact and manageable, it is often beneficial to align the initial guess with the structure of the homogeneous solution of the linear operator. To this end, two practical guidelines can be followed when choosing the initial approximation $u_0(x)$:

(i) The initial guess should inherently satisfy any initial or boundary conditions posed by the nonlinear differential equation.

(ii) The chosen functions should be easy to manipulate particularly with respect to integration and should contribute positively to the convergence of the series solution.

Elementary functions such as polynomials, exponential functions, trigonometric terms, and rational expressions are frequently used due to their tractability and effectiveness in producing convergent series. These functions typically require less computational effort, which accelerates the recursive solution process and facilitates the derivation of higher-order approximations. Generally, the most efficient initial approximation is the one that balances simplicity with the ability to encode necessary problem constraints. This balance offers a practical approach while still allowing flexibility in shaping the series representation. Finally, it is important to note that the notion of a "best" initial guess is somewhat theoretical. In principle, the ideal initial guess would be the exact solution of the differential equation but if such a solution were available, there would be no need to apply HAM. Therefore, the practical objective is to select an initial approximation that is sufficiently accurate and compatible with the HAM framework, following the two principles outlined above.

2.2.2 Choice of auxilliary linear operator

When solving nonlinear differential equations using the Homotopy Analysis Method (HAM), it is necessary to select a suitable auxiliary linear operator. This operator should simplify the process of solving the deformation equations and help the approximate series converge to the true solution of the original nonlinear problem. Typically, the nonlinear operator $\mathcal{M}$ is decomposed into two parts:

$$\mathcal{M} = \mathcal{T} + \mathcal{P}, \tag{2.23}$$

where

- $\mathcal{T}$: the strictly linear part
- $\mathcal{P}$: the strictly nonlinear part

The auxiliary linear operator $\mathscr{A}$ is then chosen to resemble or match the linear part $\mathcal{T}$ as closely as possible. There are several commonly used strategies for selecting the auxiliary

linear operator. One basic strategy is to take the auxiliary linear operator directly as the linear part of the original nonlinear operator. For example, consider the equation:

$$\frac{d^2u}{dx^2} + \frac{du}{dx} - u^2 + 1 = 0$$

Here, the auxiliary linear operator becomes:

$$\mathscr{A}(u) = \frac{d^2u}{dx^2} + \frac{du}{dx}$$

Another approach involves selecting only the highest-order linear derivative from the equation. For instance:

$$\frac{d^2u}{dx^2} + \frac{du}{dx} - (u^2 + 1)\frac{du}{dx} = 0$$

In this case, we choose:

$$\mathscr{A}(u) = \frac{d^2u}{dx^2}$$

A more inclusive method takes into account all linear derivatives or functions appearing in the equation. This is known as complete differential matching, and it follows these rules:

- If a term involves a product of derivatives, select the highest-order derivative.
- If a derivative is multiplied by a nonlinear function of u, select the highest-order derivative in that term.
- If a term includes a nonlinear function of u alone, include the function u itself.

For example:

$$\frac{d^3u}{dx^3} \cdot \frac{du}{dx} - u \cdot \frac{d^2u}{dx^2} + \frac{du}{dx} - u^2 = 0$$

Then we take:

$$\mathscr{A}(u) = \frac{d^3u}{dx^3} - \frac{d^2u}{dx^2} + \frac{du}{dx} - u$$

In practice, the choice of the auxiliary linear operator also depends on the type of problem. For initial value problems (IVPs), a simple operator such as the highest-order derivative may be sufficient, since it simplifies integration and allows straightforward satisfaction of initial conditions. However, for boundary value problems (BVPs), it is often necessary to include multiple terms in the auxiliary linear operator to ensure that the boundary conditions (especially those at infinity) can be satisfied. In some advanced cases, particularly in

partial differential equations, one might even select a higher-order operator than the original equation, offering more flexibility in ensuring convergence and control over the approximate solution. See[49].

2.2.3 Optimal selection of the convergence control parameter in the HAM

The Homotopy Analysis Method (HAM) is distinguished by the auxiliary convergence control parameter ς, whose proper selection critically affects the convergence and accuracy of the solution series. Several approaches exist to determine the optimal value of ς [49, 28]:

Constant ς-curves

The constant ς-curve technique involves plotting a physical quantity (e.g., $u'(0)$ or $u''(0)$) derived from the truncated series solution against various values of ς. The interval where the quantity is stable is referred to as the *valid region* of ς. While intuitive and easy to implement, this method:

- Provides only an approximate interval of convergence.
- Does not yield an exact optimal value.
- Offers only local convergence information.

It is generally considered outdated in modern HAM applications.

Squared residual minimization

A more rigorous method involves minimizing the residual error of the governing equation. For a truncated series of order M, the residual is defined by the L^2-norm, which is commonly used in the literature, and given by:

$$Er(\varsigma) = \left(\int_{\Gamma} \left(\mathcal{M} \left[\sum_{k=0}^{M} u_k(x, \varsigma) \right] \right)^2 dx \right)^{\frac{1}{2}}, \tag{2.24}$$

we continue by applying the squared residual error E to estimate the optimal value of h.

$$E(\varsigma) = \int_{\Gamma} \left(\mathcal{M} \left[\sum_{k=0}^{M} u_k(x, \varsigma) \right] \right)^2 dx, \tag{2.25}$$

and the optimal value ς_{opt} satisfies:

$$\frac{d\,E(\varsigma)}{d\varsigma} = 0. \tag{2.26}$$

Despite its theoretical strength, this method is computationally expensive due to the complexity of integration especially for strongly nonlinear problems or infinite domains. A discretized version is often used:

$$E(\varsigma) \approx \bar{\mathbf{\Delta}} = \frac{1}{N+1} \sum_{j=0}^{N} \left(\mathcal{M} \left[\sum_{k=0}^{M} u_k(x_j, \varsigma) \right] \right)^2, \tag{2.27}$$

where N is the number of discrete points with $x_j = j\Delta x$, and $\Delta x = \frac{\text{length of } \Gamma}{N}$.

Important consequences and remarks

Several important insights and practical observations arise from the theoretical developments above:

- **Ratio method:** The ratio method provides a computationally efficient approach for determining the optimal value of the convergence-control parameter ς. It relies on analyzing the ratio between two successive homotopy terms, often using the L^p-norm:

  $$\beta = \frac{\|u_{k+1}\|_p}{\|u_k\|_p}.$$

  To ensure convergence of the homotopy series, it is sufficient that $\beta < 1$. The optimal value of ς corresponds to the minimum of β:

  $$\frac{d\beta}{d\varsigma} = 0.$$

  This method avoids evaluating the nonlinear operator, making it significantly less computationally expensive than residual-based methods. Moreover, it often yields results comparable to residual minimization, especially for higher-order approximations. Importantly, it is not always necessary for β to attain a strict minimum. If such a minimum

does not exist, any value of ς for which $\beta < 1$ holds is sufficient to ensure convergence. The optimal ς obtained from residual error analysis can also be used to evaluate β and confirm convergence.

- **Domain of validity:** Enforcing the ratio condition for large k helps identify the domain in x where the solution remains valid, thus linking the convergence-control parameter ς to the solution's spatial domain.

- **Validation of ς-curves:** The graphical ς-curves can be supported analytically by examining the ratio of successive derivatives at a fixed point:

$$\frac{|u_{k+1}^{(m)}(x_0)|}{|u_k^{(m)}(x_0)|} < 1,$$

allowing the convergence interval of ς to be determined.

- **Root-finding problems:** For nonlinear equations of the form $f(x) = 0$, the ratio

$$\frac{|x_{k+1}|}{|x_k|} < 1$$

provides a simple and direct criterion for identifying the convergence region of ς.

- **Error monitoring:** When an exact or numerical reference solution $u(x)$ is available, the absolute error

$$\text{err} = \int_\Gamma |u_M(x) - u(x)| dx$$

can be used to validate the selected value of ς.

- **Sufficiency but not necessity:** The condition $\beta < 1$ is sufficient but not necessary. Convergence may still occur (or fail) even if $\beta \to 1$ or becomes undefined. Thus, careful interpretation is essential.

- **Unknown parameter estimation:** In parameterized differential equations involving unknowns, tracking the ratios of their approximated values can aid in estimation and reduce the need for complex integrations.

- **Convergence acceleration:** Methods such as homotopy Padé approximants and optimal initial guesses can further enhance convergence and expand the valid region for ς.

2.2.4 The auxiliary function

In this section, we focus on the auxiliary function $H(x)$ [28], which appears in the homotopy formulation as

$$(1-p)L[u-u_0] = p\varsigma\, H(x)\,\mathcal{M}[u]. \tag{2.28}$$

It is often assumed that $H(x) \neq 0$ for all x within the considered domain, an assumption that is both natural and analytically advantageous. Under this condition, the above homotopy can be rewritten in an equivalent form:

$$(1-p)\tilde{\mathscr{A}}[u-u_0] = p\varsigma\,\mathcal{M}[u], \tag{2.29}$$

where the modified auxiliary linear operator is defined as

$$\tilde{\mathscr{A}}[u] = \frac{1}{H(x)}\,\mathscr{A}[u]. \tag{2.30}$$

Since $H(x) \neq 0$ throughout the domain, this operator is well defined. As indicated in [49], one may determine an optimal auxiliary linear operator to ensure both accuracy and convergence of the homotopy series. Consequently, the specific choice of $H(x)$ can be deduced from the desired properties of this operator. When $H(x)$ is a non-vanishing function over the entire domain, it is sufficient and indeed most common in practice to simply take $H(x) = 1$. This simplification does not compromise the generality of the method and significantly facilitates the analytical construction of the homotopy series. However, when $H(x)$ vanishes at certain points or over specific intervals, analytical and numerical difficulties may arise. For instance, the modified operator $\tilde{\mathscr{A}}$ may exhibit singularities, and the deformation equations might fail to represent the nonlinear problem accurately on portions of the domain. In summary:

- If $H(x)$ vanishes over a finite interval, the resulting solution $u(x)$ may not satisfy the original nonlinear equation throughout the domain.
- If $H(x)$ vanishes only on isolated points (a set of measure zero), the solution remains theoretically valid but computationally more complex due to potential singularities.

Therefore, to ensure the stability, simplicity, and consistency of the Homotopy Analysis Method (HAM), it is generally recommended to employ a non-vanishing auxiliary function,

most conveniently chosen as $H(x) = 1$. In the remainder of this work, we adopt the simplified case $H(x) = 1$.

2.3 Numerical tests

Example 2.1. *Consider the following second-order nonlinear ordinary differential equation:*

$$\frac{d^2u}{dx^2} + \frac{du}{dx} + u^2 = f(x), \quad x \in [0, \kappa] \tag{2.31}$$

subject to the initial conditions:

$$u(0) = 1, \quad u'(0) = -1 \tag{2.32}$$

We aim to apply the Homotopy Analysis Method (HAM) to construct an approximate analytical solution. The nonlinear operator is given by:

$$\mathcal{M}[u(x)] = \frac{d^2u}{dx^2} + \frac{du}{dx} + u^2 - e^{-2x} \tag{2.33}$$

Applying HAM, we construct the zeroth-order deformation equation:

$$(1 - p)\mathscr{A}[\phi(x; p) - u_0(x)] = \varsigma p\mathcal{M}[\phi(x; p)] \tag{2.34}$$

where $p \in [0, 1]$ is the embedding parameter, ς is a nonzero auxiliary parameter, and $\phi(x; p)$ is a family of functions satisfying:

$$\phi(x; 0) = u_0(x), \quad \phi(x; 1) = u(x). \tag{2.35}$$

Expanding $Y(x; q)$ in a power series in p:

$$\phi(x; p) = u_0(x) + \sum_{m=1}^{\infty} u_m(x)p^m, \tag{2.36}$$

subject to the initial conditions

$$u(0) = u'(0) = 0. \tag{2.37}$$

Substituting into the deformation equation and differentiating s times with respect to p, set-

ting $p = 0$, and dividing by $s!$, we obtain the s-th order deformation equation:

$$\mathscr{A}[u_s(x) - \chi_s u_{s-1}(x)] = \varsigma \mathscr{R}_s(x) \tag{2.38}$$

where χ_s and $\mathscr{R}_s$ are defined by (2.8) and (2.9) respectivelly.

We consider two choices for the linear operator. The first one is the highest derivative in the equation:

$$\mathscr{A}[u(x)] = \frac{d^2u}{dx^2} \tag{2.39}$$

while the second is an extended version:

$$\mathscr{A}[u(x)] = \frac{d^2u}{dx^2} + \frac{du}{dx} \tag{2.40}$$

Case 1: $f(x) = e^{-2x}, \mathscr{A}(u) = u'', u_0(x) = 1 - x + \frac{x^2}{2}$

The exact solution is known to be $u(x) = e^{-x}$. For the first-order approximation ($s = 1$), we compute:

$$u_1''(x) = \varsigma \mathscr{R}_1(x) = \varsigma(u_0''(x) + u_0'(x) + u_0^2(x) - e^{-2x}) \tag{2.41}$$

Using $u_0(x) = 1 - x + \frac{x^2}{2}$, we find:

$$u_1''(x) = \varsigma(\frac{x^4}{4} - x^3 + 2x^2 - x + 1 - e^{-2x}) \tag{2.42}$$

Integrating twice and applying the conditions $u_1(0) = 0$, $u_1'(0) = 0$, we obtain:

$$u_1(x) = \varsigma(\frac{x^6}{120} - \frac{x^5}{20} + \frac{x^4}{6} - \frac{x^3}{6} + \frac{x^2}{2} - \frac{x}{2} + \frac{1}{4} - \frac{e^{-2x}}{4}). \tag{2.43}$$

For the second-order approximation ($s = 2$):

$$u_2''(x) = u_1''(x) + \varsigma(u_1''(x) + u_1'(x) + u_1^2). \tag{2.44}$$

Then, integrating twice with the conditions $u_2(0) = 0$, $u_2'(0) = 0$, we find $u_2(x)$, though the expression may become lengthy and is typically computed symbolically or numerically.

$$\begin{aligned} u_2(x) =& \varsigma \left(\frac{\varsigma x^{10}}{10800} - \frac{\varsigma x^9}{1080} + \frac{17\varsigma x^8}{3360} - \frac{11\varsigma x^7}{840} + \frac{x^6(14\varsigma + 3)}{360} - \frac{x^5(13\varsigma + 6)}{120} \right. \\ &+ \frac{x^4(15\varsigma + 8)}{48} - \frac{x^3(3\varsigma + 2)}{12} + \frac{x^2(\varsigma + 1)}{2} - \frac{\varsigma x^2 e^{-2x}}{16} - \frac{x(7\varsigma + 8)}{16} \\ &\left. - \frac{\varsigma(7\varsigma + 8)e^{-2x}}{32} + \frac{(7\varsigma + 8)}{32} \right) \end{aligned} \tag{2.45}$$

The approximate solution up to the second order is:

$$u(x) \approx u_0(x) + u_1(x) + u_2(x) \tag{2.46}$$

This expression provides an analytic approximation to the exact solution e^{-x}, and the convergence of the series can be controlled by the parameter ς. Due to the complexity of the algebraic computations involved in deriving higher-order terms $u_m(x)$ of the HAM series, we employ symbolic computation software such as `MATLAB` to automate the calculations up to a desired order M. This allows us to efficiently construct the approximate solution:

$$u(x) \approx u_0(x) + u_1(x) + \cdots + u_M(x) \tag{2.47}$$

The convergence and accuracy of the series solution depend strongly on the choice of the auxiliary parameter ς. To determine a suitable value of ς, we use several techniques, including:

- ς**-curves**: plotting the value of $u(x)$ at a fixed point versus different values of ς, and identifying the convergence region.
- **Residual error analysis**: computing the residual error and minimizing it with respect to ς.

These methods help to select an optimal ς that ensures fast convergence and high accuracy of the HAM approximation.

ς-curves

We consider the ς-curve approach using the first and the second derivative of the approximate solution at $x = 1$. Specifically, for an approximation of order $M = 4$, we compute:

$$\frac{d^2}{dx^2}\left(u_0(x) + u_1(x) + u_2(x) + u_3(x) + u_4(x)\right)\Big|_{x=0} \tag{2.48}$$

This derivative is evaluated symbolically for various values of ς, and the corresponding graph is plotted (see Fig. 2.1). The result shows a relatively flat and smooth behavior within the interval $-1.1 < \varsigma < -0.3$, indicating a stable region for convergence. However, this is only a preliminary estimate. In subsequent sections, we verify and refine this interval using the residual error analysis to obtain the most appropriate value of ς.

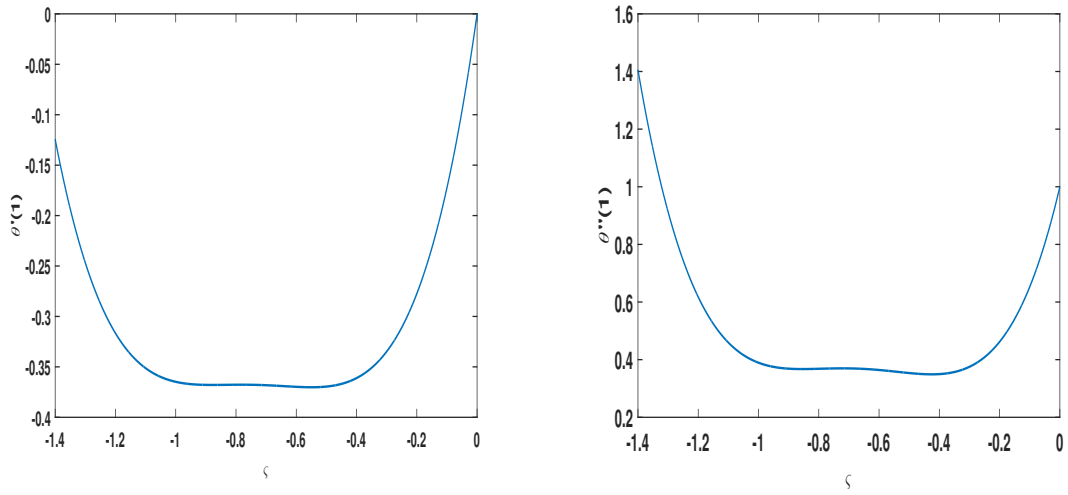

Figure 2.1: ς-curves showing the variation of the first and second derivatives at $x = 1$ for $M = 4$ in Example 2.1.

Residual error analysis

Another common technique to determine the optimal convergence-control parameter ς is the residual error analysis. The residual error $E(\varsigma)$ is defined as the integral of the squared residual of the original differential equation over the domain, which provides a global measure of the accuracy of the approximate solution:

$$E(\varsigma) = \int_0^{\kappa} \left[\mathcal{M}\left(\sum_{s=0}^{M} u_s(x;\varsigma)\right)\right]^2 dx, \tag{2.49}$$

where $\mathcal{M}$ is the nonlinear operator defined earlier, and $u_s(x;\varsigma)$ are the terms of the HAM series depending on ς. To find the optimal value of ς, we differentiate $E(\varsigma)$ with respect to ς and set the derivative equal to zero:

$$\frac{dE}{d\varsigma} = 0. \tag{2.50}$$

Solving this equation yields a set of candidate values for ς, which generally include both real and complex roots. Since only real values of ς are physically meaningful, the complex roots are discarded, and the real roots are considered as possible optimal parameters. For the case $M = 4$, the solutions found are:

$$\varsigma_1 \approx -0.885, \quad \varsigma_2 \approx -0.857, \quad \varsigma_3 \approx -0.8442. \tag{2.51}$$

Further evaluation of the residual error $E(\varsigma)$ at these points allows selection of the best ς that minimizes the error and thus ensures better convergence and accuracy of the HAM approximation. It is worth noting that as M increases, the complexity of the computations and the time required to obtain these values increase significantly, which is a practical limitation of this method. To reduce the computational complexity associated with the Residual Error Analysis method, one can alternatively use equation (2.27) as simpler substitute. These equations provide a more straightforward and less time-consuming approach to obtaining results, especially at higher orders where calculations become increasingly complex and slow. Table 2.1 shows the approximate values of the constant ς obtained by using equation (2.27)

Table 2.1: Approximate values of ς computed using equation (2.27) for Example 2.1.

Order M	ς	$\sqrt{E}$
1	-0.669	5.44444e-02
2	-0.804	9.07610e-03
3	-0.861	1.15641e-03
4	-0.885	9.67643e-05
5	-0.891	6.20924e-06
6	-0.885	9.88224e-07
7	-0.902	5.44208e-08
8	-0.911	6.39829e-09

for orders 1,2,..., and 8. This simplified method significantly reduces computational time compared to the Residual Error Analysis approach, enabling efficient evaluation of ς even for higher orders where the original method becomes increasingly complex and time-consuming.

Figure 2.2 illustrates how the ς-curves associated with this method can be used to determine the optimal value of the constant ς over the domain $[0, 1]$, thereby enhancing the accuracy of the results.

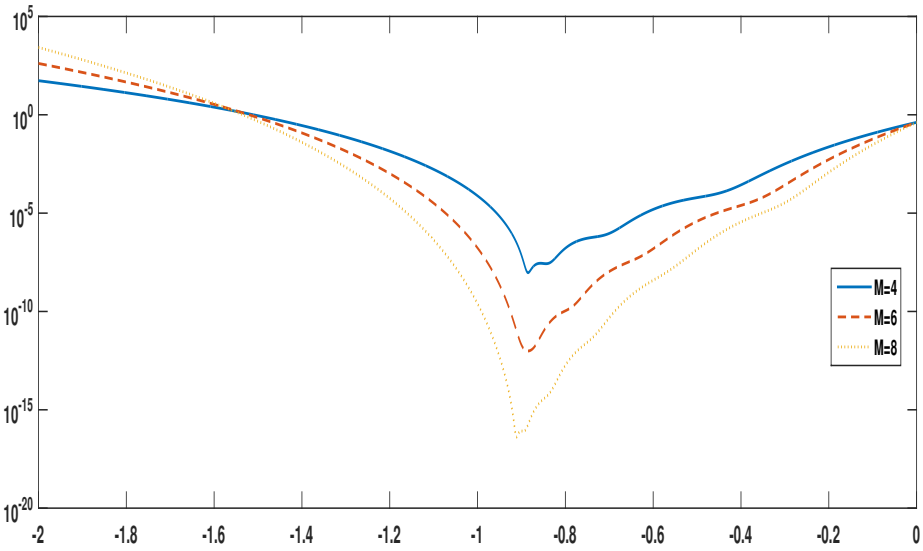

Figure 2.2: Variation of the ς-curves for different values of M over the domain $(0, 1)$ for Example 2.1.

Case 2: $f(x) = e^{-2x}, \mathscr{A}(u) = u'' + u', u_0(x) = 1 - x + \frac{x^2}{2}$

Table 2.2: Computed values of ς and $\sqrt{E}$ using the second linear operator for $f(x) = e^{-2x}, u_0(x) = 1 - x + \frac{x^2}{2}, N = 10$ and $\kappa = 1$ in Example 2.1.

M	2	4	6	8
ς	-0.909	-0.964	-0.973	-0.976
$\sqrt{E}$	3.3317e-03	1.3393e-05	3.2407e-08	6.0867e-11

It is observed from the Table 2.2 that, for **Case 2**, where the nonlinear term is defined by $f(x) = e^{-2x}$ and the auxiliary linear operator is chosen as $\mathscr{A}(u) = u'' + u'$ with the initial approximation $u_0(x) = 1 - x + \frac{x^2}{2}$, the obtained results show a significant improvement in accuracy compared to those reported in Table 2.1, which were obtained using the first linear operator. Indeed, the values of the convergence-control parameter ς in Table 2.1 converge more rapidly when the second operator is used, and the corresponding mean residual error $\sqrt{E}$ decreases exponentially as the order M increases. This clearly demonstrates that

the appropriate selection of the auxiliary linear operator has a direct impact on the performance of the Homotopy Analysis Method (HAM). Specifically, the second operator leads to faster convergence and higher accuracy, confirming its superiority for this type of nonlinear problem.

Case 3: $f(x) = 0, \mathscr{A}(u) = u'' + u, u_0(x) = 1 - x$

Table 2.3: Computed values of ς and $\sqrt{E}$ using the second linear operator for $f(x) = 0, u_0(x) = 1 - x, N = 10$ and $\kappa = 1$ in Example 2.1.

M	2	4	6	8
ς	-0.854	-0.943	-1	-0.971
$\sqrt{E}$	6.7918e-03	2.9107e-05	3.8320e-08	2.5972e-10

Table 2.3 shows that the error $\sqrt{E}$ decreases rapidly as the order M increases, demonstrating the effectiveness and numerical stability of the method. It is also evident that the choice of the parameter ς, the linear operator $\mathscr{A}$, and the initial approximation u_0 plays a crucial role in determining the accuracy of the results, as various combinations of these elements can lead to precise and convergent solutions.

Example 2.2. *Consider the Burgers' equation:*

$$\frac{\partial u}{\partial t} + u\frac{\partial u}{\partial x} = \nu\frac{\partial^2 u}{\partial x^2}, \tag{2.52}$$

with the initial condition

$$u(x, 0) = x. \tag{2.53}$$

Choosing the linear operator as the time derivative,

$$\mathscr{A}[u] = \frac{\partial u}{\partial t}, \tag{2.54}$$

the nonlinear operator is

$$\mathcal{M}[u] = \frac{\partial u}{\partial t} + u\frac{\partial u}{\partial x} - \nu\frac{\partial^2 u}{\partial x^2} \tag{2.55}$$

and the initial approximation equal to the initial condition,

$$u_0(x, t) = x, \tag{2.56}$$

we note that

$$\frac{\partial u_0}{\partial t} = 0, \quad \frac{\partial u_0}{\partial x} = 1, \quad \frac{\partial^2 u_0}{\partial x^2} = 0. \tag{2.57}$$

Applying the HAM, we get the first-order deformation equation

$$\frac{\partial u_1}{\partial t} = \varsigma \mathscr{R}_0(x) = \varsigma(\frac{\partial u_0}{\partial t} + u_0 \frac{\partial u_0}{\partial x} - \nu \frac{\partial^2 u_0}{\partial x^2}) = \varsigma x. \tag{2.58}$$

with the initial condition $u_1(x, 0) = 0$, whose solution is

$$u_1(x, t) = \varsigma t x. \tag{2.59}$$

Thus, the M^{th}-order approximation to the solution is

$$u(x, t) \approx u_0(x, t) + u_1(x, t) + u_2(x, t) + \cdots + u_M(x, t) + \cdots \tag{2.60}$$

$$= x + \varsigma t \cdot x + \varsigma t \cdot x(\varsigma + \varsigma t + 1)^1 + \cdots + \varsigma t \cdot x(\varsigma + \varsigma t + 1)^{M-1} \tag{2.61}$$

$$= x + \varsigma t x \sum_{k=0}^{M-1} (\varsigma + \varsigma t + 1)^k. \tag{2.62}$$

The convergence control parameter ς governs the behavior of the homotopy series and plays a crucial role in ensuring its convergence. It is observed that when $\varsigma = -1$, the series converges to the exact solution as the approximation order tends to infinity:

$$\lim_{M \to \infty} \left(x + \varsigma t x \sum_{k=0}^{M-1} (\varsigma + \varsigma t + 1)^k \right) = \frac{x}{1 + t}. \tag{2.63}$$

Table 2.4 presents numerical results for different values of t and x using HAM with varying the order M. As the value of M increases , the numerical solution converges rapidly towards the exact solution. This clearly demonstrates the consistency and convergence of the numerical method. Furthermore, the inclusion of an optimal convergence control parameter ς significantly enhances the accuracy and rate of convergence of the approximate solution. By carefully choosing this parameter, the numerical method achieves faster convergence with fewer terms, confirming the reliability and efficiency of the approach over the considered domain. Figure 2.2 illustrates the behavior of the squared residual error as a function of the convergence-control parameter ς for different truncation orders M The results correspond to the application of the SHAM to the Burgers' equation over the two-dimensional domain

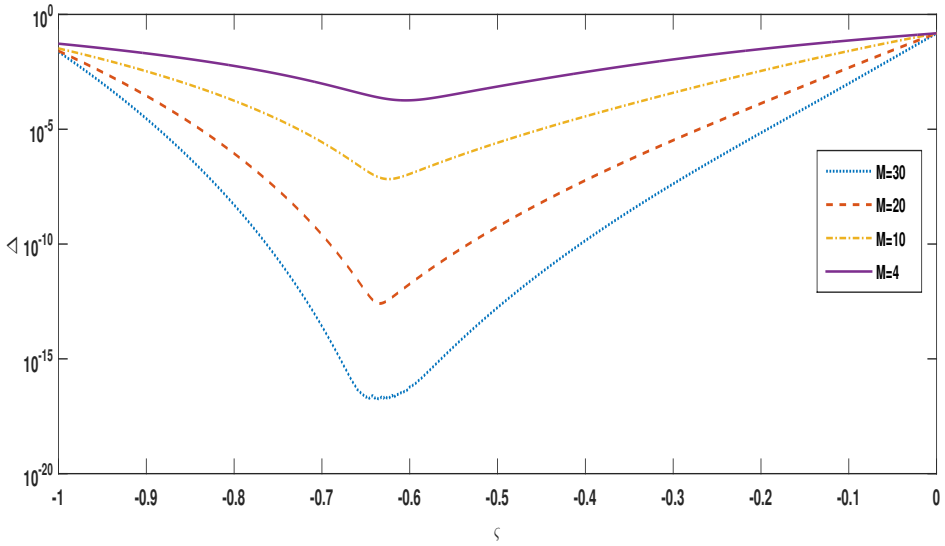

Figure 2.3: Squared residual error defined in (2.27) vs. ς for $(x,t) \in (0,1) \times (0,1)$ in Example 2.2.

$(0,1) \times (0,1)$. Each curve shows how the mean residual error varies with ς for a given order M, enabling the determination of the optimal value ς_{opt} at the minimum point of the curve.It is observed that as M increases, the curves become steeper and the minimum error decreases, indicating better convergence and higher accuracy of the SHAM solution. The consistent convergence of ς_{opt} for higher M values confirms the stability and reliability of the method. Hence, identifying the optimal ς is crucial for achieving the best numerical performance of SHAM when solving nonlinear problems such as the Burgers' equation. Figure 2.4 shows the exact three-dimensional surface of Example 2.2, corresponding to the classical Burgers equation, which serves as a reference for assessing the accuracy of the numerical results. Figure 2.5 displays the approximate solution obtained using the SHAM at order $M = 30$, demonstrating a very close agreement with the exact solution over the entire computational domain. Figure 2.6 presents the absolute error distribution, where the error remains extremely small and uniformly distributed. These observations confirm the high efficiency, and accuracy of the proposed SHAM approach in solving nonlinear partial differential equations such as the Burgers equation.

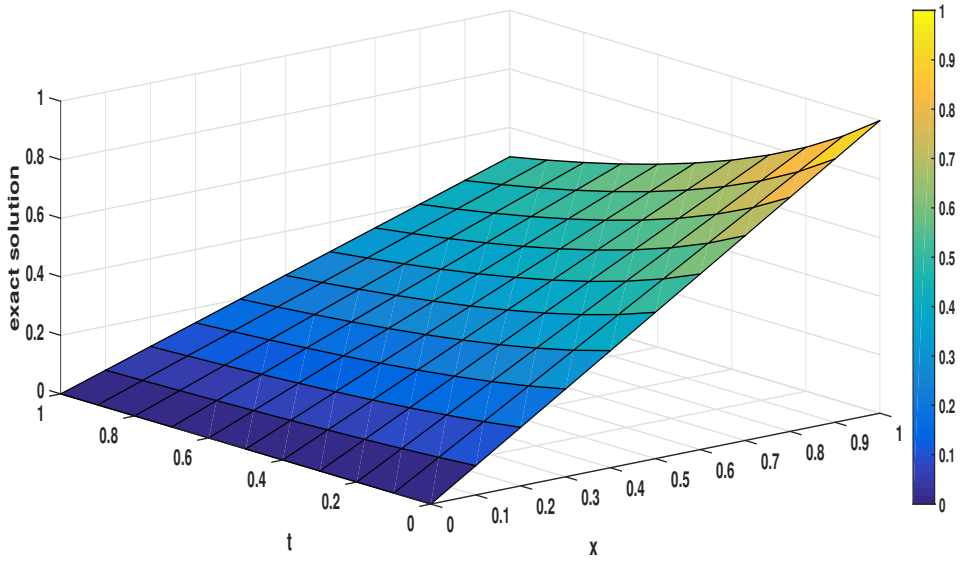

Figure 2.4: Exact solution for $(x,t) \in (0,1) \times (0,1)$ in Example 2.2.

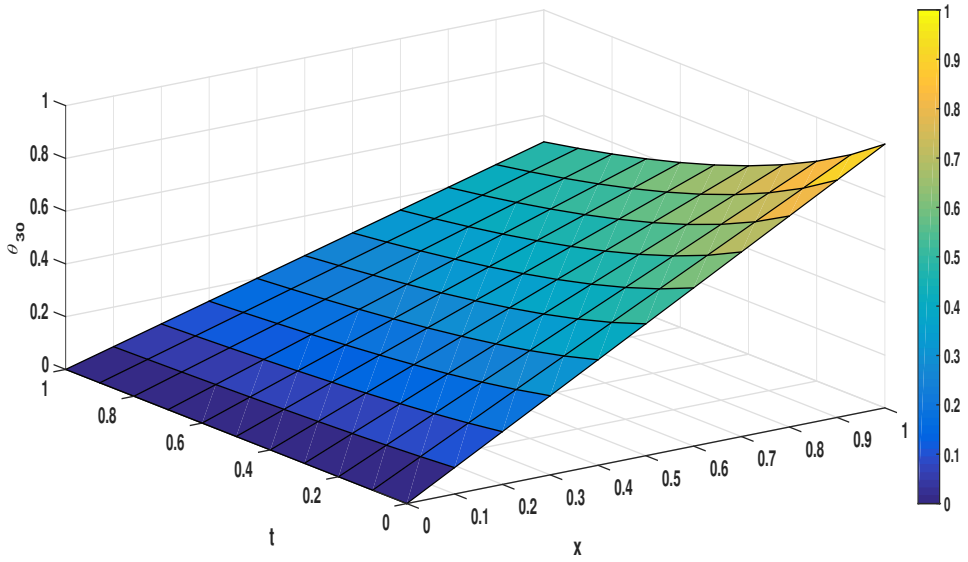

Figure 2.5: Approximate solution for $(x,t) \in (0,1) \times (0,1)$ and $M = 30$ in Example 2.2.

2.4 Generalised homotopy analysis method

Liao [27] in 1999 further introduced more artificial degrees of freedom by constructing the zeroth-order deformation equation in a more general form:

$$[1-\alpha(p)]\mathscr{A}[\phi(x,t;p)-u_0(x,t)] = \varsigma\beta(p)\mathcal{M}[\phi(x,t;p)], \quad p \in [0,1], \tag{2.64}$$

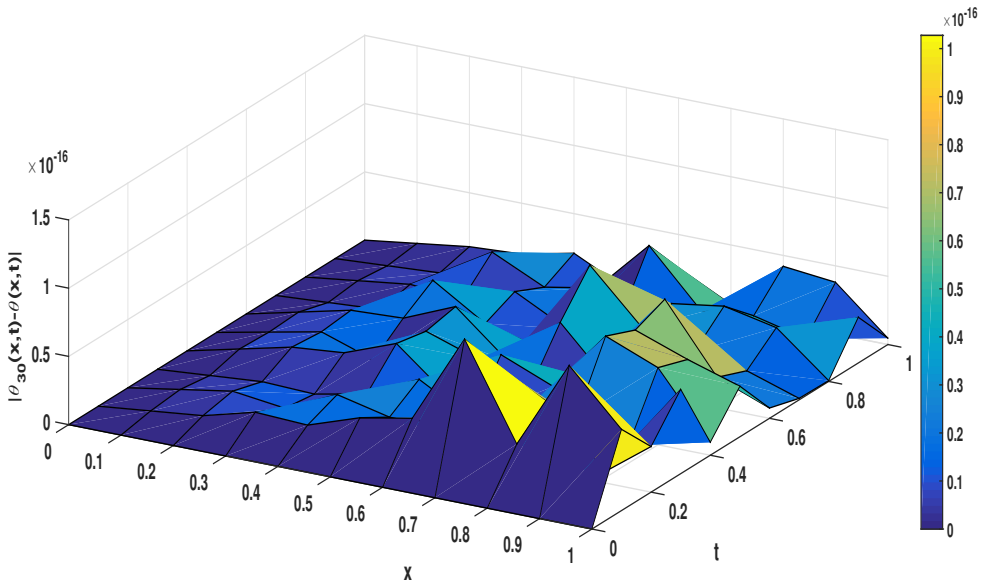

Figure 2.6: Absolute error for $(x,t) \in (0,1) \times (0,1)$ and $M = 30$ in Example 2.2.

where $\alpha(p)$ and $\beta(p)$ are analytic functions satisfying

$$\alpha(0) = \beta(0) = 0, \quad \alpha(1) = \beta(1) = 1, \tag{2.65}$$

and their Maclaurin series exist and are convergent for $|p| \leq 1$:

$$\alpha(p) \sim \sum_{m=1}^{\infty} \alpha_m p^m, \quad \beta(p) \sim \sum_{m=1}^{\infty} \beta_m p^m, \tag{2.66}$$

which implies:

$$\alpha(1) = \sum_{k=1}^{\infty} \alpha_k = 1, \quad \beta(1) = \sum_{k=1}^{\infty} \beta_k = 1, \tag{2.67}$$

where α_k and β_k are constants. This kind of generalization provides us a larger possibility to guarantee the convergence of the homotopy series of original nonlinear equations. In addition, realizing the extremely large freedom in constructing a homotopy of equations, Liao [28] introduced in 2003 a non-zero auxiliary function $H(x,t)$ to further generalize the zeroth-order deformation equation:

$$[1 - \alpha(p)]\mathscr{A}[\phi(x,t;p) - u_0(x,t)] = \varsigma H(x,t)\beta(p)\mathcal{M}[\phi(x,t;p)], \tag{2.68}$$

where the analytic functions $\alpha(p)$ and $\beta(p)$ satisfy and their Maclaurin series satisfy (2.66), respectively. Moreover, Liao [28] also proposed a more generalized zeroth-order deformation equation:

$$[1-\alpha(p)]\mathscr{A}[\phi(x,t;p)-u_0(x,t)]=\varsigma H(x,t)\beta(p)\mathcal{M}[\phi(x,t;p)]+\mathcal{A}[\phi(x,t;p),x,t;p], \tag{2.69}$$

where $\mathcal{A}$ is a nonlinear operator satisfying

$$\mathcal{A}[\phi(x,t;p),x,t;p]=0, \quad \text{when } p=0 \text{ and } p=1. \tag{2.70}$$

Using the generalized forms (2.68) and (2.69), Liao [28] proved that several existing methods, such as the Lyapunov artificial small parameter method [33], the Adomian Decomposition Method (ADM) [2], and the δ-expansion method [19], are special cases of the HAM. Furthermore, Sajid and Hayat [43] demonstrated that the so-called "homotopy perturbation method" proposed in 1998 [15, 16] is in fact equivalent to the early HAM developed by Liao in 1992 [31], meaning that the "homotopy perturbation method" brings "nothing new except its name" [43]. This demonstrates the generality and validity of HAM from another perspective. Clearly, there exist an infinite number of analytic functions $\alpha(q)$ and $\beta(q)$ satisfying (2.4) and (2.67), as well as infinite nonlinear operators $\mathcal{A}$ satisfying (2.70). Thus, the zeroth-order deformation equation (2.69) is indeed very general. Hence, the homotopy approximations provided by HAM offer many artificial degrees of freedom, giving us numerous ways to ensure the convergence of the homotopy series.

Table 2.4: Comparison of SHAM approximations for various M values with the exact solution of the fractional Burgers' equation over $(0,1)\times(0,1)$.

t	x	M				exact
		$M=2$	$M=4$	$M=10$	$M=20$	
		$\varsigma=-0.588$	$\varsigma=-0.604$	$\varsigma=-0.624$	$\varsigma=-0.634$	
0.1	0.2	0.1840864	0.182048817	0.1818183490804	0.18181818181894	0.18181818181818
	0.4	0.3681727	0.364097634	0.3636366981608	0.36363636363787	0.36363636363636
	0.6	0.5522591	0.546146450	0.5454550472412	0.54545454545681	0.54545454545455
	0.8	0.7363455	0.728195267	0.7272733963216	0.72727272727574	0.72727272727273
	1	0.9204318	0.910244084	0.9090917454020	0.90909090909468	0.90909090909091
0.5	0.2	0.1342616	0.133338538	0.13333333333341	0.1333333333333	0.13333333333333
	0.4	0.2685232	0.266677077	0.26666666666682	0.2666666666666	0.26666666666666
	0.6	0.4027848	0.400015615	0.40000000000023	0.4000000000000	0.4
	0.8	0.5370464	0.533354153	0.53333333333364	0.5333333333333	0.53333333333333
	1	0.6713080	0.666692692	0.66666666666705	0.6666666666666	0.66666666666666
1	0.2	0.1030976	0.100187177	0.10000008800692	0.10000000000037	0.1
	0.4	0.2061952	0.200374355	0.20000017601383	0.20000000000073	0.2
	0.6	0.3092928	0.300561532	0.30000026402075	0.30000000000110	0.3
	0.8	0.4123904	0.400748709	0.40000035202767	0.40000000000146	0.4
	1	0.5154880	0.500935887	0.50000044003459	0.50000000000183	0.5

Chapter 3

Spectral homotopy analysis method with Chebeshev polynomials

CHAPTER 3

SPECTRAL HOMOTOPY ANALYSIS METHOD WITH CHEBYSHEV POLYNOMIALS

In the application of the Spectral Homotopy Analysis Method (SHAM) as presented in [30, 37, 38, 46], the target equation (2.1) is decomposed into its linear component, nonlinear component, and source term, yielding the following form:

$$\mathscr{A}(y(t)) + \mathscr{M}(y(t)) = f(t), \qquad t \in [a, b], \tag{3.1}$$

where $\mathscr{A}$ denotes the linear operator, $\mathscr{M}$ the nonlinear operator, and $f(t)$ the known source function corresponding to equation (2.1). A key distinction from the standard Homotopy Analysis Method (HAM) lies in the choice of the initial guess: in SHAM, the initial approximation is taken as the exact solution of the linear equation.

$$\mathscr{A}\left(y_0(t)\right) = f(t), \tag{3.2}$$

with boundary conditions

$$B\left(y_0(t), y_0'(t), \ldots\right) = 0, \quad t \in [a, b]. \tag{3.3}$$

The zeroth-order deformation equation becomes

$$(1-p)\mathscr{A}\left(Y(t;p)-y_0(t)\right)=p\varsigma\left(\mathscr{L}(Y(t;p))+\mathscr{M}(Y(t;p))-f(t)\right),p\in[0,1]. \tag{3.4}$$

The s^{th}-order deformation equation reads

$$\mathscr{A}\left(y_s(t)-(\chi_s+\varsigma)\,y_{s-1}(t)\right)=\varsigma\mathscr{R}_{s-1}\left(y_0,y_1,\ldots,y_s\right), \tag{3.5}$$

where

$$\mathscr{R}_{s-1}\left(y_0,y_1,\ldots,y_{s-1}\right)=\frac{1}{(s-1)!}\frac{\partial^{s-1}\{\mathscr{M}(Y(t;p))-f(t)\}}{\partial p^{s-1}}. \tag{3.6}$$

3.1 SHAM using Chebychev polynomials

Substituting (1.18),(1.21) and (1.25) in (3.5) to get a matrix equation defined by

$$\mathcal{A}\mathbf{Y}_s=(\chi_s+\varsigma)\mathcal{A}\mathbf{Y}_{s-1}+\varsigma\mathcal{R}, \tag{3.7}$$

where $\mathcal{A}$ and $\mathcal{R}$ denote the matrix and vector, respectively, obtained by applying the Chebyshev discretization transformations from equations (1.18), (1.21), and (1.25) to the linear operator $\mathscr{A}$ and the nonlinear residual $\mathscr{R}_{s-1}$. The solution vectors at the m^{th} and $(m-1)^{\text{th}}$ iterations are given by:

$$\begin{aligned}\mathbf{Y}_s&=\left(\mathcal{Y}_s(\eta_0),\mathcal{Y}_s(\eta_1),\ldots,\mathcal{Y}_s(\eta_N)\right)^T,\\ \mathbf{Y}_{s-1}&=\left(\mathcal{Y}_{s-1}(\eta_0),\mathcal{Y}_{s-1}(\eta_1),\ldots,\mathcal{Y}_{s-1}(\eta_N)\right)^T.\end{aligned} \tag{3.8}$$

After imposing the boundary conditions appropriately on equation (3.7), the resulting system becomes:

$$\mathcal{A}\mathbf{Y}_s=(\chi_s+\varsigma)\,\bar{\mathcal{A}}\mathbf{Y}_{s-1}+\varsigma\,\bar{\mathcal{R}}, \tag{3.9}$$

where $\bar{\mathcal{A}}$ and $\bar{\mathcal{R}}$ are the modified matrix and vector resulting from incorporating the boundary conditions into equation (3.7). Consequently, the solution at the m^{th} level can be updated recursively as:

$$\mathbf{Y}_s=(\chi_s+\varsigma)\,\mathcal{A}^{-1}\bar{\mathcal{A}}\mathbf{Y}_{s-1}+\varsigma\,\mathcal{A}^{-1}\bar{\mathcal{R}}, \tag{3.10}$$

where $\mathcal{A}^{-1}$ denotes the inverse of the matrix $\mathcal{A}$. This recursive relation provides an efficient way to compute successive approximations $\mathcal{Y}_s$.

3.1.1 SHAM and transformation of the initial guess

In the traditional Homotopy Analysis Method (HAM), the initial approximation must satisfy the given boundary conditions and is usually constructed as a linear combination of basis functions. Although solving the associated auxiliary linear problem (e.g., equation (3.2)) directly is sometimes feasible, it may be algebraically cumbersome or result in no solution. In such cases, one resorts to a suitable initial guess that satisfies the boundary conditions alone. To simplify the handling of boundary conditions and particularly to enforce homogeneous conditions, SHAM introduces a transformation of the original problem. This transformation redefines the unknown function such that the new form inherently satisfies the boundary constraints. Following the approach in [30, 37, 46], the transformation is introduced as follows:

$$y(t) = \mathcal{Y}(\eta) = \mathcal{Y}_0(\eta) + u(\eta) \quad \text{and} \quad f(t) = \mathscr{F}(\eta), \quad t \in [a, b],\ \eta \in [-1, 1] \tag{3.11}$$

Substituting (3.11) in (3.1) yields

$$\mathscr{A}(u(\eta)) + \mathscr{M}(u(\eta)) = g(\eta), \tag{3.12}$$

subject to

$$T\left(u(\eta), u'(\eta), \ldots\right) = 0, \tag{3.13}$$

where T is a linear operator and

$$g(\eta) = \mathscr{F}(\eta) - \mathscr{A}\left(\mathcal{Y}_0(\eta)\right) - \mathscr{M}\left(\mathcal{Y}_0(\eta)\right). \tag{3.14}$$

The zeroth-order deformation equation within the Homotopy Analysis Method (HAM) framework is formulated as follows:

$$(1-p)\mathscr{A}\left(\phi(\eta;p) - u_0(\eta)\right) = p\varsigma\left(\mathscr{A}[\phi(\eta;p)] + \mathscr{M}(\phi(\eta;p)) - g(\eta)\right), \quad p \in [0,1], \tag{3.15}$$

where $\phi(\eta;p)$ denotes a family of functions continuously deforming from the initial guess $u_0(\eta)$ to the exact solution as p varies from 0 to 1. The corresponding s^{th}-order deformation

equation is given by:

$$\mathscr{A}\left(u_s(\eta) - (\chi_s + \varsigma)\, u_{s-1}(\eta)\right) = \varsigma\, \mathscr{R}_{s-1}(u_0, u_1, \ldots, u_{s-1}), \tag{3.16}$$

where the nonlinear residual $\mathscr{R}_{s-1}$ is defined by:

$$\mathscr{R}_{s-1}(u_0, u_1, \ldots, u_{s-1}) = \frac{1}{(s-1)!} \frac{\partial^{s-1}}{\partial p^{s-1}} \left\{\mathscr{M}(\phi(\eta; p)) - g(\eta)\right\}. \tag{3.17}$$

The homotopy series solution is thus expressed as:

$$y(t) = \mathcal{Y}_0(\eta) + u_0(\eta) + \sum_{k=1}^{+\infty} u_k(\eta), \tag{3.18}$$

where $u_0(\eta)$ is the solution to the auxiliary linear problem:

$$\mathscr{A}\left(u_0(\eta)\right) = g(\eta). \tag{3.19}$$

By applying the same Chebyshev spectral transformations used previously (leading to equation (3.10)), we derive the discrete form of the s^{th}-order deformation equation:

$$\mathbf{U}_s = (\chi_s + \varsigma)\, \mathcal{B}^{-1}\bar{\mathcal{B}}\mathbf{U}_{s-1} + \varsigma\, \mathcal{B}^{-1}\bar{\mathcal{R}}, \tag{3.20}$$

where the vectors of discrete solutions at the current and previous iterations are given by:

$$\begin{aligned} \mathbf{U}_s &= \left(u_s(\eta_0), u_s(\eta_1), \ldots, u_s(\eta_N)\right)^T, \\ \mathbf{U}_{s-1} &= \left(u_{s-1}(\eta_0), u_{s-1}(\eta_1), \ldots, u_{s-1}(\eta_N)\right)^T. \end{aligned} \tag{3.21}$$

The recursive formula (3.20) enables the computation of higher-order approximations u_s efficiently within the spectral-HAM framework.

3.2 Numerical tests

In this section, we demonstrate the performance and accuracy of the proposed spectral method through its application to classical nonlinear problems, namely the Van der Pol and Duffing oscillators. The effectiveness of the method is evaluated by computing the numerical

error $\mathcal{E}$ using the following error formulas:

- If we have the analytical solution

$$\mathcal{E}_1 = \max_j |y(t_j) - y_M(t_j)|, \quad j = 0, 1, \ldots, N. \tag{3.22}$$

- In cases where the analytical solution is unavailable, we estimate the error using the residual-based metric proposed in [46], defined as:

$$\mathcal{E}_2 = \max_j |\mathscr{A}(y_M(t_j)) + \mathscr{M}(y_M(t_j)) - f(t_j)|, \quad j = 0, 1, \ldots, N, \tag{3.23}$$

  where $y_M(t)$ is the truncated series approximation of the solution given by:

$$y(t) \approx y_M(t) = \mathcal{Y}_0(\eta) + \sum_{s=1}^{M} \mathcal{Y}_s(\eta). \tag{3.24}$$

To investigate the numerical convergence behavior of the proposed method, we define an optimal convergence-controlling parameter, denoted by ς, which is employed throughout our simulations. The empirical rate of convergence is then computed using the following logarithmic expression:

$$\mathcal{O} = \frac{\log(\mathcal{E}(M_1)) - \log(\mathcal{E}(M_2))}{\log(M_1) - \log(M_2)}, \tag{3.25}$$

where $\mathcal{E}(M_1)$ and $\mathcal{E}(M_2)$ denote the errors corresponding to $M = M_1$ and $M = M_2 = M_1 + 1$, respectively. In addition to error analysis, we present plots for both the approximate solution and the corresponding error curves. We also visualize the variation of the convergence parameter to determine its optimal value. All numerical computations were carried out using `MATLAB 2015`.

3.2.1 Van der Pol equation

In this subsection, the Van der Pol oscillator is used as a benchmark problem to assess the accuracy and efficiency of the proposed spectral-HAM approach. Notably, the method maintains high fidelity with the exact solution even over extended domains where the dynamics exhibit pronounced oscillatory behavior.

Example 3.1. *Consider the nonlinear second-order differential equation representing a Van*

der Pol oscillator as presented in [20, 21]:

$$\frac{d^2y}{dt^2} + \frac{dy}{dt} + y + y^2\frac{dy}{dt} = 2\cos(t) - \cos^3(t), \quad t \in [0, \kappa], \quad \kappa \to \infty, \tag{3.26}$$

subject to the initial conditions:

$$y(0) = 0, \quad \textit{and} \quad \left.\frac{dy}{dt}\right|_{t=0} = 1. \tag{3.27}$$

The exact solution of this problem is known to be:

$$y(t) = \sin(t). \tag{3.28}$$

To apply the Chebyshev-based spectral method, we map the physical domain $[0, \kappa]$ to the reference interval $[-1, 1]$ via the linear transformation:

$$t = \frac{\kappa}{2}(\eta + 1), \quad \eta \in [-1, 1]. \tag{3.29}$$

We then perform the transformation

$$y(t) = \mathcal{Y}(\eta) = \mathcal{Y}_0(\eta) + u(\eta). \tag{3.30}$$

Thus, the equation becomes

$$\frac{4}{\kappa^2}\frac{d^2\mathcal{Y}}{d\eta^2} + \frac{2}{\kappa}\frac{d\mathcal{Y}}{d\eta} + \mathcal{Y} + \frac{2}{\kappa}\mathcal{Y}^2\frac{d\mathcal{Y}}{d\eta} = 2\cos(\frac{\kappa}{2}(\eta+1)) - \cos^3(\frac{\kappa}{2}(\eta+1)), \quad \eta \in [-1, 1], \tag{3.31}$$

with the initial conditions

$$\mathcal{Y}(-1) = 0, \quad \text{and} \quad \frac{d\mathcal{Y}}{dt}|_{\eta=-1} = \frac{2}{\kappa}. \tag{3.32}$$

where

$$\begin{aligned}\mathcal{Y}_0(\eta) = \; & \frac{125\sin(\frac{\kappa}{2}(\eta+1)) - 3\sin(\frac{3}{2}\kappa(\eta+1)) + 4\cos(\frac{3}{2}\kappa(\eta+1))}{200} \\ & + \frac{10\kappa(\eta+1) - 1}{50}e^{-\frac{\kappa}{2}(\eta+1)},\end{aligned} \tag{3.33}$$

where $\mathcal{Y}_0$ satisfies the initial conditions (3.27) and is a solution of the equation

$$\mathscr{A}\left(\mathcal{Y}_0(\eta)\right) = 2\cos(\frac{\kappa}{2}(\eta+1)) - \cos^3(\frac{\kappa}{2}(\eta+1)), \quad \mathscr{L}(\mathcal{Y}) = \mathcal{Y}'' + 2\mathcal{Y}' + \mathcal{Y}. \tag{3.34}$$

Substituting equation (3.30) and (3.33) into equation (3.31) gives

$$\frac{4}{\kappa^2}\frac{d^2u}{d\eta^2} + \frac{2}{\kappa}(1+\mathcal{Y}_0^2)\frac{du}{d\eta} + (1+\frac{4}{\kappa}\mathcal{Y}_0\frac{d\mathcal{Y}_0}{d\eta})u + \frac{2}{\kappa}\frac{d\mathcal{Y}_0}{d\eta}u^2 + 2\mathcal{Y}_0 u\frac{du}{d\eta} + u^2\frac{du}{d\eta} + \varphi(\eta) = 0, \tag{3.35}$$

$$\varphi(\eta) = \frac{4}{\kappa^2}\frac{d^2\mathcal{Y}_0}{d\eta^2} + \frac{d\mathcal{Y}_0}{d\eta} + \mathcal{Y}_0^2\frac{d\mathcal{Y}_0}{dt} - 2\cos(\frac{\kappa}{2}(\eta+1)) + \cos^3(\frac{\kappa}{2}(\eta+1)),$$

and

$$u(-1) = \frac{du}{d\eta}|_{\eta=-1} = 0. \tag{3.36}$$

We select the linear and nonlinear operators for (3.35) as follows:

$$\mathscr{A}(u) = \frac{4}{\kappa^2}\frac{d^2u}{d\eta^2} + \frac{2}{\kappa}(1+\mathcal{Y}_0^2)\frac{du}{dx} + (1+\frac{4}{\kappa}\mathcal{Y}_0\frac{d\mathcal{Y}_0}{d\eta})u. \tag{3.37}$$

$$\mathscr{M}(u) = \mathscr{A}(u) + \frac{2}{\kappa}\frac{d\mathcal{Y}_0}{d\eta}u^2 + \frac{4}{\kappa}\mathcal{Y}_0 u\frac{du}{d\eta} + \frac{2}{\kappa}u^2\frac{du}{d\eta}. \tag{3.38}$$

The initial approximation u_0 for solving (3.35) with SHAM is obtained by solving

$$\mathscr{A}\left(u_0\right) + \varphi(\eta) = 0, \tag{3.39}$$

with

$$u_0(-1) = \frac{du_0}{d\eta}|_{\eta=-1} = 0. \tag{3.40}$$

Applying the Chebychev spectral collocation method (ChebSCM) to (3.39) gives,

$$\mathbf{A}U_0 = -\Phi, \tag{3.41}$$

under the specified initial conditions

$$u_0\left(\eta_N\right) = 0, \quad \sum_{k=0}^{N}\mathbf{D}_{Nk}u_0\left(\eta_k\right) = 0; \quad \mathbf{D} = \frac{2}{\kappa}D, \tag{3.42}$$

and

$$\begin{aligned}
\mathbf{A} &= \mathbf{D}^2 + \operatorname{diag}\left(1 + (\mathbf{Y}_0)^2\right)\mathbf{D} + \operatorname{diag}\left(1 + 2\mathbf{Y}_0\right) \\
U_0 &= \left[u_0\left(\eta_0\right), u_0\left(\eta_1\right), \ldots, u_0\left(\eta_N\right)\right]^T, \\
\mathbf{\Phi} &= \left[\varphi\left(\eta_0\right), \varphi\left(\eta_1\right), \ldots, \varphi\left(\eta_N\right)\right]^T, \\
\mathbf{Y}_0 &= \left[\mathcal{Y}_0\left(\eta_0\right), \mathcal{Y}_0\left(\eta_1\right), \ldots, \mathcal{Y}_0\left(\eta_N\right)\right]^T.
\end{aligned} \tag{3.43}$$

Hence, under the HAM framework, the zeroth-order and s^{th}-order deformation equations, respectively are:

$$(1-p)\mathscr{A}\left(\phi(\eta;p) - u_0(\eta)\right) = p\varsigma\{\mathscr{M}\left(\phi(\eta;p)\right) + \phi(\eta)\}. \tag{3.44}$$

$$\mathscr{A}\left(u_s(\eta) - (\chi_s + \varsigma)\, u_{s-1}(\eta)\right) = \varsigma\mathscr{R}_{s-1}\left(u_0, u_1, \ldots, u_{s-1}\right), \tag{3.45}$$

where

$$\mathscr{R}_{s-1}\left[u_0, u_1, \ldots, u_{s-1}\right] = \frac{1}{(s-1)!}\frac{\partial^{s-1}\{\mathscr{M}\left(\phi(\eta;p)\right) + \phi(\eta)\}}{\partial p^{s-1}}|_{p=0}. \tag{3.46}$$

Hence, the approximation of $y(t)$ obtained using the HAM is

$$y(t) = \mathcal{Y}_0(\eta) + u_0(\eta) + \sum_{s=1}^{+\infty} u_s(\eta). \tag{3.47}$$

Substituting (3.37),(3.38)and (3.46) in (3.45) gives

$$\begin{aligned}
\mathscr{A}\left(u_s\right) &= \varsigma\left(\frac{2}{\kappa}\frac{d\mathcal{Y}_0}{d\eta}\sum_{n=0}^{s-1} u_s u_{s-1-n} + 2\mathcal{Y}_0\sum_{n=0}^{s-1} u_s u'_{s-1-n} + \sum_{n=0}^{s-1} u'_{s-1-n}\sum_{i=0}^{n} u_{n-i}u_i\right) \\
&\quad +\varsigma\left(1-\chi_s\right)\varphi(\eta) + \left(\chi_s + \varsigma\right)\mathscr{A}\left(u_{s-1}\right),
\end{aligned} \tag{3.48}$$

subject to

$$u_s(\eta_N) = \frac{du}{d\eta}|_{\eta=\eta_N} = 0. \tag{3.49}$$

Applying the ChebSCM to equation (3.48) gives:

$$\begin{aligned}
\mathbf{A}U_s &= \varsigma\left(\frac{2}{\kappa}\mathbf{Y}'_0\sum_{n=0}^{s-1} U_s U_{s-1-n} + 2\mathbf{Y}_0\sum_{n=0}^{s-1} U_s U'_{s-1-n} + \sum_{n=0}^{s-1} U'_{s-1-n}\sum_{i=0}^{n} U_{n-i}U_i\right) \\
&\quad +\varsigma\left(1-\chi_s\right)\Phi + \mathbf{A}U_{s-1}
\end{aligned} \tag{3.50}$$

and

$$u_s\left(\eta_N\right) = 0, \quad \sum_{k=0}^{N}\mathbf{D}_{Nk}u_s\left(\eta_k\right) = 0. \tag{3.51}$$

where

$$\begin{aligned}
\mathbf{A} &= \mathbf{D}^2 + \operatorname{diag}\left(1 + (\mathbf{Y}_0)^2\right)\mathbf{D} + \operatorname{diag}\left(1 + 2\mathbf{Y}_0\right) \\
U_s &= [u_s(\eta_0), u_s(\eta_1), \ldots, u_s(\eta_N)]^T, \\
U_s' &= [u_s'(\eta_0), u_s'(\eta_1), \ldots, u_s'(\eta_N)]^T, \\
\mathbf{Y}_0' &= [\mathcal{Y}_0'(\eta_0), \mathcal{Y}_0'(\eta_1), \ldots, \mathcal{Y}_0'(\eta_N)]^T
\end{aligned} \tag{3.52}$$

Starting from the initial approximation u_0, the subsequent terms u_s can be computed recursively by solving equation (3.50). Once the initial guess y_0, the first approximation u_0, and the recursive solutions u_s are obtained, they are substituted into the series expression (3.47) to construct the approximate solution $y(t)$ to the original problem defined in (3.26). Figure3.1 presents the error curves used to determine the optimal value of the convergence-

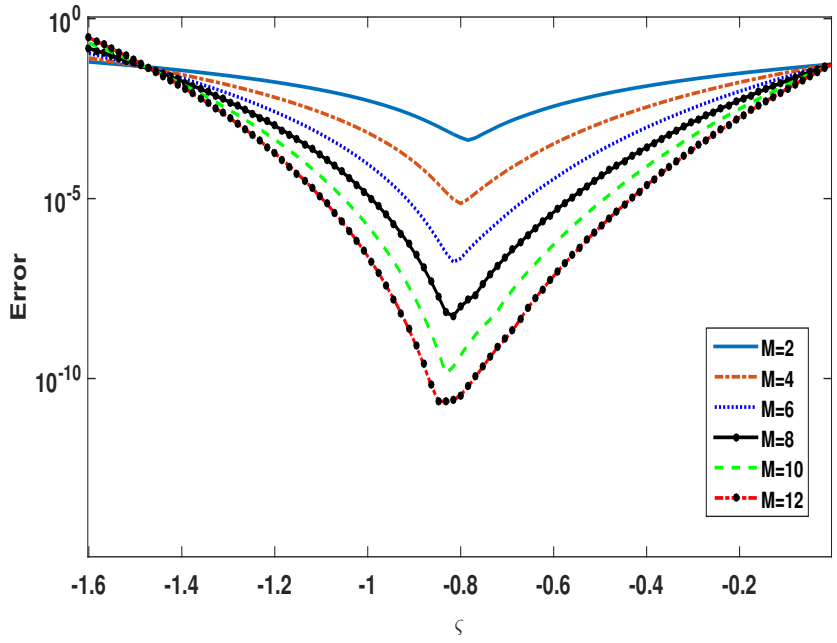

Figure 3.1: $\mathcal{E}_1$ as a function of ς for $N = 30$ and $\kappa = 5$.

control parameter ς for the case $\kappa = 5$ with $N = 30$ collocation points.

Table 3.1: $\mathcal{E}_1$ at selected ς for $\kappa = 5$ and $N = 30$.

M	ς	$\mathcal{E}_1$
2	-0.78	4.0943e-04
4	-0.80	7.2814e-06
6	-0.82	1.9459e-07
8	-0.82	4.4286e-09
10	-0.82	1.7431e-10
12	-0.84	2.2987e-11

Table 3.1 illustrates the variation of the approximation error with respect to the number of terms M in the series solution, demonstrating the rapid convergence and efficiency of the proposed method.

Table 3.2 presents the approximate solutions obtained using the SHAM method for various values of the order M, alongside the exact solution. The close agreement between the approximate and exact values highlights the accuracy and efficiency of the SHAM approach. Even for relatively small values of M, the method yields highly accurate results, thereby confirming its robustness and suitability for solving this class of nonlinear problems.

Table 3.2: Comparison between SHAM and exact solutions with $\kappa = 1$ and $N = 16$.

t	$M = 2$	$M = 4$	$M = 6$	Exact sol
	$\varsigma = -0.97$	$\varsigma = -0.97$	$\varsigma = -0.95$	
0	0	0	0	0
0.084	8.4165507e-02	8.4165506685e-02	8.41655066857e-02	8.41655066866e-02
0.222	2.2039059e-01	2.2039058518e-01	2.20390585175e-01	2.20390585177e-01
0.309	3.0378062e-01	3.0378060089e-01	3.03780600879e-01	3.03780600881e-01
0.402	3.9167829e-01	3.9167822317e-01	3.91678223115e-01	3.91678223117e-01
0.5	4.7942572e-01	4.7942553872e-01	4.79425538603e-01	4.79425538604e-01
0.597	5.6261504e-01	5.6261470821e-01	5.62614708047e-01	5.62614708048e-01
0.691	6.3757182e-01	6.3757140236e-01	6.37571402222e-01	6.37571402223e-01
0.778	7.0170346e-01	7.0170310487e-01	7.01703104786e-01	7.01703104788e-01
0.916	7.9301060e-01	7.9301045079e-01	7.93010450729e-01	7.93010450732e-01
1	8.4147158e-01	8.4147098493e-01	8.41470984805e-01	8.41470984808e-01

Table 3.3 presents a comparison among three methods: the proposed SHAM, HPTM [21], and LDM [20]. The absolute errors computed at points within the interval $[0, 1]$ clearly demonstrate the superior accuracy of the SHAM method. The evaluation points correspond to the values listed in Table 3.2, rounded to one decimal place, based on the Gauss-Lobatto

Table 3.3: Absolute error variation using SHAM ($\varsigma = -0.97$, $N = 16$, $\kappa = 1$), HPTM and LDM.

t	SHAM($M = 2$)	SHAM($M = 4$)	LDM [20]	HPTM [21]
0	0	0	0	0
0.1	3.90812e-13	1.78914e-12	4.8e-06	4.3e-07
0.2	3.05398e-09	1.93409e-12	8.5e-05	7.1e-05
0.3	1.83222e-08	9.57590e-12	4.51e-04	3.76e-04
0.4	6.99433e-08	4.80444e-11	1.466e-03	1.257e-03
0.5	1.81757e-07	1.15306e-10	3.601e-03	3.259e-03
0.6	3.29779e-07	1.64206e-10	7.387e-03	7.2e-03
0.7	4.17136e-07	1.41603e-10	1.3334e-02	1.4247e-02
0.8	3.58849e-07	8.21438e-11	2.1876e-02	2.5967e-02
0.9	1.48613e-07	5.56166e-11	3.3295e-02	4.4405e-02
1	5.99500e-07	1.23401e-10	4.7687e-02	7.2126e-02

collocation nodes over this interval. These results confirm that SHAM consistently achieves lower absolute errors relative to the other two methods when solving this class of problems.

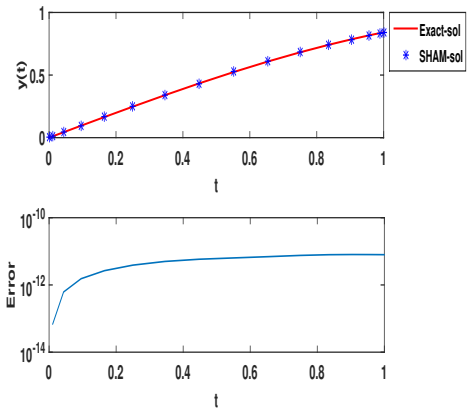

(a) $M = 6$, $N = 15$, $\varsigma = -0.96$, $\kappa = 1$.

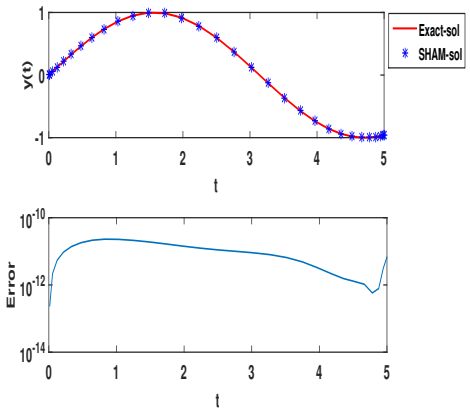

(b) $M = 12$, $N = 30$, $\varsigma = -0.84$, $\kappa = 5$.

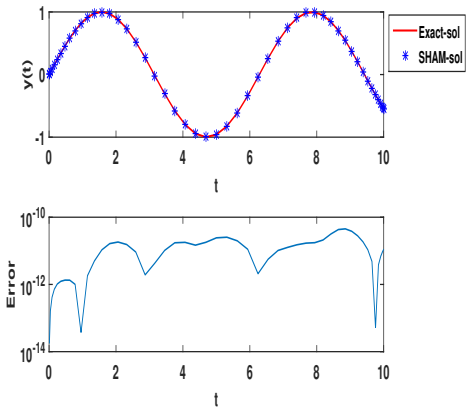

(c) $M = 14$, $N = 50$, $\varsigma = -0.78$, $\kappa = 10$.

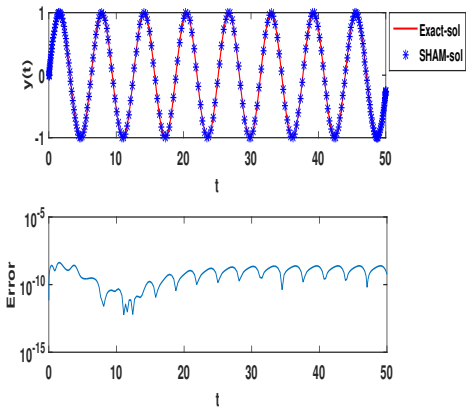

(d) $M = 14$, $N = 250$, $\varsigma = -0.74$, $\kappa = 50$.

Figure 3.2: Exact and approximate solutions with error behavior.

Figure 3.2 illustrates both the exact and numerical solutions of equation (3.26), demonstrating excellent agreement between the two. The associated approximation error confirms the high level of accuracy achieved by the proposed method. Furthermore, Figure 3.2d highlights the pronounced oscillatory behavior of the solution, offering additional validation of the method's ability to accurately capture such dynamics. Notably, the results presented here outperform those reported in [21] (see Fig. 7, p. 5).

Table 3.4 demonstrates a gradual decrease in the accuracy of the numerical solution as the

Table 3.4: $\mathcal{E}_1$ for various κ.

κ	1	5	10	15	20	50
$\mathcal{E}_1$	5.6520e-12	2.3631e-11	4.5047e-11	1.2212e-10	2.2429e-10	4.2414e-09

value of κ increases. Nevertheless, the accuracy remains satisfactory even for $\kappa = 50$, where the error is approximately 4.2414×10^{-9}. This result is particularly significant considering the pronounced oscillatory behavior of the solution over such a large interval.

3.2.2 Duffing equation

We examine three illustrative examples, including both damped and undamped cases, to validate the effectiveness of the proposed method. The evaluation is conducted through error analysis and graphical comparisons.

Example 3.2. *Consider the damped Duffing equation as presented in [2]:*

$$\frac{d^2y}{dt^2} + 2\frac{dy}{dt} + y + 8y^3 = e^{-3t}, \quad t \in [0, \kappa], \quad \kappa \to \infty, \tag{3.53}$$

subject to the initial conditions:

$$y(0) = \frac{1}{2}, \quad \textit{and} \quad \left.\frac{dy}{dt}\right|_{t=0} = -\frac{1}{2}. \tag{3.54}$$

The exact analytical solution to this problem is given by: $y(t) = \frac{1}{2}e^{-t}$.

Using the relations (3.29)-(3.30) gives

$$\frac{4}{\kappa^2}\frac{d^2u}{d\eta^2} + \frac{4}{\kappa}\frac{du}{d\eta} + (1 + 24\mathcal{Y}_0^2)u + 24\mathcal{Y}_0u^2 + 8u^3 + \varphi(\eta) = 0, \tag{3.55}$$

$$\mathcal{Y}_0(\eta) = \frac{3}{4}e^{-\frac{\kappa}{2}(\eta+1)} - \frac{1}{4}\kappa(\eta+1)e^{-\frac{\kappa}{2}(\eta+1)} - \frac{1}{4}e^{-\frac{3}{2}\kappa(\eta+1)}, \tag{3.56}$$

$$\varphi(\eta) = \frac{4}{\kappa^2}\frac{d^2\mathcal{Y}_0}{d\eta^2} + \frac{4}{\kappa}\frac{d\mathcal{Y}_0}{d\eta} + \mathcal{Y}_0 + 8\mathcal{Y}_0^3(-\frac{\kappa}{2}(\eta+1)) - e^{-\frac{3}{2}\kappa(\eta+1)},$$

under the conditions (3.36), we select the linear and nonlinear operators for (3.55) as:

$$\mathscr{A}(u) = \frac{4}{\kappa^2}\frac{d^2u}{d\eta^2} + \frac{4}{\kappa}\frac{du}{d\eta} + (1+24\mathcal{Y}_0^2)u, \tag{3.57}$$

$$\mathscr{M}(u) = \mathscr{A}(u) + 24\mathcal{Y}_0u^2 + 8u^3. \tag{3.58}$$

u_0 is a solution of (3.39) with the conditions (3.40). Applying the ChebSCM on equation (3.39) gives (3.41) subject to conditions (3.42), with

$$\mathbf{A} = \mathbf{D}^2 + 2\mathbf{D} + \mathrm{diag}\left(1 + 24\mathbf{Y}_0^2\right). \tag{3.59}$$

Hence, under the HAM framework, the zeroth-order deformation equation and the corresponding s^{th}-order counterpart with equations (3.57) and (3.58) give:

$$\begin{aligned}\mathscr{A}\left(u_s\right) &= \varsigma\left(24\mathcal{Y}_0\sum_{n=0}^{s-1}u_su_{s-1-n} + 8\sum_{n=0}^{s-1}u_{s-1-n}\sum_{i=0}^{n}u_{n-i}u_i\right)\\ &\quad +\varsigma\left(1-\chi_s\right)\varphi(\eta) + \left(\chi_s+\varsigma\right)\mathscr{A}\left(u_{s-1}\right),\end{aligned} \tag{3.60}$$

with the conditions (3.49). Applying the Chebyshev Spectral Collocation Method (ChebSCM) to equation (3.60) yields the following recursive formulation:

$$\begin{aligned}\mathbf{A}U_s &= \varsigma\left(24Y_0\sum_{n=0}^{s-1}U_sU_{s-1-n} + 8\sum_{n=0}^{s-1}U_{s-1-n}\sum_{i=0}^{n}U_{n-i}U_i\right)\\ &\quad +\varsigma(1-\chi_s)\Phi + \mathbf{A}U_{s-1},\end{aligned} \tag{3.61}$$

subject to the initial conditions specified in (3.51). Here, the matrix $\mathbf{A}$ is defined as

$$\mathbf{A} = \mathbf{D}^2 + \mathrm{diag}\left(1+\mathbf{Y}_0^2\right)\mathbf{D} + \mathrm{diag}\left(1+2\mathbf{Y}_0\right), \tag{3.62}$$

where $\mathbf{D}$ is the Chebyshev differentiation matrix and $\mathbf{Y}_0$ is the initial approximation vector. Starting from the initial approximation u_0, the higher-order terms u_s are computed recursively by solving equation (3.61). Finally, substituting the initial guess y_0, the zeroth-order

term u_0, and the subsequent solutions u_s into the series expression (3.47) yields the approximate solution $y(t)$ for the Duffing equation (3.53). Figure 3.3 illustrates the variation of the

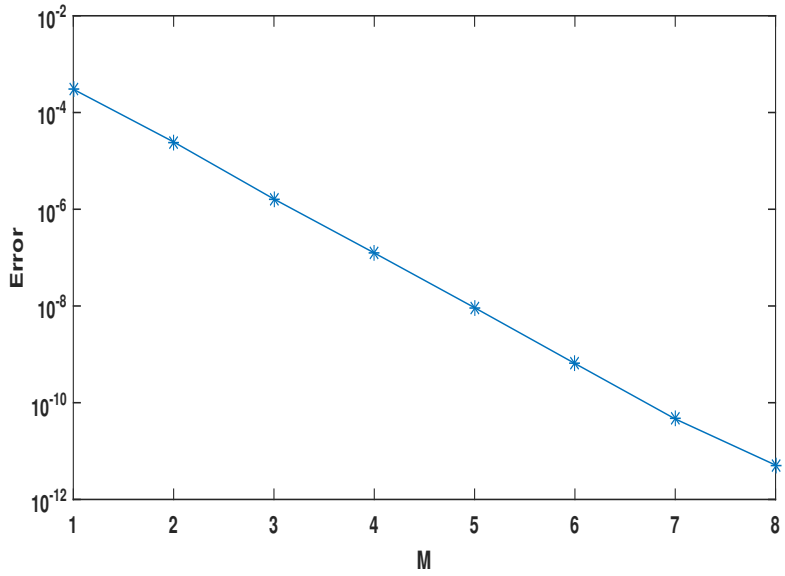

Figure 3.3: Behavior of the error $\mathcal{E}_1$ as a function of M for $N = 30$ and $\kappa = 6$.

approximation error with respect to the order M, for values ranging from 1 to 8.

Table 3.5: $\mathcal{E}_1$ and $\mathcal{O}$ at $\mathscr{C}_0$ when $N = 30$ and $\kappa = 6$.

M	ς	$\mathcal{E}_1$	$\mathcal{O}$
1	-0.92	3.0251e-04	-3.62
2	-0.90	2.4629e-05	-6.70
3	-0.92	1.6256e-06	-8.92
4	-0.90	1.2489e-07	-11.68
5	-0.90	9.2140e-09	-14.57
6	-0.90	6.4720e-10	-17.13
7	-0.90	4.6158e-11	-16.46
8	-0.90	5.1278e-12	–

Table 3.5 presents both the error and the corresponding rate of convergence as the order M increases, under the influence of the convergence-control parameter ς. These results clearly demonstrate the rapid convergence and high efficiency of the proposed method. Table 3.6 reports the results obtained using the proposed SHAM approach, corresponding to the solution of equation (3.53) after applying the transformations defined in equations (3.18) and (3.19).

Table 3.6: Comparison between absolute errors at selected $t \in [0;1]$ for various order M when $N = 30$ and $\kappa = 1$.

	SHAM			SHAM*		
t	$M = 2$ $\varsigma = -0.98$	$M = 4$ $\varsigma = -0.99$	$M = 8$ $\varsigma = -0.87$	$M = 2$ $\varsigma = -1.16$	$M = 4$ $\varsigma = -0.96$	$M = 8$ $\varsigma = -1.68$
0	0	0	0	0	0	0
0.10	2.4438e-12	1.9461e-11	1.9457e-11	9.9573e-05	9.4718e-09	4.9729e-12
0.21	1.4567e-09	3.7098e-11	3.6827e-11	3.8265e-04	1.9118e-09	9.4840e-12
0.30	9.2647e-09	4.7271e-11	4.5510e-11	6.6313e-04	1.8494e-07	1.2099e-11
0.40	3.3695e-08	5.4622e-11	4.7649e-11	9.3701e-04	9.6635e-07	1.4229e-11
0.5	7.7816e-08	5.9276e-11	4.0525e-11	1.1058e-03	2.9337e-06	3.9936e-11
0.60	1.1848e-07	6.1860e-11	2.5609e-11	1.0988e-03	6.2725e-06	3.2854e-10
0.70	1.1544e-07	6.2091e-11	8.8604e-12	9.1052e-04	1.0180e-05	1.7784e-09
0.80	5.4301e-08	6.0599e-11	3.6020e-12	5.9552e-04	1.3124e-05	5.8467e-09
0.90	6.8155e-08	5.3236e-11	1.0458e-11	5.9225e-05	1.3458e-05	1.7376e-08
1	1.1129e-07	6.2238e-12	7.9145e-12	5.0525e-04	8.4901e-06	3.3119e-08

Table 3.7: Comparison between absolute errors at selected $t \in [0;20]$ for various order M when $N = 60$ and $\kappa = 20$.

	SHAM			SHAM*		
t	$M = 2$ $\varsigma = -0.9$	$M = 4$ $\varsigma = -0.9$	$M = 8$ $\varsigma = -0.92$	$M = 2$ $\varsigma = -0.26$	$M = 4$ $\varsigma = -0.18$	$M = 8$ $\varsigma = -0.16$
0	0	0	0	0	0	0
1.91	8.6962e-06	9.1249e-09	2.5896e-11	7.5105e-02	7.2543e-02	4.0381e-02
4.12	1.9040e-05	1.1175e-07	1.0901e-11	2.9191e-02	2.9283e-02	2.9560e-02
5.93	7.1776e-06	5.8527e-08	1.0041e-11	7.2149e-03	7.2115e-03	7.2117e-03
7.92	1.5784e-06	1.4573e-08	3.0245e-12	1.3511e-03	1.3501e-03	1.3503e-03
10	2.7486e-07	2.6827e-09	5.9544e-13	2.1723e-04	2.1683e-04	2.1698e-04
12.08	4.4057e-08	4.4305e-10	9.9111e-14	3.3652e-05	3.3452e-05	3.3540e-05
14.07	7.3016e-09	7.4758e-11	1.4732e-14	5.7297e-06	5.6111e-06	5.6637e-06
15.87	1.3833e-09	1.4325e-11	9.5734e-16	1.2756e-06	1.1966e-06	1.2295e-06
18.09	1.7667e-10	1.8475e-12	8.9651e-16	3.0872e-07	2.5626e-07	2.6937e-07
20	2.9397e-11	3.0969e-13	5.1313e-17	1.1133e-05	9.1256e-06	1.5212e-05

For comparison, results from the classical SHAM method (denoted as SHAM*) are also included, where the solution was computed directly using the standard formulation. It is evident that the proposed approach yields significantly improved accuracy over the classical SHAM method. Furthermore, Table 3.7 demonstrates the robustness and effectiveness of the algorithm even when applied over large time intervals.

Table 3.8 show that the numerical solutions always maintain their good accuracy.

Table 3.8: $\mathcal{E}_1$ for various κ.

κ	1	6	12	24	50	100
$\mathcal{E}_1$	7.1370e-12	5.1278e-12	1.0168e-12	5.8231e-12	4.1395e-12	1.4916e-11

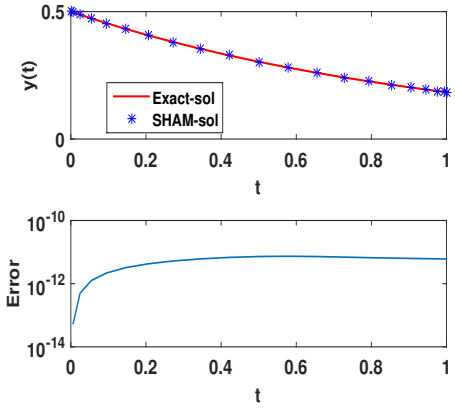

(a) $M = 5$, $N = 20$, $\varsigma = -0.98$, $\kappa = 1$.

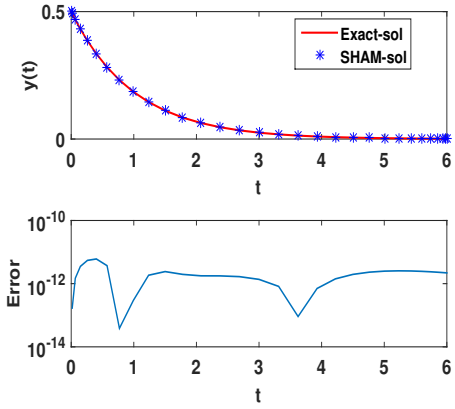

(b) $M = 8$, $N = 30$, $\varsigma = -0.9$, $\kappa = 6$.

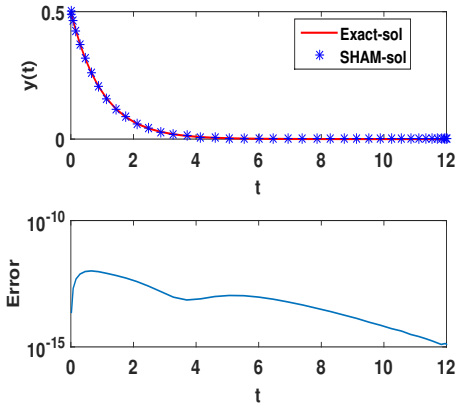

(c) $M = 10$, $N = 40$, $\varsigma = -0.92$, $\kappa = 12$.

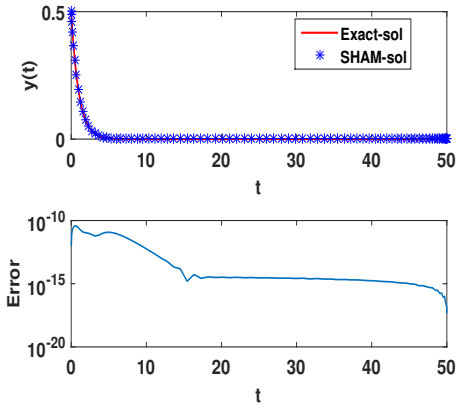

(d) $M = 8$, $N = 80$, $\varsigma = -0.92$, $\kappa = 50$.

Figure 3.4: Exact and approximate solutions with error behavior

Figure 3.4 depicts both the exact and numerical solutions of equation (3.53). It is evident that the numerical results closely match the exact solution. The corresponding approximation error further confirms the high accuracy and reliability of the proposed method. Table 3.9 presents the error $\mathcal{E}_1$ for approximation orders ranging from 2 to 12, comparing the performance of the proposed SHAM method with that of the classical SHAM* approach. The results clearly demonstrate that the proposed method achieves significantly improved convergence, highlighting its superiority in delivering more accurate solutions across a range of approximation orders.

Table 3.9: Comparison between the error $\mathcal{E}_1$ for various order M using SHAM and SHAM*.

	$\kappa = 1; N = 30$		$\kappa = 20; N = 60$	
Order M	$\mathcal{E}_1$ (SHAM)	$\mathcal{E}_1$ (SHAM*)	$\mathcal{E}_1$ (SHAM)	$\mathcal{E}_1$ (SHAM*)
2	2.3700e-05	8.5293e-02	1.2445e-07	1.1263e-03
4	1.2155e-07	8.4361e-02	8.2458e-11	1.3913e-05
6	9.0366e-10	8.2567e-02	5.2943e-11	2.8966e-07
8	5.8936e-11	8.7441e-02	5.1264e-11	3.3119e-08
10	6.0148e-11	8.8255e-02	5.2184e-11	6.8170e-10
12	6.0177e-11	7.6333e-02	5.1948e-11	1.8091e-11

Example 3.3. *Let us consider the damping Duffing equation [3, 8]:*

$$\frac{d^2y}{dt^2} + \frac{dy}{dt} + y^3 = 0, \quad t \in [0, \kappa], \quad \kappa \to \infty, \tag{3.63}$$

with the initial conditions

$$y(0) = 1, \quad \textit{and} \quad \left.\frac{dy}{dt}\right|_{t=0} = 1. \tag{3.64}$$

Using the transformations (3.29) and (3.30) gives:

$$\mathscr{A}\left(y_0(t)\right) = 0, \quad \mathscr{A}(y) = y'' + y' + y. \tag{3.65}$$

$$\frac{4}{\kappa^2}\frac{d^2u}{d\eta^2} + \frac{2}{\kappa}\frac{du}{d\eta} + (1 + 3\mathcal{Y}_0^2(t))u + 3\mathcal{Y}_0(\eta)u^2 + u^3 + \varphi(\eta) = 0 \tag{3.66}$$

where

$$\mathcal{Y}_0(\eta) = 2e^{-\frac{\kappa}{4}(\eta+1)} \sin\left(\frac{\sqrt{3}}{4}\kappa(\eta+1) + \frac{\pi}{6}\right), \tag{3.67}$$

and

$$\varphi(\eta) = \frac{4}{\kappa^2}\frac{d^2\mathcal{Y}_0}{d\eta^2} + \frac{2}{\kappa}\frac{d\mathcal{Y}_0}{d\eta} + \mathcal{Y}_0(\eta) + \mathcal{Y}_0^3(\eta),$$

subject to the initial conditions (3.36).

We choose the linear operator of (3.66)

$$\mathscr{L}(u) = \frac{4}{\mathscr{A}^2}\frac{d^2u}{d\eta^2} + \frac{2}{\mathscr{A}}\frac{du}{d\eta} + (1 + 3\mathcal{Y}_0^2(\eta))u \tag{3.68}$$

the nonlinear operator is defined as

$$\mathscr{M}(u) = \mathscr{A}(u) + 3\mathcal{Y}_0(\eta)u^2 + u^3 \tag{3.69}$$

To solve equation (3.66), we begin by computing u_0, which is the solution of the system defined by equations (3.39)–(3.40), using the Spectral Homotopy Analysis Method (SHAM). By applying the ChebSCM to equation (3.39), we obtain the discrete system given in equation (3.41), subject to the initial conditions specified in (3.42), where

$$\mathbf{A} = \mathbf{D}^2 + \mathbf{D} + \mathrm{diag}(1 + 3\mathbf{Y}_0^2). \tag{3.70}$$

Hence, the zeroth-order deformation equation and s^{th}-order deformation equation with equations (3.57) and (3.58) give:

$$\begin{aligned}\mathscr{A}(u_s) =& \varsigma(1-\chi_s)\varphi(\eta) + (\chi_s + \varsigma)\mathscr{A}(u_{s-1}) \\ &+ \varsigma\left(3\mathcal{Y}_0\sum_{n=0}^{s-1} u_s u_{s-1-n} + \sum_{n=0}^{s-1} u_{s-1-n}\sum_{i=0}^{n} u_{n-i}u_i\right),\end{aligned} \tag{3.71}$$

subject to the initial condition (3.49). Now, applying the ChebSCM on equation (3.71) gives:

$$\mathbf{A}U_s = \varsigma(1-\chi_s)\Phi + \mathbf{A}U_{s-1} + \varsigma\left(3Y_0\sum_{n=0}^{s-1} U_s U_{s-1-n} + \sum_{n=0}^{s-1} U_{s-1-n}\sum_{i=0}^{n} U_{n-i}U_i\right), \tag{3.72}$$

with conditions (3.51), where

$$\mathbf{A} = \mathbf{D}^2 + \mathbf{D} + \mathrm{diag}\left(1 + 3\mathbf{Y}_0^2\right). \tag{3.73}$$

Now, substuting the initial guess y_0, the initial approximation u_0 and the solution u_s in (3.47) gives the solution y of our problem (3.63). Figure 3.5 illustrates, on the left-hand side, the error curves used to determine the optimal convergence-control parameter ς. Table 3.10 presents the variation in the approximation error as the order increases, clearly highlighting the rapid convergence achieved by the proposed method. The Figure 3.6 illustrates the numerical solution and the absolute error of the problem (3.63). Through the error curve, we deduce the effectiveness of our method used to solve this problem.

Table 3.11 presents the results obtained using our SHAM method alongside those from the

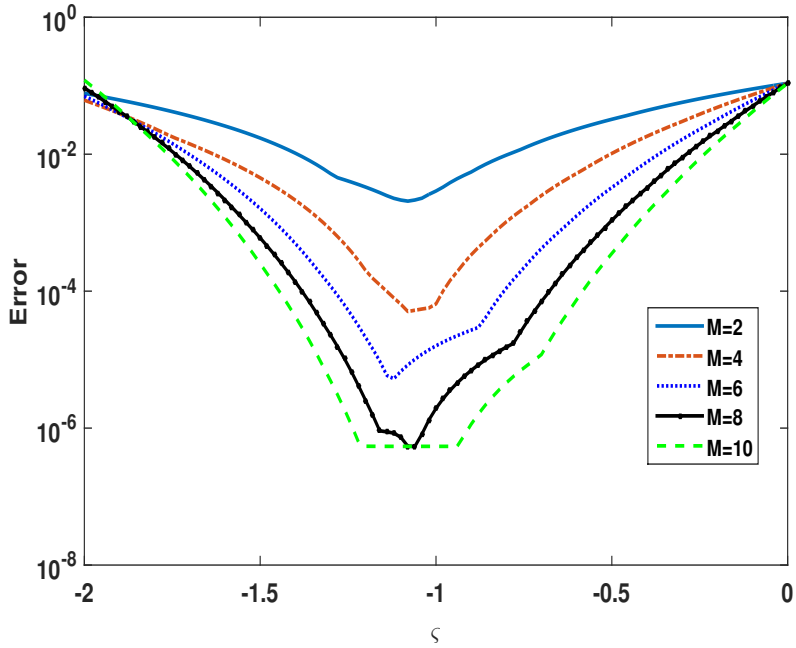

Figure 3.5: $\mathcal{E}_2$ as a function of ς for $N = 60$, $\kappa = 10$.

Table 3.10: $\mathcal{E}_2$ at selected ς when $N = 60$ and $\kappa = 10$.

M	ς	$\mathcal{E}_2$
2	-1.08	2.0629e-03
4	-1.08	5.0400e-05
6	-1.12	5.2447e-06
8	-1.06	5.4166e-07
10	-1.08	5.4106e-07
12	-0.84	5.4106e-07

classical SHAM*. It is evident that our approach delivers significantly improved accuracy compared to the classical method.

Example 3.4. *Let us consider the undamped Duffing equation as presented in [3, 8]:*

$$\frac{d^2y}{dt^2} + 3y - 2y^3 = \cos(t)\sin(2t), \quad t \in [0, \kappa], \quad \kappa \to \infty, \tag{3.74}$$

with the initial conditions

$$y(0) = 0, \quad \textit{and} \quad \left.\frac{dy}{dt}\right|_{t=0} = 1. \tag{3.75}$$

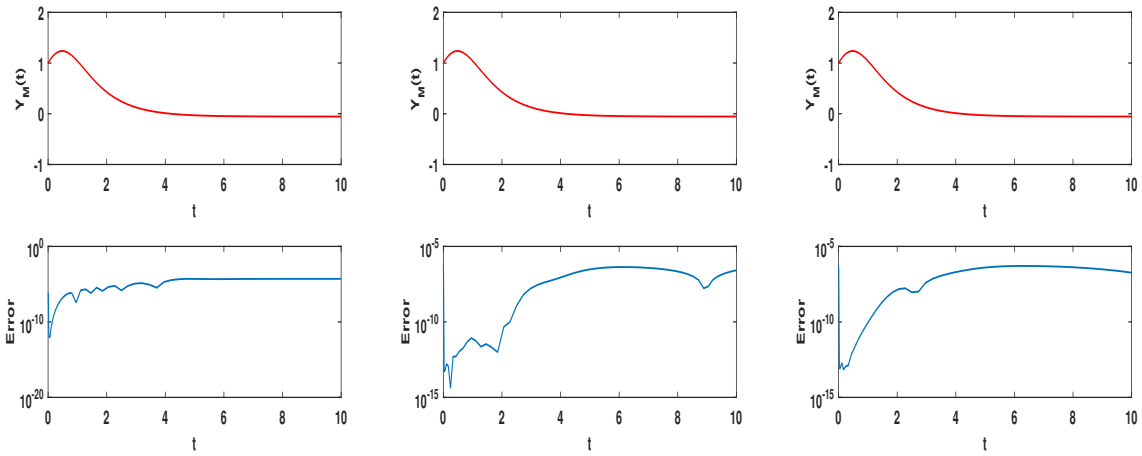

(a) $M = 4, \varsigma = -1.08$. (b) $M = 8, \varsigma = -1.06$. (c) $M = 12, \varsigma = -0.84$.

Figure 3.6: Numerical solutions with absolute error behavior for $N = 60$ and $\kappa = 10$.

Table 3.11: Comparison between absolute errors at selected $t \in [0; 1]$ for various order M when $N = 30$ and $\kappa = 1$.

	SHAM			SHAM*		
t	$M = 2$ $\varsigma = -1.02$	$M = 4$ $\varsigma = -1.02$	$M = 8$ $\varsigma = -1.14$	$M = 2$ $\varsigma = -1.15$	$M = 4$ $\varsigma = -1.08$	$M = 8$ $\varsigma = -0.98$
0,10	1.4063e-10	3.2489e-11	3.2716e-11	4.4078e-03	8.0083e-06	1.9218e-12
0,21	1.1046e-08	1.2397e-11	1.2625e-11	9.1183e-03	1.6441e-05	2.1225e-12
0,30	9.4002e-08	2.7758e-11	2.5737e-11	1.1374e-02	2.2527e-05	2.9765e-12
0,40	4.7359e-07	1.7853e-10	1.7434e-10	9.9335e-03	3.5939e-05	1.0006e-11
0,50	1.5241e-06	5.3286e-10	5.9268e-10	1.0406e-03	7.3896e-05	1.0730e-10
0,60	3.1502e-06	8.3623e-10	1.3499e-09	1.7208e-02	1.2541e-04	1.0680e-09
0,70	3.7882e-06	2.1352e-10	2.1104e-09	4.0187e-02	8.6406e-05	7.0086e-09
0,79	1.0278e-06	1.7256e-09	2.2397e-09	5.5366e-02	1.6189e-04	2.8150e-08
0,91	9.4839e-06	4.0434e-09	6.6537e-10	3.7257e-02	6.1064e-04	9.0087e-08
1	2.1483e-05	6.0259e-09	5.3284e-09	4.9826e-02	2.0184e-05	1.9054e-07

Using the transformations (3.29) and (3.30) gives:

$$\mathscr{A}\left(y_0(t)\right) = 0, \quad \mathscr{A}(y) = y'' + 3y. \tag{3.76}$$

$$\frac{4}{\kappa^2}\frac{d^2u}{d\eta^2} + (3 - 6\mathcal{Y}_0^2)u - 6\mathcal{Y}_0u^2 - 2u^3 + \varphi(\eta) = 0 \tag{3.77}$$

where

$$\mathcal{Y}_0(\eta) = \frac{\sin^3(\frac{\kappa}{2}(\eta+1))}{3} + \frac{\sqrt{3}}{3}\sin(\sqrt{3}\frac{\kappa}{2}(\eta+1)), \tag{3.78}$$

and

$$\varphi(\eta) = \frac{4}{\kappa^2}\frac{d^2\mathcal{Y}_0}{d\eta^2} + 3\mathcal{Y}_0 - 2\mathcal{Y}_0^3 - \cos(\frac{\kappa}{2}(\eta+1))\sin(\kappa(\eta+1)),$$

Based on the initial conditions (3.36), we employ the same procedure as in the first example to derive the solution for problem (3.74).

Figure 3.7 presents both the analytical and numerical solutions of equation (3.74), demonstrating a strong agreement between them. Furthermore, the approximation errors emphasize the high level of accuracy attained by the numerical solution in comparison to the exact one.

Tables 3.12 and 3.13 illustrate the effectiveness of our approximation method. As the order

Table 3.12: Comparison between SHAM and exact solutions for $M = 10, 20, 30$ with $\kappa = \pi$ and $N = 40$.

t	$M = 10$ $\varsigma = -1.34$	$M = 20$ $\varsigma = -1.34$	$M = 30$ $\varsigma = -1.32$	Exact sol
0	0	0	0	0
0.300	2.955154e-01	2.9551581577e-01	2.95515815660e-01	2.95515815660e-01
0.648	6.031978e-01	6.0319862354e-01	6.03198623316e-01	6.03198623318e-01
0.970	8.247028e-01	8.2470398201e-01	8.24703981718e-01	8.24703981720e-01
1.204	9.335160e-01	9.3351734777e-01	9.33517347477e-01	9.33517347478e-01
1.571	9.999990e-01	9.9999999997e-01	9.99999999993e-01	1
1.937	9.335198e-01	9.3351734606e-01	9.33517347470e-01	9.33517347478e-01
2.172	8.247098e-01	8.2470397917e-01	8.24703981707e-01	8.24703981720e-01
2.494	6.032066e-01	6.0319861901e-01	6.03198623304e-01	6.03198623318e-01
2.842	2.954977e-01	2.9551581061e-01	2.95515815643e-01	2.95515815660e-01
π	-2.895083e-04	-1.329572210e-07	-9.2389540463e-11	1.22464679915e-16

Table 3.13: Absolute error variation for $M = 2, 4, 6$ with $\kappa = \pi$ and $N = 40$.

t	$M = 4$ $\varsigma = -1.44$	$M = 10$ $\varsigma = -1.34$	$M = 20$ $\varsigma = -1.34$	$M = 30$ $\varsigma = -1.32$
0	0	0	0	0
0.300	1.80219e-06	4.42150e-07	1.13546e-10	1.51545e-14
0.646	3.50623e-06	8.50345e-07	2.20186e-10	2.40774e-12
0.970	9.97980e-06	1.14498e-06	2.84103e-10	2.16094e-12
1.204	6.39417e-05	1.34816e-06	2.91726e-10	1.97509e-13
1.571	5.30010e-04	1.07985e-06	3.12168e-11	6.58507e-12
1.937	3.23277e-04	2.41107e-06	1.41628e-09	7.19536e-12
2.172	1.25352e-04	5.84263e-06	2.54661e-09	1.36522e-11
2.494	2.51178e-04	7.98412e-06	4.30520e-09	1.43658e-11
2.842	1.21092e-03	1.81190e-05	5.04913e-09	1.76206e-11
π	2.37030e-03	2.89508e-04	1.32957e-07	9.23897e-11

M increases from 4 to 30, the error notably decreases, ranging approximately from 10^{-4} to 10^{-12}. This demonstrates that the accuracy of the solution improves significantly with higher values of M.

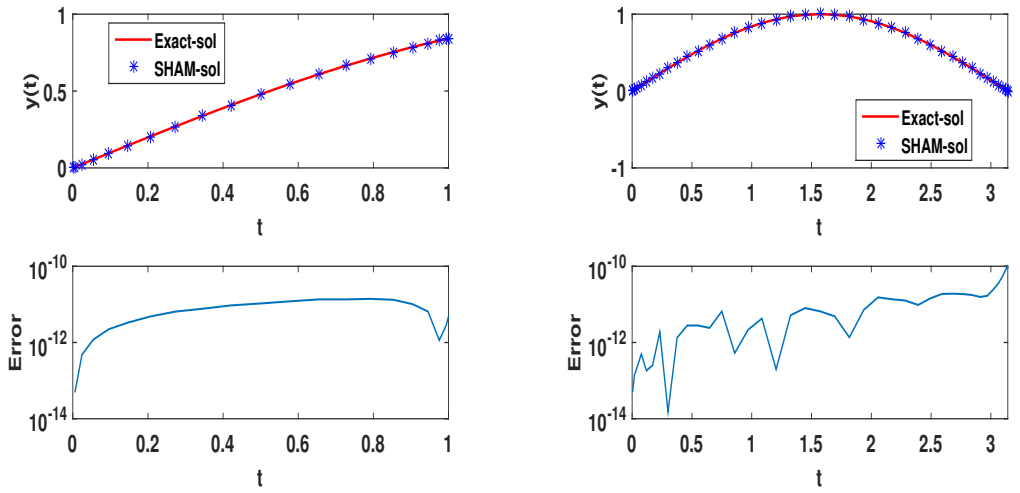

(a) $N = 20, \varsigma = -1.32, \kappa = 1, M = 14.$ (b) $N = 40, \varsigma = -1.32, \kappa = \pi, M = 30.$

Figure 3.7: Exact and approximate solutions with error behavior.

3.3 Conclusion

In this work, spectral methods were chosen for their proven efficiency, complemented by the use of collocation points to enhance the speed of convergence. The methodology involved iteratively refining the numerical solution, carefully selecting a suitable linear operator, and defining an initial approximation. To evaluate the accuracy of the proposed approach, we calculated the errors, which remained consistently low even over long time intervals, as evidenced in Table 3.8. The swift convergence behavior is highlighted in Table 3.5 through the convergence rate $\mathcal{O}$. Furthermore, the method demonstrated strong capability in dealing with highly oscillatory problems, as illustrated in Figure 3.2d. Importantly, the outcomes we obtained surpass the accuracy reported in [21].

Chapter 4

SHAM using Chelyshkov polynomials

CHAPTER 4

SHAM USING CHELYSHKOV POLYNOMIALS

4.1 SHAM using Chelyshkov polynomials

The spectral method is carried out on the interval $[a, b]$ by introducing the transformation $x = (b-a)t + a$, valid for $a \leq x \leq b$. This allows us to rewrite the solution given in (1.28) and its derivative (1.29) in matrix form at the collocation points:

$$\begin{aligned} \boldsymbol{\mathcal{Y}} &= \boldsymbol{C}(t)\boldsymbol{E} \\ \boldsymbol{\mathcal{Y}}' &= \frac{1}{b-a}\frac{d\boldsymbol{C}(t)}{dt}\boldsymbol{E} \\ \boldsymbol{\mathcal{Y}}'' &= \frac{1}{(b-a)^2}\frac{d^2\boldsymbol{C}(t)}{dt^2}\boldsymbol{E} \end{aligned} \tag{4.1}$$

where

$$\boldsymbol{\mathcal{Y}} = [y(x_0), \cdots, y(x_N)]^T, \ \boldsymbol{E} = [a_0, \cdots, a_N]^T, \text{ and } \boldsymbol{C}(t) = [C_{N0}(t)\ C_{N1}(t) \cdots C_{NN}(t)].$$

Substituting (1.28) and (4.1) in (3.5), we obtain

$$\mathcal{B}E_k = (\delta_k + \varsigma)\mathcal{B}E_{k-1} + \varsigma\mathcal{R}, \tag{4.2}$$

where $\mathcal{B}$ and $\mathcal{R}$ denote the matrix and vector, respectively, resulting from the application of the Chelyshcov transformations (1.28) and (4.1) to $\mathcal{L}$ and R_{k-1}, respectively. Moreover,

$$\mathbf{E}_k \quad = \quad (e_{k_0}, e_{k_1}, \ldots, e_{k_N})^T . \tag{4.3}$$

By appropriately imposing the boundary conditions in equation (4.2), we obtain

$$\mathcal{B}E_k = (\delta_k + \varsigma)\bar{\mathcal{B}}E_{k-1} + \varsigma\bar{\mathcal{R}}, \tag{4.4}$$

where $\bar{\mathcal{B}}$ and $\bar{\mathcal{R}}$ represent the modified matrix and vector, respectively, resulting from the implementation of the conditions at the boundaries on the right-hand side of the equation (4.2). Therefore

$$E_k = (\delta_k + \varsigma)\mathcal{B}^{-1}\bar{\mathcal{B}}E_{k-1} + \varsigma\mathcal{B}^{-1}\bar{\mathcal{R}}. \tag{4.5}$$

Here, $\mathcal{B}^{-1}$ denotes the inverse of the matrix $\mathcal{B}$. Equation (4.5) defines an iterative relation that facilitates the computation of k^{th}-order approximation $A_k, k \geq 1$.

The following transformation is introduced to guarantee homogeneous boundary conditions [6, 7, 30, 37, 46]:

$$y(x) = u(t) + y_0(x). \tag{4.6}$$

Substituting (4.6) into (3.1) yields

$$\mathscr{A}(u(t)) + \mathcal{M}(u(t)) = \mathscr{H}(x),$$

subject to

$$P\left(u(t), u'(t), \ldots\right) = 0, \quad t = \frac{x-a}{b-a}, \quad a \leq x \leq b,$$

where P is a linear operator, and

$$\mathscr{H}(x) = f(x) - \mathscr{A}\left(y_0(x)\right) - \mathcal{M}\left(y_0(x)\right).$$

Then, the zeroth-order deformation equation within the context of HAM becomes

$$(1-\varrho)\mathscr{A}\left(\phi(t;\varrho) - u_0(t)\right) = \varrho\varsigma\left(\mathscr{A}(\phi(t;\varrho)) + \mathcal{M}(\phi(t;\varrho)) - \mathscr{H}(x)\right), \quad 0 \leq \varrho \leq 1,$$

where $\phi(x;\varrho)$ is an unknown function. The deformation equation of order k reads

$$\mathscr{A}\left(u_k(x)-(\delta_k+\varsigma)\,u_{k-1}(x)\right)=\varsigma\mathscr{R}_{k-1}\left(x\right), \tag{4.7}$$

where

$$\mathscr{R}_{k-1}\left(x\right)=\frac{1}{(k-1)!}\frac{\partial^{k-1}\left(\mathcal{M}(\phi(t;\varrho))-\mathscr{H}(x)\right)}{\partial\varrho^{k-1}}\bigg|_{\varrho=0}.$$

Hence, the homotopy series solution is

$$y(x)=y_0(x)+u_0(t)+\sum_{k=1}^{+\infty}u_k(t). \tag{4.8}$$

The starting approximation $u_0(x)$ is obtained by solving the equation

$$\mathscr{A}\left(u_0(t)\right)=\mathscr{H}(x), \tag{4.9}$$

with

$$u_0(0)=u'(0)=0. \tag{4.10}$$

To solve (4.9), we use Chelyshkov spectral collocation method, so

$$\mathbf{B}A_0=\mathbf{H}, \tag{4.11}$$

subject to

$$U_0(0)=U_0'(0)=0, \tag{4.12}$$

where

$$\begin{aligned} U_0 &= \mathbf{C}(t)A_0, \\ \mathbf{H} &= (\mathscr{H}(x_0),\mathscr{H}(x_1),...,\mathscr{H}(x_{N-1}))^T. \end{aligned}$$

By following the same procedure that led to equation (4.5), we derive

$$\begin{cases} \boldsymbol{A}_0=\mathcal{B}^{-1}\bar{\mathbf{H}} \\ \boldsymbol{A}_k=(\delta_k+\varsigma)\mathcal{B}^{-1}\bar{\mathcal{B}}\boldsymbol{A}_{k-1}+\varsigma\mathcal{B}^{-1}\bar{\mathcal{R}}. \end{cases} \tag{4.13}$$

Equation (4.13) thus defines an iterative relation that facilitates the computation of kthorder approximations $A_k, k \geq 1$.

$$\begin{aligned} \boldsymbol{U} &= \boldsymbol{C}(t)\boldsymbol{A} \\ \mathbf{A}_k &= (a_{k_0}, a_{k_1}, \ldots, a_{k_N})^T \\ \boldsymbol{U} &= (u(t_0), u(t_1), ..., u(t_N))^T . \end{aligned} \tag{4.14}$$

4.2 Numerical tests

We now consider the use of SHAM for solving Lane-Emden-type equations. The performance of the method is assessed by calculating the absolute error through the expression:

$$\mathcal{E} = \max_j |y(x_j) - y_N(x_j)|, \quad j = 0, 1, ..., N. \tag{4.15}$$

To analyse the numerical convergence behavior, the convergence rate is estimated based on the error defined by (3.25). where $\mathcal{E}(M)$ represents the error calculated for order M
We display the graphs of the computed solution, the corresponding error distribution, and the profile used to determine the optimal convergence-control parameter. All numerical experiments are performed using MATLAB 2015.

4.2.1 Nonlinear case

Example 4.1. *We focus on a Lane-Emden-type model described by:*

$$y'' + \frac{2}{x}y' + y^2 = e^{x^2}(6 + 4x^2) + e^{2x^2}, \quad x \in [0, \kappa]. \tag{4.16}$$

This problem is equipped with the values $y(0) = 1$ and $y'(0) = 0$ at the origin. Its exact solution is given by $y(x) = \exp(x^2)$.

The linear and nonlinear operators are considered as follows :

$$L(y) = y'' + \frac{2}{x}y', \qquad N(y) = y'' + \frac{2}{x}y' + y^2$$

To simplify the numerical treatment, we rescale the domain $[0, \kappa]$ to the unit interval $[0, 1]$ via the transformation

$$x = \kappa t, \quad t \in [0, 1]. \tag{4.17}$$

Applying the following substitution:

$$y(x) = y_0(x) + u(t), \tag{4.18}$$

with $y_0(x) = x^2 + 1$ taken as an initial approximation, and inserting it into equation (4.16), we arrive at:

$$\frac{1}{\kappa^2}u'' + \frac{2}{\kappa x}u' + 2y_0u + u^2 = \mathscr{H}(x), \tag{4.19}$$

accompanied by the conditions:

$$u(0) = u'(0) = 0,$$

and the source term $\mathscr{H}(x)$ is defined as:

$$\mathscr{H}(x) = -y_0'' - \frac{2}{x}y_0' - y_0^2 + e^{x^2}(6 + 4x^2) + e^{2x^2}.$$

Accordingly, the modified linear and nonlinear operators are given by:

$$\mathscr{A}(u) = \frac{1}{\kappa^2}u'' + \frac{2}{\kappa x}u' + 2y_0u, \qquad \mathcal{M}(u) = \frac{1}{\kappa^2}u'' + \frac{2}{\kappa x}u' + 2y_0u + u^2.$$

By replacing $l\mathscr{A}$, $\mathcal{M}$ in (4.7), we have:

$$\mathscr{A}(u_k) = (\delta_k + \varsigma)\mathscr{A}(u_{k-1}) + \varsigma\left[-(1-\delta_k)\mathscr{H} + \sum_{i=0}^{k-1} u_i u_{k-i-1}\right], \tag{4.20}$$

such that

$$u_k(0) = u_k'(0) = 0. \tag{4.21}$$

Using Eqs. (1.28) and (4.1), the equation (4.20) becomes:

$$\mathbf{B}\mathbf{A}_k = (\delta_k + \varsigma)\mathbf{B}\mathbf{A}_{k-1} + \varsigma\left[-(1-\delta_k)\mathbf{H} + \sum_{i=0}^{k-1}(\mathbf{C}(t)\mathbf{A}_i)(\mathbf{C}(t)\mathbf{A}_{k-i-1})\right]. \tag{4.22}$$

Where

$$\mathbf{B} = \frac{1}{\kappa^2}\mathbf{C}''(t) + \mathbf{diag}(\frac{2}{Lx})\mathbf{C}'(t) + 2\mathbf{diag}(y_0)$$
$$\mathbf{A}_k = (a_{k_0}, a_{k_1}, ..., a_{k_N})^T.$$

Imposing initial conditions (4.21) appropriately in the equation (4.22) yields

$$\begin{cases} \mathbf{A}_0 = \mathbf{B}^{-1}\bar{\mathbf{H}}, \\ \mathbf{A}_k = (\delta_k + \varsigma)\mathbf{B}^{-1}\bar{\mathbf{B}}\mathbf{A}_{k-1} + \varsigma\mathbf{B}^{-1}\left[-(1-\delta_k)\bar{\mathbf{H}} + \sum_{i=0}^{k-1}(\mathbf{C}(t)\mathbf{A}_i)(\mathbf{C}(t)\mathbf{A}_{k-i-1})\right]. \end{cases} \tag{4.23}$$

Matrix $\bar{\mathbf{B}}$ is a modified version of matrix $\mathbf{B}$, where the first and second rows have been set to zero, while all other entries remain unchanged. Similarly, vector $\bar{\mathbf{H}}$ is derived from vector $\mathbf{B}$, with the first two elements set to zero, to match the given initial data.

Figure 4.1 presents error curves that aid in determining the optimal value of the parameter

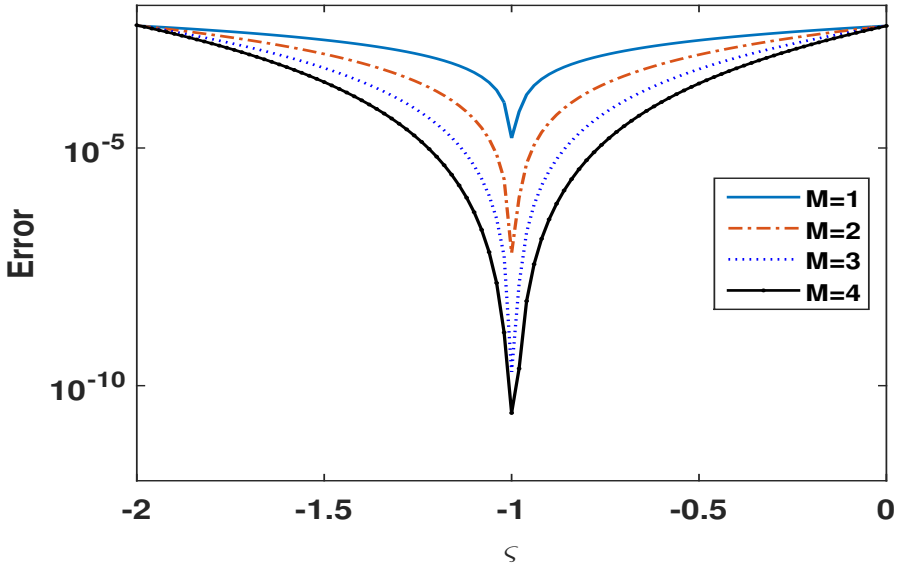

Figure 4.1: Error as a function of ς for Example 4.1.

that controls convergence ς with $N = 15$ and $\kappa = 1$.

Table 4.1 displays numerical results produced by applying SHAM across different approximation levels, alongside the corresponding exact values. The comparison illustrates the method's strong performance in terms of precision and computational efficiency, underscoring its robustness and suitability for addressing this class of equations. Figure 4.2 depicts a comparison between the computed and analytical solutions. The near-perfect overlap of the two curves confirms the remarkable precision achieved by the method. This observation is reinforced by the corresponding absolute error plot, which remains nearly flat and close to zero throughout the domain, showcasing the accuracy and efficiency of the implemented approach. Table 4.2 illustrates the error and convergence rate as the parameter ς varies with

Table 4.1: Evaluating the SHAM against the exact solution for the case $\kappa = 1$, $\varsigma = -1$, and $N = 15$ for Example 4.1.

x	$M = 1$	$M = 2$	$M = 4$	Exact sol
0	1.000000000000	1.000000000000	1.00000000000000	1.00000000000000
0,01	1.000119389072	1.000119388948	1.00011938896677	1.00011938896472
0,04	1.001870344531	1.001870343790	1.00187034390147	1.00187034388881
0,1	1.009160329211	1.009160328329	1.00916032846104	1.00916032844618
0,17	1.027746601134	1.027746600205	1.02774660034397	1.02774660032811
0,5	1.064494459734	1.064494458793	1.06449445893373	1.06449445891786
0,35	1.126780418881	1.126780417947	1.12678041808730	1.12678041807137
0,45	1.221973676149	1.221973675257	1.22197367539461	1.22197367537915
0,55	1.356619280159	1.356619280035	1.35661928016785	1.35661928015284
0,65	1.534771277802	1.534771289422	1.53477128954642	1.53477128953225
0,75	1.755054537280	1.755054656926	1.75505465697248	1.75505465696030
0,83	2.006714650913	2.006715379109	2.00671537833900	2.00671537832539
0,9	2.266267841814	2.266270715690	2.26627071000402	2.26627070998778
0,96	2.497801725244	2.497809288944	2.49780926730229	2.49780926727809
0,99	2.659829279484	2.659842739357	2.65984269168939	2.65984269166280
1	2.718265589756	2.718281890413	2.71828182847822	2.71828182845905

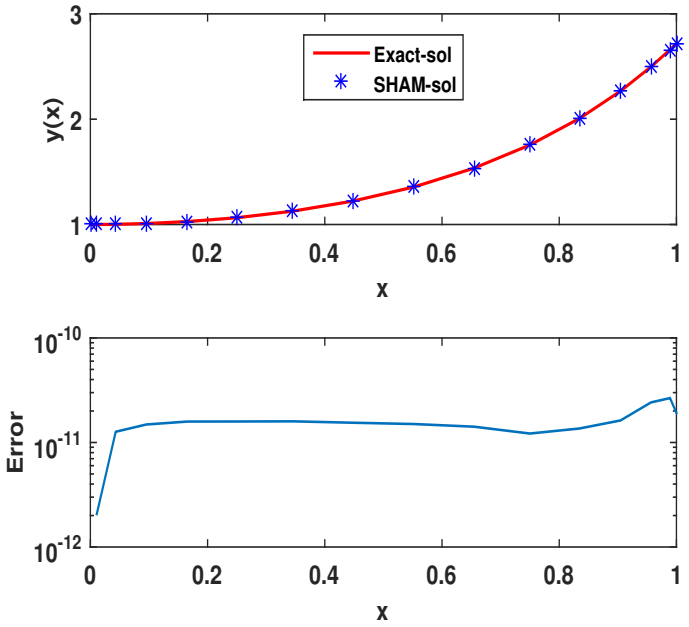

Figure 4.2: Exact vs. approximate solution with absolute error for $M = 4$, $N = 15$, and $\varsigma = -1$ for Example 4.1.

the order M, varies from 1 to 4. The results indicate good convergence, confirming the efficiency and reliability of the SHAM.

Table 4.2: Error norm and the order of convergence when $N = 15$ for Example 4.1.

Order (M)	ς	$\mathcal{E}$	$\mathcal{O}$
1	-1	1.62387e-05	-8.03402
2	-1	6.19541e-08	-14.20895
3	-1	1.94984e-10	-6.92565
4	-1	2.65898e-11	———

Example 4.2. *Consider the nonlinear differential equation defined in [48]:*

$$y'' + \frac{2}{x}y' + y^3 = 6 + x^6, \quad x \in (0, \kappa], \tag{4.24}$$

where $y(0) = 0,\ y'(0) = 0$ *and* $y(x) = x^2$.

Using the relation (4.18) gives:

$$\frac{1}{\kappa^2}u'' + \frac{2}{\kappa x}u' + 3y_0^2u + 3y_0u^2 + u^3 = g(x), \tag{4.25}$$

with

$$u(0) = u'(0) = 0,$$

where

$$\mathscr{H}(x) = -y_0'' - \frac{2}{x}y_0' - y_0^3 + 6 + x^6$$

, and $y_0(x) = x^2 + \frac{x^8}{72}$ is chosen as a solution of the linear part of (4.24).

The modified linear operator and the corresponding nonlinear operator are defined as:

$$\mathscr{A}(u) = \frac{1}{\kappa^2}u'' + \frac{2}{\kappa x}u' + 3y_0^2u, \qquad \mathcal{M}(u) = \frac{1}{\kappa^2}u'' + \frac{2}{\kappa x}u' + 3y_0^2u + 3y_0u^2 + u^3.$$

By replacing $\mathscr{A}$, $\mathcal{M}$and (4.8) in (4.7) , we have:

$$\mathscr{A}(u_k) = (\delta_k+\varsigma)\mathscr{A}(u_{k-1})+\varsigma\left[-(1-\delta_k)\mathscr{H} + 3y_0^2\sum_{i=0}^{k-1}u_iu_{k-i-1} + \sum_{i=0}^{k-1}u_{k-i-1}\sum_{p=0}^{i}u_{i-p}u_p\right]. \tag{4.26}$$

Using Eqs. (1.28) and (4.1), the equation (4.26) becomes:

$$\mathbf{B}\mathbf{A}_k = (\delta_k + \varsigma)\mathbf{B}\mathbf{A}_{k-1} + \varsigma\left[-(1-\delta_k)\mathbf{H} + 3y_0\sum_{i=0}^{k-1}(\mathbf{C}(t)\mathbf{A}_i)(\mathbf{C}(t)\mathbf{A}_{k-i-1})\right.$$

$$+\sum_{i=0}^{k-1}(\mathbf{C}(t)\mathbf{A}_{k-i-1})\sum_{p=0}^{i}(\mathbf{C}(t)\mathbf{A}_{i-p})(\mathbf{C}(t)\mathbf{A}_p)\Bigg],$$

where

$$\mathbf{B}=\frac{1}{\kappa^2}\mathbf{C}''(t)+\mathbf{diag}(\frac{2}{\kappa x})\mathbf{C}'(t)+3\mathbf{diag}(y_0^2).$$

In the end, we find this system:

$$\begin{cases}\mathbf{A}_0=\mathbf{B}^{-1}\bar{\mathbf{H}},\\ \mathbf{A}_k=(\delta_k+\varsigma)\mathbf{B}^{-1}\bar{\mathbf{B}}\mathbf{A}_{k-1}+\varsigma\mathbf{B}^{-1}\Bigg[-(1-\delta_k)\bar{\mathbf{H}}+3y_0\sum_{i=0}^{k-1}(\mathbf{C}(t)\mathbf{A}_i)(\mathbf{C}(t)\mathbf{A}_{k-i-1})\\ \qquad+\sum_{i=0}^{k-1}(\mathbf{C}(t)\mathbf{A}_{k-i-1})\sum_{p=0}^{i}(\mathbf{C}(t)\mathbf{A}_{i-p})(\mathbf{C}(t)\mathbf{A}_p)\Bigg].\end{cases}\tag{4.27}$$

Table 4.3 presents the rate of convergence $\mathcal{O}$, and the error $\mathcal{E}$, with the corresponding op-

Table 4.3: Error $\mathcal{E}$ and the order of convergence when $N=8$ for Example 4.2.

Order (M)	ς	$\mathcal{E}$	$\mathcal{O}$
1	-1	3.15242e-09	-9.77852
2	-1	3.58935e-12	-16.77144
3	-1	3.99680e-15	-14.09029
4	-1	6.93889e-17	———

timal parameter ς as the order M increases from 1 to 4. The results demonstrate consistent convergence, underscoring the accuracy and robustness of the SHAM approach.

Table 4.4 displays the variation in the order M from 1 to 4. The results clearly indicate

Table 4.4: Errors variation for $M=1,2,3,4$ with $\varsigma=-1$, $\kappa=1$, and $N=8$ for Example 4.2.

x	$M=1$	$M=2$	$M=3$	$M=4$
0.038	2.17409e-10	1.88135e-13	2.04481e-16	1.04083e-17
0.146	1.28739e-09	1.11298e-12	1.21084e-15	6.24501e-17
0.309	1.54188e-09	1.34134e-12	1.45717e-15	6.93889e-17
0.5	1.62489e-09	1.46744e-12	1.55431e-15	5.55111e-17
0.691	1.67594e-09	1.69353e-12	1.83187e-15	5.55112e-17
0.854	1.85855e-09	2.14395e-12	2.33147e-15	0
0.962	2.56109e-09	2.98483e-12	3.33067e-15	0
1	3.15242e-09	3.58935e-12	3.99680e-15	0

a significant decrease in error with increasing order, emphasizing the effectiveness of the

SHAM in enhancing accuracy over the interval $[0, 1]$.

Figure 4.3 presents both the exact and numerical solutions of equation (4.24). The close

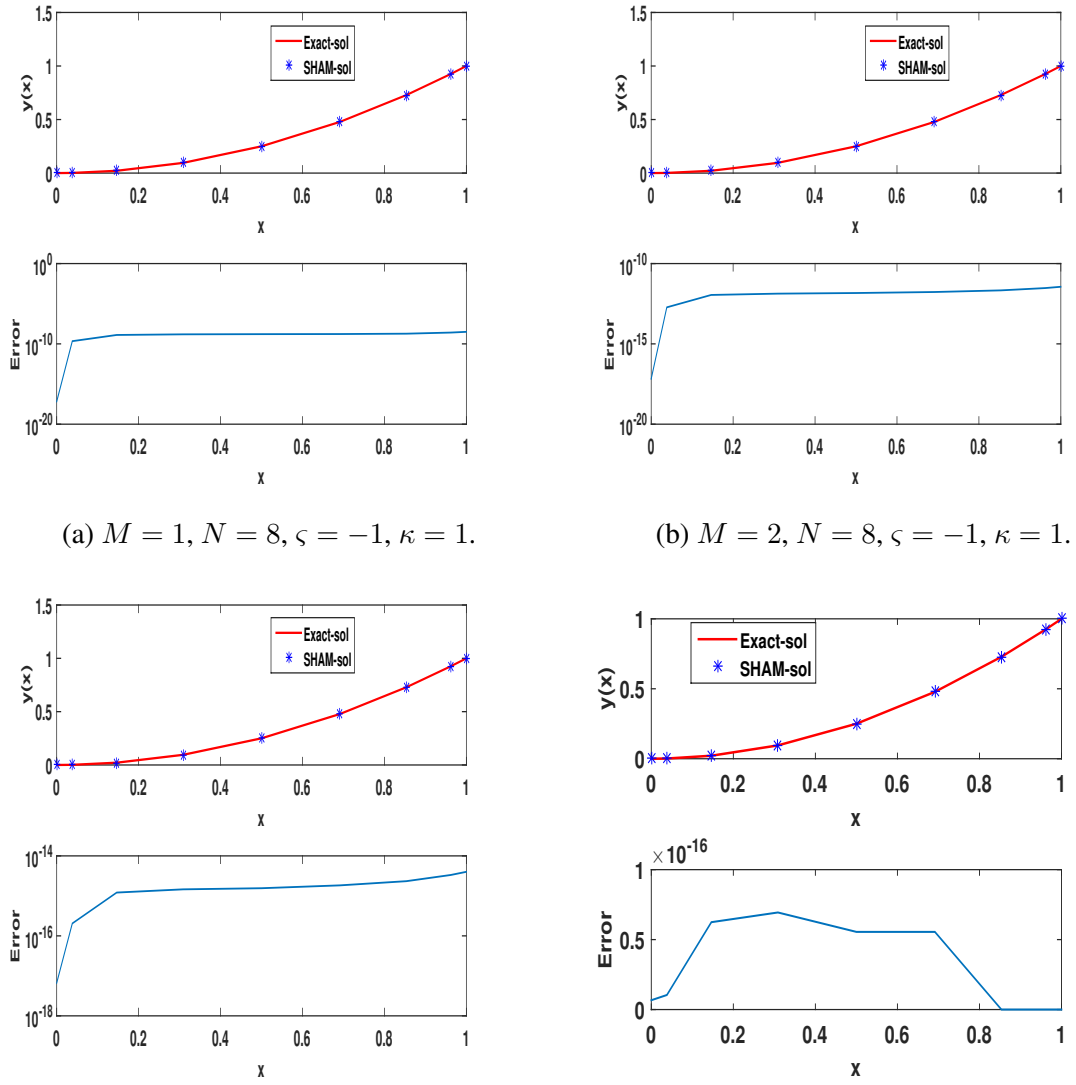

(a) $M = 1, N = 8, \varsigma = -1, \kappa = 1.$ (b) $M = 2, N = 8, \varsigma = -1, \kappa = 1.$

(c) $M = 3, N = 8, \varsigma = -1, \kappa = 1.$ (d) $M = 4, N = 8, \varsigma = -1, \kappa = 1.$

Figure 4.3: Analysis of exact and approximate solutions with error trends, for Example 4.2.

agreement between them highlights the precision of the numerical approach, while the associated error curves further confirm the accuracy and reliability of the proposed method.

4.2.2 Linear case

Example 4.3. *We now consider a homogeneous Lane-Emden-type equation, as discussed in [40, 48, 50]:*

$$y'' + \frac{2}{x}y' - 2(2x^2 + 3)y = 0, \quad x \in (0, \kappa], \tag{4.28}$$

with $y(0) = 1$ *and* $y'(0) = 0$. *The exact solution is* $y(x) = \exp(x^2)$.

Using the relation (4.18) gives:

$$\frac{1}{\kappa^2}u'' + \frac{2}{\kappa x}u' - 2(2x^2+3)u = \mathscr{H}(x), \tag{4.29}$$

such that

$$u(0) = u'(0) = 0,$$

where

$$\mathscr{H}(x) = -y_0'' - \frac{2}{x}y_0' - (4x^2+6)y_0 \quad \text{and} \quad y_0(x) = x^2 + 1.$$

The linear operator is defined as:

$$\mathscr{A}(u) = \frac{1}{\kappa^2}u'' + \frac{2}{\kappa x}u'.$$

By replacing $\mathscr{A}$ and (4.8) in (4.7), we have:

$$\mathscr{A}(u_k) = (\delta_k + \varsigma)\mathscr{A}(u_{k-1}) + \varsigma\left[-(1-\delta_k)\mathscr{H} - 2(2x^2+3)u_{k-1}\right]. \tag{4.30}$$

Substituting Eqs. (1.28) and (4.1) into the equation (4.30) gives:

$$\mathbf{B}\mathbf{A}_k = (\delta_k + \varsigma)\mathbf{B}\mathbf{A}_{k-1} + \varsigma\left[-(1-\delta_k)\mathbf{H} - 2(2x^2+3)\left((\mathbf{C}(t)\mathbf{A}_{k-1})\right]\right., \tag{4.31}$$

where

$$\mathbf{B} = \frac{1}{\kappa^2}\mathbf{C}''(t) + diag(\frac{2}{\kappa x})\mathbf{C}'(x) - 2\mathbf{diag}(2x^2+3), \tag{4.32}$$

and

$$u_k(0) = u_k'(0) = 0.$$

Finally, we solve this system:

$$\begin{cases} \mathbf{A}_0 = \mathbf{B}^{-1}\bar{\mathbf{H}}, \\ \mathbf{A}_k = (\delta_k + \varsigma)\mathbf{B}^{-1}\bar{\mathbf{B}}\mathbf{A}_{k-1} + \varsigma\mathbf{B}^{-1}\left[-(1-\delta_k)\bar{\mathbf{H}} - 2(2x^2+3)(\mathbf{C}(t)\mathbf{A}_{k-1})\right]. \end{cases} \tag{4.33}$$

Table 4.5 provides a comparative assessment of the error rates obtained using three distinct approaches: the proposed SHAM method, the LT-HPM method from [48], and the ADM

Table 4.5: Error variation using SHAM, LT-HPM and ADM for $M = 4, L = 1$ and $N = 15$ for Example 4.3.

x	SHAM	LT-HPM [48], ADM [50]
0	0	0
0.01	4.4595e-12	0
0.04	2.6948e-11	0
0.10	3.2293e-11	1.2434e-14
0.17	3.5306e-11	3.0831e-12
0.25	3.7788e-11	1.9898e-10
0.35	4.6569e-11	5.3770e-09
0.45	7.3402e-11	7.8328e-08
0.55	5.6659e-12	7.1212e-07
0.65	7.3054e-10	4.4137e-06
0.75	1.4939e-09	1.9680e-05
0.83	5.1594e-09	6.5194e-05
0.90	3.3396e-08	1.6351e-04
0.96	8.4202e-08	3.1372e-04
0.99	1.3252e-07	4.6303e-04
1	1.5147e-07	5.2707e-04

technique from [50]. The results reveal that SHAM consistently yields the lowest error, underscoring its advantage in minimizing computational inaccuracies. Moreover, SHAM exhibits rapid convergence toward accurate solutions, confirming its efficiency and suitability for solving problems that demand both high precision and fast computational performance.

Table 4.6 provides a side-by-side comparison of the numerical results produced by SHAM, LT-HPM, and ADM with the exact solution of the problem under consideration. The results indicate that the approximations produced by the proposed SHAM exhibit a high degree of accuracy, closely aligning with the exact solution. This demonstrates the superior precision and reliability of SHAM compared to the other methods, underscoring its effectiveness in solving complex mathematical problems. Moreover, the improved accuracy of SHAM highlights its potential for applications requiring highly precise numerical approximations and rapid convergence to optimal solutions. Figure 4.4 illustrates the exact solution together with the approximations produced by the three different methods for visual comparison. At first glance, all solution curves appear to overlap. However, upon magnifying a specific region of the graph, it becomes evident that the SHAM curve closely follows the exact solution, whereas the curves corresponding to the LT-HPM and ADM methods deviate from it. This highlights the superior accuracy and effectiveness of SHAM in providing highly precise numerical approximations, reinforcing its reliability in solving complex mathematical

Table 4.6: Comparison between SHAM, LT-HPM, ADM and the exact solution with $M = 4, L = 1$ and $N = 15$ for Example 4.3.

x	SHAM	LT-HPM [48], ADM [50]	Exact sol
0	1.000000000000000	1.000000000000000	1.000000000000000
0.0109	1.000119388969177	1.000119388964718	1.000119388964718
0.0432	1.001870343915754	1.001870343888806	1.001870343888806
0.0955	1.009160328478472	1.009160328446166	1.009160328446179
0.1654	1.027746600363419	1.027746600325030	1.027746600328113
0.2500	1.064494458955647	1.064494458718876	1.064494458917859
0.3455	1.126780418117939	1.126780412694419	1.126780418071369
0.4477	1.221973675452556	1.221973597050772	1.221973675379154
0.5523	1.356619280147169	1.356618568034100	1.356619280152835
0.6545	1.534771288801716	1.534766875817270	1.534771289532253
0.7500	1.755054655466403	1.755034977180114	1.755054656960298
0.8346	2.006715383484737	2.006650184084876	2.006715378325386
0.9045	2.266270743383852	2.266107204814253	2.266270709987778
0.9568	2.497809351479664	2.497495550209225	2.497809267278094
0.9891	2.659842824183984	2.659379657298854	2.659842691662801
1.0000	2.718281979931200	2.717754761889216	2.718281828459046

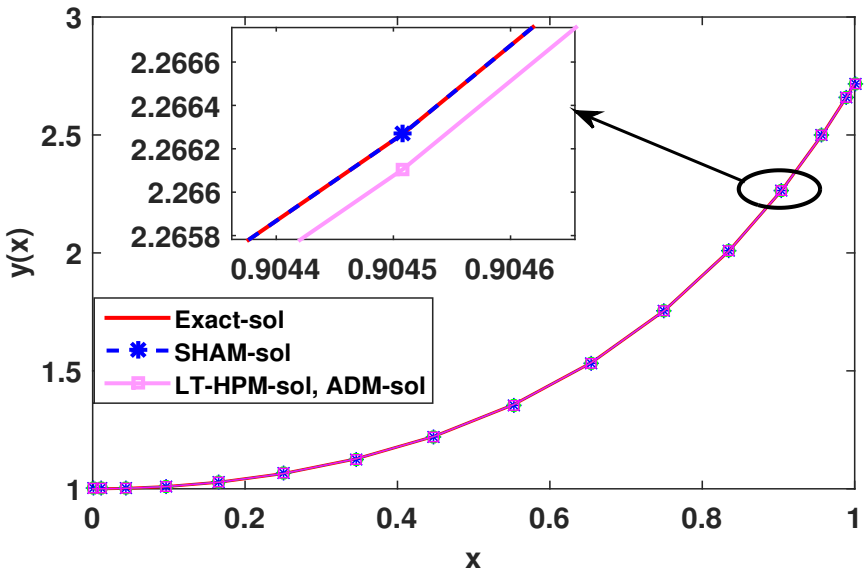

Figure 4.4: A review of the exact solution versus the approximations using SHAM, LT-HPM and ADM for Example 4.3.

problems. Figure 4.5 further supports this conclusion by displaying the corresponding error curves. It clearly shows that the error associated with SHAM remains significantly lower across the entire domain compared to the other two methods. This demonstrates the high accuracy and stability of SHAM in minimizing computational errors, further validating its advantage over traditional approaches in numerical problem-solving.

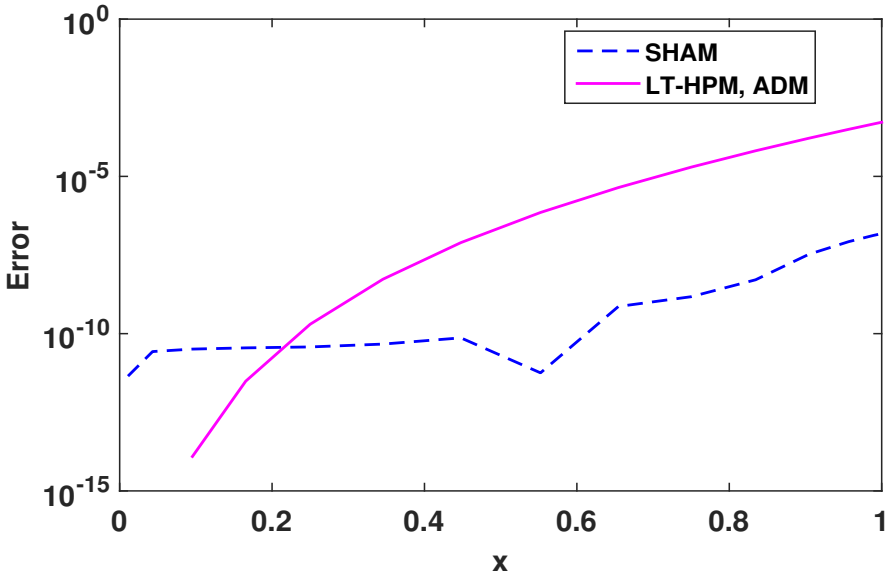

Figure 4.5: Comparison of errors using SHAM, LT-HPM and ADM for Example 4.3.

Example 4.4. *Consider the following linear ordinary differential equation [40, 48, 50]:*

$$y'' + \frac{8}{x}y' + xy = -30x + 44x^3 - x^4 + x^5, \quad x \in (0, \kappa], \tag{4.34}$$

with $y(0) = 0$ *and* $y'(0) = 0$. *The analytical solution is* $y(x) = x^4 - x^3$.

By applying the SHAM and heeding the steps used in the previous examples, we ultimately get the following system:

$$\begin{cases} \mathbf{A}_0 = \mathbf{B}^{-1}\bar{\mathbf{H}}, \\ \mathbf{A}_k = (\delta_k + \varsigma)\mathbf{B}^{-1}\bar{\mathbf{B}}\mathbf{A}_{k-1} + \varsigma\mathbf{B}^{-1}\left[-(1-\delta_k)\bar{\mathbf{H}} + x(\mathbf{C}(t)\mathbf{A}_{k-1})\right], \end{cases} \tag{4.35}$$

where

$$\mathbf{B} = \frac{1}{\kappa^2}\mathbf{C}''(t) + \mathbf{diag}(\frac{8}{\kappa x})\mathbf{C}'(t) + \mathbf{diag}(x). \tag{4.36}$$

Table 4.7 presents the computed solutions using the SHAM at various approximation orders, alongside the exact values. The high degree of agreement between the two confirms the method's precision and effectiveness. This consistency demonstrates the robustness of SHAM in accurately resolving problems of this nature.

Example 4.5. *Let us take the linear ordinary differential equation defined as follows [40,*

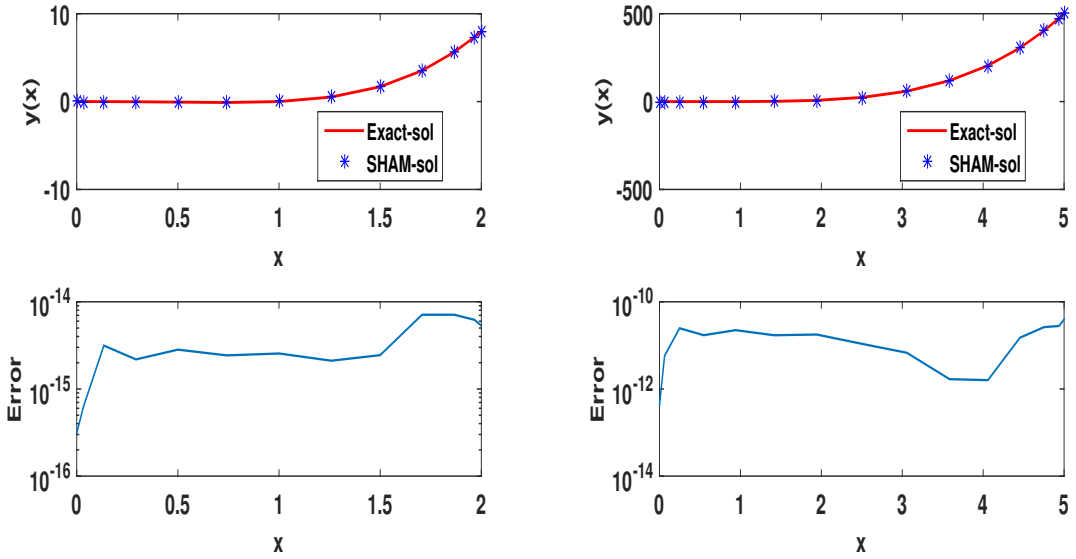

(a) $M = 8$, $N = 12$, $\varsigma = -1$, $\kappa = 2$.

(b) $M = 18$, $N = 14$, $\varsigma = -0.86$, $\kappa = 5$.

Figure 4.6: Exact and approximate solutions with associated error behavior for Example 4.4.

Table 4.7: Evaluating the SHAM against the exact solution for $\kappa = 2$ and $N = 12$ for Example 4.4.

x	$M = 2$	$M = 4$	$M = 6$	exact sol
	$\varsigma = -1$	$\varsigma = -0.98$	$\varsigma = -0.98$	
0,03	-0.00003821495944	-0.00003821375774	-0.00003821376051	-0.00003821376050
0,13	-0.00208256768829	-0.00208256228698	-0.00208256229943	-0.00208256229943
0,29	-0.01776695677000	-0.01776695295773	-0.01776695296637	-0.01776695296637
0,50	-0.06250000488399	-0.06249999998924	-0.06250000000000	-0.06250000000000
0,74	-0.10538262249315	-0.10538261825424	-0.10538261826217	-0.10538261826216
1,00	-0.00000000412393	0.00000000000559	-0.00000000000001	-0.00000000000000
1,26	0.51628101093195	0.51628100311101	0.51628100312440	0.51628100312440
1,50	1.68750010127633	1.68749999996172	1.68750000000003	1.68750000000000
1,71	3.51776729034637	3.51776695305564	3.51776695296648	3.51776695296637
1,87	5.62708270380479	5.62708256266238	5.62708256229949	5.62708256229943
1,97	7.33913855727115	7.33913982927560	7.33913982889804	7.33913982889826
2,00	7.99999765554067	8.00000000026357	7.99999999999965	8.00000000000000

48, 50]:

$$y'' + \frac{2}{x}y' + y = x^3 + x^2 + 12x + 6, \quad x \in [0, \kappa] \tag{4.37}$$

with $y(0) = 0, y'(0) = 0$ *and* $y(x) = x^2 + x^3$.

By employing the same approach and following the established methodology, the application of the SHAM leads to the following results.

Table 4.8 provides a quantitative comparison of the errors associated with the SHAM and

Table 4.8: Error variation using SHAM and HFC methods with $\kappa = 10$ for Example (4.5).

x	HFC error [40]	x	SHAM error
0	0	0	7.36383e-14
0.01	1.47e-06	0.11	1.77180e-08
0.10	1.82e-06	0.43	1.04241e-07
0.50	1.41e-06	0.95	1.11839e-07
1.00	1.25e-06	1.65	8.73862e-08
2.00	6.93e-07	2.50	4.01795e-08
3.00	7.58e-08	3.45	7.06064e-09
4.00	3.07e-07	4.48	3.06738e-08
5.00	3.21e-07	5.52	2.03932e-08
6.00	9.74e-08	6.55	6.96787e-09
7.00	2.05e-07	7.50	2.03789e-08
8.00	7.36e-07	8.35	1.67647e-07
9.00	4.61e-06	9.05	3.35735e-07
10.00	1.24e-05	9.57	2.50299e-07
		9.89	4.37785e-08
		10.00	1.77181e-07

HFC methods [40], allowing for a precise evaluation of their accuracy. SHAM, applied using Gauss-Lobatto collocation points, consistently produces lower errors than HFC, which is based on Hermite collocation points, across various evaluation points. This reduction in error highlights the numerical superiority of SHAM, demonstrating its greater precision in approximating the exact solution. Furthermore, the results confirm that SHAM offers a more stable and accurate approach compared to HFC, making it a more reliable and efficient method for solving this class of numerical problems. Figure 4.7, structured in three panels, offers a comparative assessment of the numerical and exact solutions over the interval $[0, 10]$, using two distinct techniques: the spectral homotopy analysis method with Gauss-Lobatto nodes and the Hermite function collocation (HFC) method. The upper-left panel illustrates the solution derived via SHAM alongside the analytical solution, revealing a high level of consistency that underscores the method's precision. The lower-left panel compares the approximate solution obtained using HFC with the exact solution. A high degree of agreement is also observed, highlighting the effecacy of this approach. The right section presents the error curves associated with both methods. It is evident that the error corresponding to SHAM is lower than that of HFC, indicating the superior accuracy of SHAM.

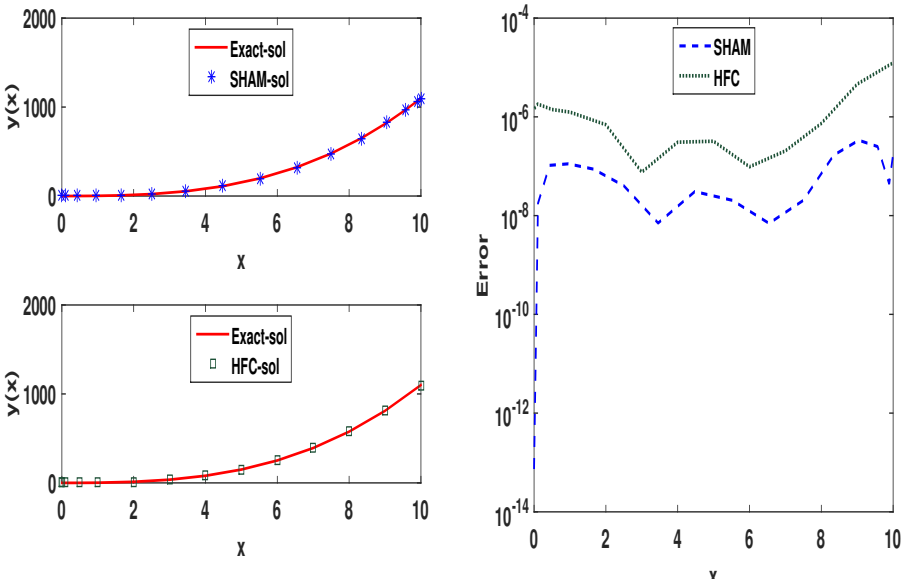

Figure 4.7: Visual representation of the exact solution alongside SHAM ($M = 20$, $N = 15$, $\varsigma = -0.82$, $\kappa = 10$) and HFC approximations, including absolute error distributions for Example 4.5.

4.3 Conclusion

In this work, we utilized collocation points to accelerate convergence and applied spectral methods to leverage their computational efficiency. The approach involves refining the numerical solution, selecting an appropriate linear operator, and establishing an initial estimate. To evaluate the performance of the proposed method, error calculations were conducted, confirming rapid convergence through the determination of the convergence rate. A comparative analysis with ADM, LT-HPM, and HFC methods further highlights the superior performance of our approach, as evidenced by the figures and tables presented. These results underscore the effectiveness of SHAM in solving the considered equations.

Chapter 5

SHAM using Chelyshkov polynomials in fractional problems

CHAPTER 5

SHAM USING CHELYSHKOV POLYNOMIALS IN FRACTIONAL PROBLEMS

In this chapter, we extend the previously developed Spectral Homotopy Analysis Method (SHAM) [7] to address *fractional-order nonlinear differential equations*. Fractional calculus has gained significant attention in recent decades due to its ability to describe memory and hereditary properties inherent in many physical, biological, and engineering systems. The incorporation of fractional derivatives allows for a more realistic modeling of complex dynamical behaviors that cannot be captured by classical integer-order formulations. In what follows, we adapt the SHAM framework based on Chelyshkov polynomials [7] to fractional operators while maintaining the same spectral matrix formulation introduced in the previous chapter.

As defined previously, the linear operator $\mathscr{A}$ may include a fractional derivative term and can be expressed in the general form:

$$\mathscr{A}(y(t)) = D_t^{\alpha} y(t) + \mathcal{P}(y(t)), \tag{5.1}$$

where D_t^{α} denotes the fractional derivative of order $\alpha > 0$, and $\mathcal{P}$ represents any additional linear operator acting on $y(t)$. In the general case, two positive real orders α and β may

appear in the model to represent different fractional differentiation effects. The same spectral matrix formulation can be extended to represent these operators, providing a unified treatment for both integer and non-integer derivatives.

Indeed, the fractional derivative operator D_t^α of order α acting on $C(t)$ can be expressed in matrix form as

$$\boldsymbol{\mathcal{Y}}^{(\alpha)} = \frac{1}{(b-a)^\alpha} D^\alpha \boldsymbol{C}(t) \boldsymbol{E},$$

where $D^\alpha \boldsymbol{C}(t)$ denotes the fractional differentiation matrix of order α. The integer-order differentiation matrices correspond to the special cases $\alpha = 1, 2, \ldots$. This unified matrix representation allows us to handle both integer and fractional derivatives within the same spectral framework without altering the overall solution procedure.

5.1 Application of the fractional SHAM using Chelyshkov polynomials

To illustrate the effectiveness and accuracy of the proposed fractional SHAM formulation, we consider in the following example a nonlinear fractional Duffing-type equation involving two fractional derivatives of positive real orders α and β.

Example 5.1. *[1] We consider the following nonlinear fractional Duffing-type differential equation:*

$$D_x^\alpha y(x) + a\, D_x^\beta y(x) + b\, y(x) + c\, y^3(x) = g(x), \qquad x \in [0, \kappa], \tag{5.2}$$

subject to the initial conditions

$$y(0) = 1, \qquad y'(0) = 0, \tag{5.3}$$

where 1<$\alpha \leq 2$ and 0<$\beta \leq 1$ are the fractional derivative orders. The source term $g(x)$ is chosen such that the exact solution is

$$y(x) = \cos(x),$$

for the particular parameter values $a = b = c = 1$.

The linear and nonlinear operators are defined as follows:

$$L(y) = D_x^{\alpha} y(x) + a\, D_x^{\beta} y(x) + b\, y(x), \quad N(y) = D_x^{\alpha} y(x) + a\, D_x^{\beta} y(x) + b\, y(x) + c\, y^3(x).$$

To simplify the numerical treatment, the physical domain $[0, \kappa]$ is rescaled to the unit interval $[0, 1]$ via the transformation (4.17). By applying the substitution (4.18), with $y_0(x) = 1 - \frac{x^2}{2}$ chosen as an initial approximation, and substituting it into equation (5.2), we obtain:

$$\frac{1}{\kappa^{\alpha}} D^{\alpha} u + \frac{1}{\kappa^{\beta}} D^{\beta} u + (1 + 3y_0)u + 3y_0 u^2 + u^3 + \mathscr{H}(x) = 0, \tag{5.4}$$

subject to the initial conditions: $u(0) = u'(0) = 0$, where the source term $\mathscr{H}(x)$ is defined as:

$$\mathscr{H}(x) = \frac{1}{\kappa^{\alpha}} D^{\alpha} y_0 + \frac{1}{\kappa^{\beta}} D^{\beta} y_0 + y_0 + y_0^3 - g(x).$$

Accordingly, the modified linear and nonlinear operators are given by:

$$\begin{aligned} \mathscr{A}(u) &= \frac{1}{\kappa^{\alpha}} D^{\alpha} u + \frac{1}{\kappa^{\beta}} D^{\beta} u + (1 + 3y_0)u, \\ \mathcal{M}(u) &= \frac{1}{\kappa^{\alpha}} D^{\alpha} u + \frac{1}{\kappa^{\beta}} D^{\beta} u + (1 + 3y_0)u + 3y_0 u^2 + u^3. \end{aligned}$$

By substituting $\mathcal{L}$ and $\mathcal{N}$ into (4.7), we have:

$$\mathscr{A}(u_k) = (\delta_k + \varsigma)\mathcal{L}(u_{k-1}) + \varsigma \left[(1 - \delta_k)\mathscr{H} + 3y_0 \sum_{i=0}^{k-1} u_i u_{k-i-1} + \sum_{i=0}^{k-1} u_{k-i-1} \sum_{n=0}^{i} u_{i-n} u_n \right], \tag{5.5}$$

with the initial conditions:

$$u_k(0) = u_k'(0) = 0. \tag{5.6}$$

Using Eqs. (1.28) and (4.1), Eq. (5.5) can be rewritten as:

$$\begin{aligned} \mathbf{B}\mathbf{A}_k = \varsigma \Bigg[3\mathbf{Y}_0 \sum_{i=0}^{k-1} (\mathbf{C}(t)\mathbf{A}_i)(\mathbf{C}(t)\mathbf{A}_{k-i-1}) + \sum_{i=0}^{k-1} (\mathbf{C}(t)\mathbf{A}_{k-i-1}) \sum_{n=0}^{i} (\mathbf{C}(t)\mathbf{A}_{i-n})(\mathbf{C}(t)\mathbf{A}_n) \Bigg] \\ + (\delta_k + \varsigma)\mathbf{B}\mathbf{A}_{k-1} + \varsigma(1 - \delta_k)\mathbf{H}. \end{aligned} \tag{5.7}$$

where

$$\mathbf{B} = \frac{1}{\kappa^{\alpha}} \mathbf{D}^{(\alpha)} C(t) + \frac{1}{\kappa^{\beta}} D^{(\beta)} C(t) + \mathbf{diag}(1 + 3y_0),$$

$$\mathbf{A}_k = (a_{k_0}, a_{k_1}, ..., a_{k_N})^T.$$

By properly enforcing the initial conditions (5.6) in Eq. (5.7), we obtain:

$$\begin{cases} \mathbf{A}_0 = \mathbf{B}^{-1}\bar{\mathbf{H}}, \\ \mathbf{A}_k = \varsigma\mathbf{B}^{-1}\left[(1-\delta_k)\bar{\mathbf{H}} + \sum_{i=0}^{k-1}(\mathbf{C}(t)\mathbf{A}_{k-i-1})\sum_{n=0}^{i}(\mathbf{C}(t)\mathbf{A}_{i-n})(\mathbf{C}(t)\mathbf{A}_n)\right] \\ \qquad + (\delta_k + \varsigma)\mathbf{B}^{-1}\bar{\mathbf{B}}\mathbf{A}_{k-1}. \end{cases} \tag{5.8}$$

Matrix $\bar{\mathbf{B}}$ represents a modified version of matrix $\mathbf{B}$, where the first and second rows are replaced by zeros while the remaining entries remain unchanged. Similarly, the vector $\bar{\mathbf{H}}$ is obtained from $\mathbf{H}$ by setting its first two elements to zero to satisfy the prescribed initial conditions.

Table 5.1 presents the transposed numerical results obtained using the Spectral Homotopy Analysis Method (SHAM) applied to the fractional Duffing equation for different values of M. The table reports both the approximate solutions and the corresponding absolute errors for $M = 2$ and $M = 4$ with $\alpha = 1.8$ and $\beta = 0.8$, compared with the exact analytical solution $y(t) = \cos(t)$. It is observed that the SHAM approach yields highly accurate results even for small values of M, with the absolute error decreasing rapidly as M increases. This demonstrates the strong convergence behavior and computational efficiency of the proposed fractional SHAM formulation. Moreover, the accuracy improvement with higher M highlights the method's adaptability to handle fractional-order nonlinear problems such as the Duffing-type equation, confirming its robustness and reliability in approximating complex fractional dynamical systems.

Figure 5.1 illustrates the comparison between the exact and approximate solutions of Example 5.1, along with the corresponding absolute error distributions, for fractional orders $\alpha = 1.9$ and $\beta = 0.9$. The convergence-control parameter ς was optimally determined using the squared residual error (2.27) to ensure the best accuracy and stability of the solution. It is observed that the SHAM formulation based on Chelyshkov polynomials provides results in excellent agreement with the analytical solution even for low approximation orders ($M = 2$ and $M = 4$). The absolute error remains extremely small of the order of 10^{-12} to 10^{-14} which clearly demonstrates the high accuracy, stability, and rapid convergence of the proposed fractional SHAM approach.

Table 5.1: Transposed numerical results and corresponding absolute errors for $\kappa = 1$, $\alpha = 1.8$ and $\beta = 0.8$.

x	Approx. ($M = 2$)	Error ($M = 2$)	Approx. ($M = 4$)	Error ($M = 4$)	Exact Solution
	$\varsigma = -0.998$		$\varsigma = -1$		
0.0000	1.000000000000000	0	1.000000000000000	0	1.000000000000000
0.0203	0.999794904612734	1.09912e-14	0.999794904612746	5.55112e-16	0.999794904612745
0.0794	0.996851598355700	7.17204e-14	0.996851598355777	5.66214e-15	0.996851598355771
0.1726	0.985146776922874	1.42109e-13	0.985146776923027	1.15463e-14	0.985146776923016
0.2923	0.957585814432710	1.87739e-13	0.957585814432913	1.57652e-14	0.957585814432897
0.4288	0.909447634977450	9.48130e-14	0.909447634977563	1.82077e-14	0.909447634977545
0.5712	0.841275830929770	1.23435e-12	0.841275830928555	1.88738e-14	0.841275830928536
0.7077	0.759854206577774	8.21754e-12	0.759854206569574	1.74305e-14	0.759854206569557
0.8274	0.676769742726573	2.47495e-11	0.676769742701840	1.60982e-14	0.676769742701824
0.9206	0.605321381345431	3.89699e-11	0.605321381306475	1.42109e-14	0.605321381306461
0.9797	0.557233070942186	3.78825e-11	0.557233070904317	1.37668e-14	0.557233070904303
1.0000	0.540302305901792	3.36521e-11	0.540302305868154	1.37668e-14	0.540302305868140

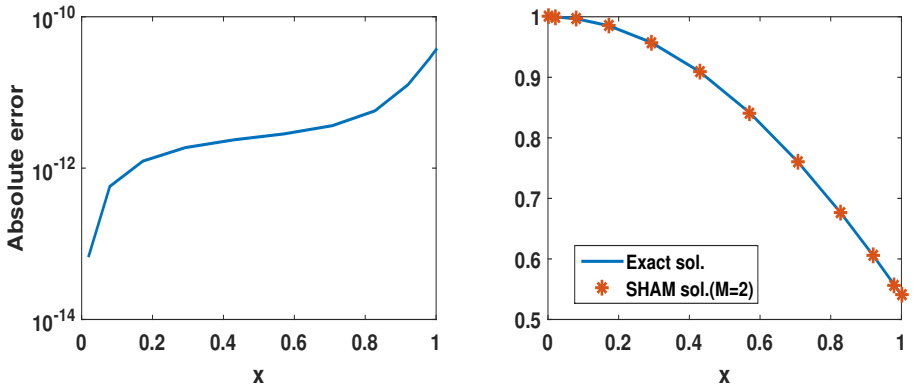

(a) $M = 2$, $N = 11$, $\varsigma = -1$, $\kappa = 1$.

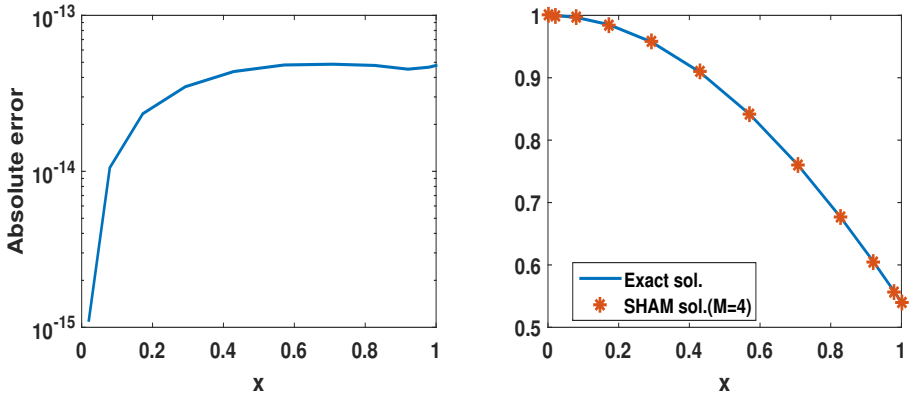

(b) $M = 4$, $N = 11$, $\varsigma = -1.002$, $\kappa = 1$.

Figure 5.1: Exact and approximate solutions with associated error behavior for $\alpha = 1.9$ and $\beta = 0.9$ in Example 5.1.

GENERAL CONCLUSION

In this dissertation, we have conducted an extensive study of the *Homotopy Analysis Method* and its spectral extension, the *Spectral Homotopy Analysis Method*, for solving nonlinear differential equations, both in their classical and fractional forms. The theoretical framework of HAM was first presented in detail, emphasizing its topological foundation, flexibility, and analytical power in dealing with strongly nonlinear problems without the need for small parameters. The essential role of the convergence-control parameter ς was discussed, highlighting how it enables the regulation of convergence and stability of the obtained series solutions. Subsequently, the study demonstrated the practical efficiency of HAM through its application to well-known nonlinear models such as the *Burgers equation* and another nonlinear problem. The obtained results confirmed the accuracy and reliability of the method while showcasing its adaptability to different types of nonlinearities. Building upon this foundation, the *Spectral Homotopy Analysis Method* was developed and applied using *Chebyshev polynomials* to solve the *Duffing* and *Van der Pol equations*. The results revealed a remarkable agreement with analytical solutions, as well as a rapid convergence and numerical stability, proving the advantage of combining spectral techniques with HAM. The method was further extended by incorporating *Chelyshkov polynomials* as spectral bases within SHAM, representing the first known application of these polynomials in this context. This new approach was successfully applied to the *Lane-Emden equation*, a classical nonlinear model in astrophysics, confirming the robustness of SHAM across different polynomial families. Finally, SHAM was generalized to the *fractional domain* and applied to the *fractional Duffing equation*, effectively demonstrating its ability to handle both fractional-order derivatives and

nonlinear dynamics simultaneously. The numerical results showed excellent convergence rates, high accuracy, and strong computational stability. Overall, this research highlights that both *HAM and SHAM* provide efficient, flexible, and accurate frameworks for tackling a wide range of nonlinear differential equations. The integration of the homotopy concept with spectral representations leads to highly stable and rapidly convergent solutions, making these methods powerful tools for modeling complex physical, biological, and engineering phenomena. Future perspectives may include extending SHAM to multi-dimensional and coupled systems, exploring adaptive strategies for optimal convergence control, and applying the method to real-world fractional models arising in viscoelasticity, fluid mechanics, and plasma physics.

Bibliography

BIBLIOGRAPHY

[1] W. M. Abd-Elhameed, O. M. Alqubori, A. K. Amin, and A. G. Atta. Numerical solutions for nonlinear ordinary and fractional duffing equations using combined fibonacci–lucas polynomials. *Axioms*, 14(4), 2025.

[2] G. Adomian. *Solving Frontier Problems of Physics: the Decomposition Method.* Springer Dordrecht, Athens, Georgia, U.S.A, 1994.

[3] M. AL-Jawary and S. Abd-AL-Razaq. Analytic and numerical solution for Duffing equations. *International Journal of Basic and Applied Sciences*, 5(2):115–119, 2016.

[4] N. Arar, B. Deghdough, S. Dekkiche, Z. Torch, and A. M. Nagy. Numerical solution of the Burgers' equation using Chelyshkov polynomials. *International Journal of Applied and Computational Mathematics*, 10(33), 2024.

[5] A. Benzahi, N. Arar, N. Abada, M. Rhaima, L. Mchiri, and A. Ben Makhlouf. Numerical investigation of Fredholm fractional integro-differential equations by least squares method and compact combination of shifted Chebyshev polynomials. *Journal of Nonlinear Mathematical Physics*, 30:1392–1408, 2023.

[6] M. Bouakkaz, N. Arar, and M. Meflah. Enhanced numerical resolution of the Duffing and Van der Pol equations via the spectral homotopy analysis method employing chebyshev polynomials of the first kind. *Journal of Applied Mathematics and Computing*, 71(1):1159–1187, 2025.

[7] M. Bouakkaz, N. Arar, M. Meflah, K. Shah, B. Abdalla, and T. Abdeljawad. A Chelyshkov-based spectral homotopy analysis method for singular nonlinear Lane–Emden-type equations. *Networks and Heterogeneous Media*, 21(3):943–967, 2026.

[8] B. Bülbül and M. Sezer. Numerical solution of Duffing equation by using an improved Taylor matrix method. *Journal of Applied Mathematics*, 2013(691614), 2013.

[9] C. Canuto, M. Y. Hussaini, A. Quarteroni, and A. T. Zang. *Spectral Method in Fluid Dynamics*. Springer, Berlin Heidelberg, 1988.

[10] V. Chauhan and P. K. Srivastava. Computational techniques based on Runge-Kutta method of various order and type for solving differential equations. *International Journal of Mathematical, Engineering and Management Sciences*, 4(2):375–386, 2019.

[11] V.S. Chelyshkov. Alternative orthogonal polynomials and quadratures. *Electron. Trans. Numer. Anal*, 25(7):17–26, 2006.

[12] Gh. A. Cordshooli and A. R. Vahidi. Solutions of Duffing-Van der Pol equation using decomposition method. *Advanced Studies in Theoretical Physics*, 5(1-4):121–129, 2011.

[13] W. Fafa, Z. Odibat, and N. Shawagfeh. The homotopy analysis method for solving differential equations with generalized caputo-type fractional derivatives. *Journal of Computational and Nonlinear Dynamics*, 18(2):021004, 2022.

[14] E. Gokmen, G. Yuksel, and M. Sezer. A numerical approach for solving Volterra type functional integral equations with variable bounds and mixed delays. *Journal of Computational and Applied Mathematics*, 311:354–363, 2017.

[15] J.H. He. An approximate solution technique depending upon an artificial parameter. *Communications in Nonlinear Science and Numerical Simulation*, 3:92–97, 1998.

[16] J.H. He. Homotopy perturbation technique. *Computer Methods in Applied Mechanics and Engineering*, 178:257–262, 1999.

[17] P. J. Hilton. *An Introduction to Homotopy Theory*. Cambridge University Press, Cambridge, 1953.

[18] S. Kamil, W. Liu, A. R. Aeshah, K. Naveed, U. K. Sami, O. Muhammad, and A. Zubair. Unraveling pine wilt disease: Comparative study of stochastic and deterministic model using spectral method. *Expert Systems with Applications*, 240:122407, 2024.

[19] A. V. Karmishin, A. T. Zhukov, and V. G. Kolosov. *Methods of Dynamics Calculation and Testing for Thin-walled Structures (in Russian)*. Mashinostroyenie, Moscow, 1990.

[20] Y. Khan, M. Madani, A. Yildirim, M. A. Abdou, and N. Faraz. A new approach to Van der Pol's oscillator problem. *Verlag der Zeitschrift für Naturforschung*, 66(10-11):620–624, 2011.

[21] Y. Khan, H. Vazquez-leal, and N. Faraz. An efficient new iterative method for oscillator differential equation. *Scientia Iranica*, 19(6):1473–1477, 2012.

[22] A. A. Kilbas, H. M. Srivastava, and J. J. Trujillo. *Theory and Applications of Fractional Differential Equations*, volume 204 of *North-Holland Mathematics Studies*. Elsevier, Amsterdam, 2006.

[23] Z. Laouar, N. Arar, and A. Ben Makhlouf. Theoretical and numerical study for Volterra-Fredholm fractional integro-differential equations based on Chebyshev polynomials of the third kind. *Complexity*, 2023:6401067, 2023.

[24] Z. Laouar, N. Arar, and A. Talaat. Efficient spectral Legendre Galerkin approach for the advection diffusion equation with constant and variable coefficients under mixed Robin boundary conditions. *Advances in the Theory of Nonlinear Analysis and its Application*, 7(1):133–147, 2023.

[25] Y. Li, T. Nohara Ben, and S. Liao. Series solutions of coupled Van der Pol equation by means of homotopy analysis method. *Journal of Mathematical Physics*, 51(6):063517, 2010.

[26] S. J. Liao. A kind of approximate solution technique which does not depend upon small parameters (ii) – an application in fluid mechanics. *International Journal of Non-Linear Mechanics*, 32:815–822, 1997.

[27] S. J. Liao. An explicit, totally analytic approximation of blasius viscous flow problems. *International Journal of Non-Linear Mechanics*, 34:759–778, 1999.

[28] S. J. Liao. *Beyond Perturbation: Introduction to the Homotopy Analysis Method*. Chapman and Hall/CRC, New York, 2003.

[29] S. J. Liao. On the homotopy analysis method for nonlinear problems. *Applied Mathematics and Computation*, 147:499–513, 2004.

[30] S. J. Liao. *Advances in the Homotopy Analysis Method*. Word Scientific, Singapor, 2014.

[31] S.J Liao. *The Proposed Homotopy Analysis Technique for the Solution of Nonlinear Problems*. Phd dissertation, Shanghai Jiao Tong University, 1992.

[32] S.J. Liao. *Homotopy Analysis Method in Nonlinear Differential Equations*. Springer, Berlin, Heidelberg, 2012.

[33] A. M. Lyapunov. *General Problem on Stability of Motion (English Translation)*. Taylor & Francis, London, 1992.

[34] J. C. Mason and D. C. Handscomb. *Chebyshev Polynomials*. Chapman and Hall/CRC, New York, 2002.

[35] S. Mengjun and W. Qinghua. On the Chebyshev spectral collocation method for the solution of highly oscillatory Volterra integral equations of the second kind. *Applied Mathematics and Nonlinear Sciences*, 9(1), 2024.

[36] A. Molabahrami and F. Khani. The homotopy analysis method to solve the Burgers–Huxley equation. *Nonlinear Analysis: Real World Applications*, 2007.

[37] S. S. Motsa and Z. G. Makukula. The spectral-homotopy analysis method (SHAM) for solutions of boundary layer problems. In R.O. Fagbenle, O.M. Amoo, S. Aliu, and A. Falana, editors, *Applications of Heat, Mass and Fluid Boundary Layers*, pages 133–148. Woodhead Publishing, 2020.

[38] S. S. Motsa, P. Sibanda, and S. Shateyi. A new spectral-homotopy analysis method for solving a nonlinear second order BVP. *Commun Nonlinear Sci Numer Simulat*, 15(9):2293–2302, 2010.

[39] Z. Odibat and S. Kumar. A robust computational algorithm of homotopy asymptotic method for solving systems of fractional differential equations. *Journal of Computational and Nonlinear Dynamics*, 14(8):081004, 2019.

[40] K. Parand, M. Dehghan, A.R. Rezaei, and S.M. Ghaderi. An approximation algorithm for the solution of the nonlinear Lane–Emden type equations arising in astrophysics using Hermite functions collocation method. *Computer Physics Communications*, 181(6):1096–1108, 2010.

[41] I. Podlubny. *Fractional Differential Equations*, volume 198 of *Mathematics in Science and Engineering*. Academic Press, New York, London, Toronto, 1999.

[42] T. J. Rivlin. *Chebychev Polynomials*. Dover Publications, New York, 2020.

[43] M. Sajid and T. Hayat. Comparison of ham and hpm methods for nonlinear heat conduction and convection equations. *Nonlinear Analysis: Real World Applications*, 9:2296–2301, 2008.

[44] S. G. Samko, A. A. Kilbas, and O. I. Marichev. *Fractional Integrals and Derivatives: Theory and Applications*. Gordon and Breach, Yverdon, 1993.

[45] S. Sen. *Topology and Geometry for Physicists*. Academic Press, Florida, 1983.

[46] P. Sibanda, S. S. Motsa, and Z. G. Makukula. A spectral-homotopy analysis method for heat transfer flow of a third grade fluid between parallel plates. *International Journal of Numerical Methods for Heat and Fluid Flow*, 22(1):4–23, 2012.

[47] Y. Talaei and M. Asgari. An operational matrix based on chelyshkov polynomials for solving multi-order fractional differential equations. *Neural Computing and Applications*, 30:1369–1376, 2018.

[48] R. Tripathi and H. Mishra. Homotopy perturbation method with Laplace transform (LT-HPM) for solvingLane–Emden type differential equations (LETDEs). *SpringerPlus*, 5, 12 2016.

[49] R. A. Van Gorder and K. Vajravelu. On the selection of auxiliary functions, operators, and convergence-control parameters in the application of the homotopy analysis

method to nonlinear differential equations: A general approach. *Communications in Nonlinear Science and Numerical Simulation*, 14:4078–4089, 2009.

[50] A-M. Wazwaz. A new method for solving singular initial value problems in the second-order ordinary differential equations. *Applied Mathematics and Computation*, 128(1):45–57, 2002.

[51] A-M. Wazwaz. The variational iteration method for solving nonlinear singular boundary value problems arising in various physical models. *Communications in Nonlinear Science and Numerical Simulation*, 16(10):3881–3886, 2011.